ÇUKUROVA UNIVERSITY
INSTITUTE OF NATURAL AND APPLIED SCIENCES

PhD THESIS

Mustafa İNCİ

MODELLING AND ANALYSIS OF FAULT RIDE THROUGH CAPABILITY OF GRID CONNECTED WIND SYSTEMS USING MULTILEVEL DYNAMIC VOLTAGE RESTORER

DEPARTMENT OF ELECTRICAL AND ELECTRONICS ENGINEERING

ADANA-2017

ÇUKUROVA UNIVERSITY
INSTITUTE OF NATURAL AND APPLIED SCIENCES

MODELLING AND ANALYSIS OF FAULT RIDE THROUGH CAPABILITY OF GRID CONNECTED WIND SYSTEMS USING MULTILEVEL DYNAMIC VOLTAGE RESTORER

Mustafa İNCİ

PhD THESIS

DEPARTMENT OF ELECTRICAL AND ELECTRONICS ENGINEERING

We certify that the thesis titled above was reviewed and approved for the award of degree of the Doctor of Philosophy by the board of jury on 08/12/2017.

……………………….…	.………….…………………	………………….……….….
Prof. Dr. Mehmet TÜMAY	Assoc. Prof. Dr. M.Emin MERAL	Assoc. Prof. Dr. M. Uğraş CUMA
SUPERVISOR	MEMBER	MEMBER

……………………….….	………………………………..
Asst. Prof. Dr. Adnan TAN	Asst. Prof. Dr. Tahsin KÖROĞLU
MEMBER	MEMBER

This PhD Thesis is written at the Department of Electrical and Electronics Engineering of Institute of Natural and Applied Sciences of Çukurova University.
Registration Number:

Prof. Dr. Mustafa GÖK
Director
Institute of Natural and Applied Sciences

This thesis was supported by TÜBİTAK for my thesis (Project Number: 115R304).

ABSTRACT

PhD THESIS

MODELLING AND ANALYSIS OF FAULT RIDE THROUGH CAPABILITY OF GRID CONNECTED WIND ENERGY SYSTEMS USING MULTILEVEL DYNAMIC VOLTAGE RESTORER

Mustafa İNCİ

ÇUKUROVA UNIVERSITY
INSTITUTE OF NATURAL AND APPLIED SCIENCES
DEPARTMENT OF ELECTRICAL AND ELECTRONICS ENGINEERING

Supervisor : Prof. Dr. Mehmet TÜMAY
Co-supervisor : Assoc.Prof. Dr. K.Çağatay BAYINDIR
Year: 2017, Pages: 181
Jury : Prof. Dr. Mehmet TÜMAY
: Assoc. Prof. Dr. M. Emin MERAL
: Assoc. Prof. Dr. M. Uğraş CUMA
: Assist. Prof. Dr. Adnan TAN
: Assist. Prof. Dr. Tahsin KÖROĞLU

In conventional dynamic voltage restorer (DVR) tied wind systems, traditional controller schemes provide only low-voltage ride through capability due to voltage dips. In order to improve the capabilities of DVR systems, multifunctional controller algorithm is designed and analyzed theoretically in multilevel DVR to compensate both voltage dips for low-voltage ride through (LVRT), voltage swells for high voltage ride through (HVRT) and voltage harmonics, simultaneously. For this purpose, different reference generation methods are performed for multifunctional compensation and compared in order to obtain better results. In addition, DVR topologies which use battery called as Topology I and share dc-link capacitors of back-back converter in doubly fed induction generator (DFIG) called as Topology II are performed. The controller methods are firstly tested in Topology I in order to obtain detection speeds for voltage dips and harmonic compensation capabilities. Following, different case studies are performed in grid connected DFIG based wind system for Topology I and II. Performance results verify the effectiveness of the multifunctional controller scheme to enhance uninterruptible voltage stability and harmonics compensation in grid connected wind systems.

Key Words: DVR, Multifunctional Compensation, Dip/Swell, Voltage Harmonics, DFIG.

ÖZ

DOKTORA TEZİ

ŞEBEKEYE BAĞLI RÜZGÂR SİSTEMLERİNİN ÇOK SEVİYELİ DİNAMİK GERİLİM İYİLEŞTİRİCİ KULLANILARAK ARIZA SONRASI SİSTEME KATKI YETENEĞİNİN MODELLENMESİ VE ANALİZİ

Mustafa İNCİ

ÇUKUROVA ÜNİVERSİTESİ
FEN BİLİMLERİ ENSTİTÜSÜ
ELEKTRİK – ELEKTRONİK MÜHENDİSLİĞİ ANABİLİM DALI

Danışman : Prof. Dr. Mehmet TÜMAY
İkinci Danışman : Doç. Dr. K.Çağatay BAYINDIR
Year: 2017, Pages: 181
Jüri : Prof. Dr. Mehmet TÜMAY
: Doç. Dr. M. Emin MERAL
: Doç. Dr. M. Uğraş CUMA
: Yrd. Doç. Dr. Adnan TAN
: Yrd. Doç. Dr. Tahsin KÖROĞLU

Klasik dinamik gerilim iyileştirici (DGİ) bağlı rüzgâr sistemlerinde klasik denetim şemaları, gerilim düşmelerine bağlı olarak sadece düşük gerilim sonrası sistem kararlılığı sağlamaktadır. DGİ sistemlerin kabiliyetlerini geliştirmek için, düşük ve yüksek gerilim sonrası sistem kararlılığı için gerilim düşmeleri/yükselmeleri ve harmoniklerini eş zamanlı telafi etmek amacı ile çok fonksiyonlu denetim algoritması çok seviyeli DGİ için tasarlanıp teorik olarak analiz edilmektedir. Bu amaçla, farklı referans üretim yöntemleri uygulanmakta ve daha iyi sonuç almak için karşılaştırılmaktadır. Ek olarak, batarya kullanılan Topoloji I ve çift beslemeli asenkron jeneratör (ÇBAJ)'deki sırt-sırta dönüştürücüdeki da-bağ sığalarını kullanan Topoloji II isimli DGİ topolojileri çalıştırılmaktadır. Denetim yöntemleri ilk olarak gerilim düşmelerinin tespit hızları ve harmonik telafi yetenekleri için Topoloji I'de karşılaştırılmaktadır. Devamında, farklı örnekleme çalışmaları şebekeye bağlı ÇBAJ tabanlı rüzgâr sisteminde Topoloji I ve II için ayrı ayrı gerçekleştirilmektedir. Performans sonuçları, şebekeye bağlı rüzgâr sistemlerinde kesintisiz gerilim kararlılığı ve harmonik telafi sağlamak için gerçekleştirilen çok fonksiyonlu denetleyicinin etkisini kanıtlamaktadır.

Anahtar Kelimeler: DGİ, Çok Fonksiyonlu Telafi, Düşme/Yükselme, Gerilim Harmoniği, ÇBAJ.

EXTENDED SUMMARY

With the development of technology and the reduction of fossil fuels, the wind energy industry has become one of the most important sources of renewable energy. Wind energy systems are used to reduce the electricity consumption in the consumer part by connecting to the electrical network. These systems are named as “Grid connected wind energy systems”. The power ratings of these systems are significantly increasing in the renewable energy industry, and the global wind power capacity in 2015 approaches to nearly 450 GW. However, the linkage and interaction of wind turbines with the grid cause serious problems due to the high power rating of the wind turbines. In this interaction, voltage problems on the grid side are the most important events affecting system stability of wind energy systems. Voltage dips / swells problems are considered to be the most important issues affecting energy quality in grid-connected wind energy systems. These problem types cause to lose its stability and cause high generator currents and electrical torque oscillations in a turbine generator. In addition, negative effects such as loss of power equipment and losses occur. After the faults in the grid, it is desirable that the wind turbines remain connected to the grid without losing the voltage stability and preventing the generation of high generator currents. This is called “Fault ride through capability”. Another problem in electrical grids is voltage harmonics, which cause to malfunction of the protection devices and overheat of the transformers / generators.

In wind energy systems connected to the grid, the most commonly used generator type in wind farms is double-fed induction generators (DFIG). It is preferred because it has variable speed control, active / reactive power control and small rating converters. In this generator type, the stator of the DFIG is directly connected to the electrical grid. The rotor is connected to the grid with a back-to-back converter to increase the rating of the electrical energy produced by the wind turbine partially (about 30%). However, the voltage dips / swells on the grids affect

the magnetic coupling between the stator and the rotor, creating transient high currents. Transient high currents increase the dc-link voltage in the back-to-back converter and cause the switching elements to be damaged. There are various protection elements applied to the wind energy systems connected to the electrical network in order to prevent these undesirable events in the turbine due to faults in the grids and to maintain system stability. One of the most popular methods used at DFIG is "Dynamic Voltage Restorers (DVR)". DVRs are special power devices with an inverter structure and are placed in series between the grid and the turbine. In this way, it provides the stability of the voltage on the turbine side by injecting the controlled voltage during the voltage dips / swells on the grid side. Conventional DVR systems applied to grid connected wind systems examine only symmetrical and asymmetric voltage dip situations. In these studies, it is discussed how to compensate for voltage dips and to prevent transient currents in the system and to contribute to the system after low voltage faults.

In this thesis, the effects of voltage dips / voltage swells and voltage harmonics problems in electrical grids and the compensation using multilevel DVR system are investigated and analyzed. For this purpose, a 5-level H-bridge diode clamped multilevel inverter is used. In the proposed system, the injected voltage has low total harmonic distortion due to the five-level H-bridge diode clamped multilevel inverter. In order to test the DVR tied wind system, the DFIG based grid-connected wind energy system is first modeled by using the PSCAD program. The wind turbine model is designed according to 0.69 kV / 50 Hz system. In the design of the wind system, the back-to-back converter is controlled using the vector control method. In the second step of the modeling, the design of the DVR system has been realized according to the wind turbine system parameters. DVR is firstly tested between the load and the grid, instead of the wind turbine, and the performance results are examined. It is ensured that the voltage on the load side is kept constant by compensating for the voltage dips / swells and harmonics on the grid side. The multilevel DVR system is tested for the first time with the aim of compensating for voltage dips / swells and harmonics seen in wind power systems connected to the grid. To accomplish these functions, a multi-functional controller algorithm has been developed.

In the optimization section, the combination of DGI and DFIG based wind system is realized. The optimization of DVR system is performed for two different topologies. In the system called Topology-I, DGI performs the compensation process by providing the energy need from the battery. In Topology II, the voltage problems are compensated from energy by using the common dc-link capacitors in the back-to-back converter in the wind turbine system. The proposed system is designed to compensate for 50% voltage dips, 30% voltage swells and voltage harmonics up to 10%.The Performance results for both systems are examined using the PSCAD program for different case studies.

In the proposed system, the multifunctional controller algorithm is implemented using different methods. By comparing the performances of the methods used in this study, the best method among methods is determined for the compensation operation. The performance results of the used methods are presented in Chapter 6. “Synchronous Reference Frame (SRF)”, “Enhanced Phase Locked Loop (EPLL)”, “Second Order Generalized Integrator based Phase Locked Loop (SOGIPLL)”, “Sliding Discrete Fourier Transform (SDFT)” and “Fast Fourier Transform (FFT)” are methods which tested in Topology I for multifunctional compensation process.

In multifunctional compensation algorithm, the most effective method is determined by comparing the compensation capacities of voltage dip and voltage harmonics using different control methods. The common feature of the used methods is that they are applicable for each phase and they are capable of obtaining the amplitudes of voltage dips /swells and harmonic signals. The reference signals are calculated by the obtained signals and compared with the triangular signals in pulse width modulation to generate controlled injected voltages. All methods are investigated for compensation for voltage harmonics and three-phase asymmetrical voltage dips. The starting/ending detection times of voltage dips and THD performance values after the compensation are presented in a tabular form. When the performance results are examined, ISRF method is determined as the fastest response method by detecting the voltage dips as fast as other methods. Using this method, the total distortion at turbine-side voltage can be reduced to approximately 1.5% for different THD levels.

In the next step, the ISRF method is tested for different case studies in Topology I and Topology II, and the performance results are given in Chapter 7.In the performance results, both topologies are examined for low voltage fault ride-through capability, high voltage ride-through capability and voltage harmonic compensation situations. In case studies, the compensation results of voltage dipp + harmonics and voltage swell + harmonics are given. When the performance data is analyzed, both topologies can simultaneously compensate for voltage dips / swells + harmonics and prevent high stator / rotor currents that occur after voltage dips / swells faults. In addition, Topology-I can achieves long-term voltage dip/swell compensation due to a separate battery. Topology II eliminates the additional energy storage requirement by using common dc-link capacitor of back-back converter in wind system. However, limited and short-term compensation is executed in Topology-II.

ACKNOWLEDGEMENTS

I would like to present my endless gratitude to my supervisors Prof. Dr. Mehmet TÜMAY and Assoc. Prof. Dr. Kamil Çağatay BAYINDIR for their support throughout this PhD journey. They have made a lot of valuable contributions to my academic knowledge and experience as well as to my intellectual life. I feel very lucky to have the chance to work with my supervisors.

I wish to express my special thanks to Asst. Prof. Dr. Adnan TAN. I think that he is one of the rare academicians bound to his work with passion. I am thankful to Res. Asst. Mehmet BÜYÜK for sharing his knowledge and being more than a colleague.

I thank to my wife Gizem CANGÜL İNCİ and my family for helping and supporting me throughout my entire life.

Finally, I cannot express my gratitude enough to those people who deceived me, left me alone when I needed them, and made me learn how long a night can be. I have realized how powerful I am thanks to them.

The financial support of the Scientific and Technological Research Council of Turkey (TÜBİTAK Project Number:115R304) during my Ph.D. is gratefully acknowledged.

CONTENTS **PAGE**

LIST OF TABLES **PAGE**

LIST OF FIGURES **PAGE**

XXI

LIST OF ABBREVIATIONS

A	: Amperes
AC	: Alternative Current
DC	: Direct Current
DFIG	: Doubly Fed Induction Generator
DFT	: Discrete Fourier Transform
DVR	: Dynamic Voltage Restorer
EPLL	: Enhanced Phase Locked Loop
F	: Frequency
FRT	: Fault Ride Through
FFT	: Fast Fourier Transform
GCWES	: Grid Connected Wind Energy System
GSC	: Grid Side Converter
GW	: Giga Watts
H-DCMI	: H-bridge Diode Clamped Multilevel Inverter
HPF	: High Pass Filter
HVRT	: High Voltage Ride Through
Hz	: Hertz
IEC	: International Electro-technical Commission
IEEE	: Institute of Electrical and Electronics Engineers
IGBT	: Insulated Gate Bipolar Transistor
ISRF	: Improved Synchronous Reference Frame
KW	: Kilo Watts
LPF	: Low Pass Filter
LVRT	: Low Voltage Ride Through
MW	: Mega Watts
P	: Power
PI	: Proportional Integrator

PMSG	: Permanent Magnet Synchronous Generator
PSCAD	: Power System Computer Aided Design
PU	: Per Unit
PWM	: Pulse Width Modulation
RSC	: Rotor Side Converter
SCIG	: Squirrel Cage Induction Generator
SOGI-PLL	: Second Order Generalized Integrator Phase Locked Loop
SDFT	: Sliding Discrete Fourier Transform
STATCOM	: Static Compensator
THD	: Total Harmonic Distortion
V	: Volts
VCO	: Voltage Controlled Oscillator
WRIG	: Wound Rotor Induction Generator
WRSG	: Wound Rotor Synchronous Generator

1. INTRODUCTION

In this chapter, general information of the thesis is given, as brief review of classical power system stability, changes and challenges in the power system with installation of renewable energy sources. The weak grid issue, which is gaining increasing importance with high penetration of wind power plants in recent years, is discussed up to an extent, together with severe grid faults. The research objectives, contributions, and the organization of the thesis are provided at the end of this chapter.

1.1. Background

Wind energy industry has become one of the most important renewable energy sources with the development of technology and reduction of fossil fuels. Wind energy systems have been connected to the electrical systems, called as grid connected wind energy systems (GCWES), are utilized to reduce the demand of utility-fed electricity for machines, illumination, heating and refreshment. The power ratings of these systems have demonstrated significant increment in renewable energy industry, which has started to improve since 1980s. But, the connection to the grid has become a serious problem due to high power ratings of wind turbines. Voltage problems at grid-side significantly affect power system stability of wind energy systems during the interaction with grid. Voltage dips and swells are the most significant issues which affects energy quality in GCWES. Voltage dips (sags) and swells are known as voltage reductions and rises which cause power losses and damage of power equipments. Furthermore, generator current and electrical torque reaches to higher values by losing voltage stability. After the faults in grid, wind turbines are required to remain grid connected during severe voltage dips and to prevent high stator/rotor currents and power losses without losing the voltage stability of turbine. This condition is defined as fault ride through (FRT) capability. Another problem called as voltage harmonics creates overheating of transformer/generators and fault operation of protective equipments.

In GCWES, the most common generator type for wind farm applications is Doubly Fed Induction Generator (DFIG) because of its advantages such as variable speed operation, active/reactive power control and smaller rated power converters. Basically, the stator of DFIG is directly tied to the grid. The rotor is connected to grid via partially back-to-back converters called as Rotor Side Converter (RSC) and Grid Side Converter (GSC) which have partial rating (nearly 30%) of power generator by wind turbine. Voltage dips at grid-side such as balanced/unbalanced faults result in high stator currents in DFIG based wind systems due to the direct connection of stator to the grid. Because of magnetic coupling between stator and rotor, high transient currents occur in rotor-side of system. High transient currents may damage solid-state devices and increase dc-link voltage of back-to-back converters.

Voltage dips/swells at grid-side voltages cause high stator currents due to the direct connection of stator to the grid. Because of magnetic coupling between stator and rotor, high transient currents occur in rotor-side of system. High transient currents damage solid-state devices and increase dc-link voltage of back-to-back converters in DFIG. To prevent these harmful conditions under unstable conditions, protection devices are applied in grid connected wind energy systems to provide FRT capability. The most popular solutions for DFIG are crowbar, STATCOM, and Dynamic Voltage Restorer (DVR). Among these topologies, crowbar is a resistive network which is connected to rotor winding in DFIG. In fault conditions, crowbar is short-circuited and DFIG behaves like an induction generator. But, high short current flows when the crowbar is active. In this situation, it absorbs a large amount of reactive power from grid, which is not applicable for grid code requirements. Other methods called as STATCOM and DVR are power electronics based devices to support reactive power at point common of coupling. DVR injects less reactive current to provide voltage stability compared with STATCOM.

1.2. Research Objectives and Contributions

Traditional DVRs used with GCWES are used to compensation for only voltage dips or unbalances during symmetrical and/or asymmetrical grid faults in (Flannery and Venkataramanan, 2009; Abdel-Baqi and Nasiri, 2011; Ibrahim et al., 2011; Leon et al., 2011; Ramirez et al., 2011; Wessels et al., 2011; Zhang et al., 2012; Alaraifi et al., 2013; Amutha and Kumar, 2013; Yao et al., 2013; Chen and Wang, 2014; Gkavanoudis and Demoulias, 2015). However, voltage harmonics cause overheating of transformers and generators, losses in transmission lines/cables in GCWES. In traditional DVR based systems, only voltage dips are compensated in (Flannery and Venkataramanan, 2009; Abdel-Baqi and Nasiri, 2011; Ibrahim et al., 2011; Ramirez et al., 2011; Wessels et al., 2011; Zhang et al., 2012; Alaraifi et al., 2013; Amutha and Kumar, 2013; Chen and Wang, 2014; Gkavanoudis and Demoulias, 2015) for FRT. Compensation of only voltage unbalances is performed in (Leon et al., 2011) and (Yao et al., 2013) in order to prevent negative sequence currents in electrical machines which cause unequal overheating and torque in stator windings of generator.

In this thesis, Dynamic Voltage Restorer (DVR) is used for the compensation of voltage dip/swell and harmonics problems in DFIG wind system. The original contributions and purposes of the proposed system are followed as:

- The simultaneous compensation of voltage dips, voltage swells and harmonics compensation is achieved in GCWES.
- Five level H-bridge diode clamped multilevel inverter is used to obtain low THD values at injected voltages.
- In order to compensate different voltage problems, multifunctional

controller algorithm is improved.

- Different voltage detection methods are used to provide better voltage stability at wind-side voltages.
- Two DVR topologies with battery (Topology I) and dc-link capacitor of back-back converter in DFIG (Topology II) are performed for case studies.
- The power flow is analyzed under voltage dips and swells.
- The system is designed and simulated to compensate up to %50 voltage dips and voltage harmonics with approximately 9.52% total harmonics distortion (THD).

1.3. The Organization of Thesis

The organization of the thesis is as follows;

Chapter 1 presents general overview, problems and solution techniques of problems in wind energy systems, briefly. It also explains the main objectives and contributions of thesis.

Chapter 2 introduces the power quality problems and its effects in grid connected wind systems. In addition, international standards related to PQ problems are given in this section.

Chapter 3 explains the wind energy in World and Turkey. Besides, the classification of wind turbines and turbine design are presented in this section. The structure of DFIG and its controller method called as Vector Control are also given in this chapter.

Chapter 4 explains the system and control method in order to compensate voltage problems in electrical grids. Multifunctional compensation technique is explained, and different control strategies are shown in this chapter.

Chapter 5 describes system topologies and controller schemes in order to compensate different voltage problems at grid side and provide the stable and smooth voltage at wind-side voltages.

Chapter 6 shows the compensation results of modelled system by using different reference signal generation methods.

Chapter 7, the system models and case studies for different multilevel inverters and different control strategies are given. In addition, performance results are given for different case studies under voltage dips, voltage swell and voltage harmonics.

Finally, Chapter 8 summarizes the contributions of the system and future work.

2. PQ ISSUE IN GCWES

In this section, the power quality problems in GCWES and their effects are presented. Also, PQ standards specified by IEC are given.

2.1. Overview

Wind energy is playing an increasingly important role in the supply of energy of most industrialized countries, and its share of the electrical generation is expected to continue to increase for many years to come (Fortman, 2015). An issue such as limited fossil fuel reserves, climate change due to CO2 emissions, brings to attention alternative technologies to generate electricity in a more sustainable manner (Chandrasekaran, 2014). In recent years there has been a lot of emphasis on renewable power integration due to environmental issues and to lower the dependence on fossil fuels (Saraf, 2012). Wind energy systems are being connected to the electrical systems, called as grid connected wind energy systems (GCWESs), are utilized to reduce the demand of utility-fed electricity for machines, illumination, heating and refreshment. The power ratings of these systems have demonstrated significant increment in renewable energy industry, which has started to improve in 1980s. As installed capacity of the wind power plants (WPPs) in power system of certain countries increases, stability of the power system becomes more critical (Göksu, 2013). With the rapid increase in penetration of wind power in the power system, it becomes necessary to require wind systems to behave as possible as conventional power plants to support the network voltage and frequency not only during steady-state conditions but also during grid disturbances (Qiao and Harley, 2008). But, the connection to the grid has become a serious problem due to high power ratings of wind turbines. The deviations and waveform distortions of physical and characteristics properties in electric grids that cause equipment failure, economical loss and several negative effects are defined as power quality (PQ) problems.

In GCWESs, the PQ problems occurred at grid-side significantly affect power system stability of wind energy systems during interaction between grid and turbine (Larsson, 2000). In grid connected wind energy systems, it is characterized in expressions of voltage and frequency. The most hazardous voltage problems which affect the stability of wind turbine are voltage dips and swells. Flickers, Harmonics and transients are different voltage problems at GCWESs. In addition to voltage problems, frequency variations are other PQ problems which affect the efficiency of wind system.

The PQ standards and grid requirements of grid connected systems are specified by IEC Standard 61400-21 of IEC-Technical Committee 88. In this paper, survey of PQ problems at GCWESs is proposed. The PQ problems are categorized in Section II, and the definitions/effects of these problems are detailed.

2.2. PQ Problems

Figure 2.1 illustrates the classification of PQ problems in GCWESs.

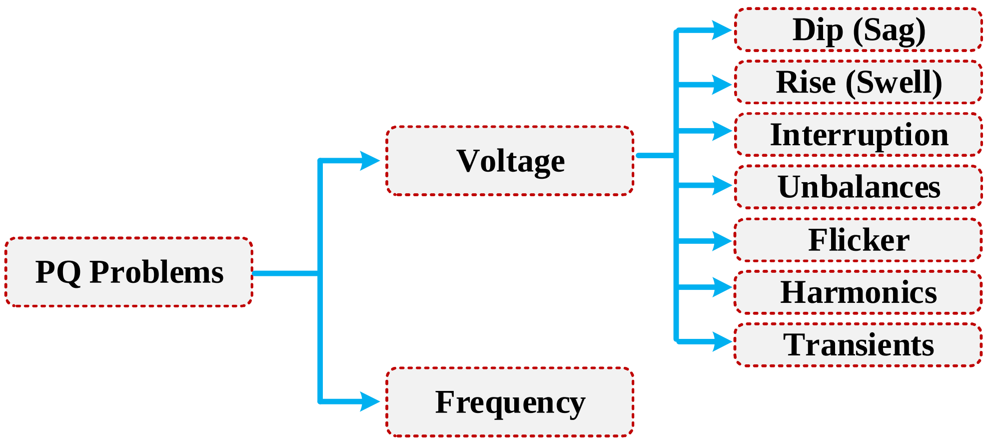

Figure 2.1 PQ problems in grid connected wind systems

2.2.1. Voltage Problems

Voltage problems are known as changes in the magnitude of voltage signals in a time duration from half period to minutes. These problems at grid-side significantly affect power system stability of wind energy systems during the interaction with grid. The most well-known PQ problems are known as variations, flicker, harmonics and transients.

2.2.1.1. Voltage Dips

Voltage dips are defined as short duration reduction in rated voltage magnitude between 10% and 90%. Figure 2.2 presents the voltage waveform of voltage dip problem in electrical systems. This problem cause high generator currents and electrical torque by losing voltage stability in GCWESs (Hansen and Michalke, 2007; Chouhan, 2010). After occurrence of voltage dips, wind turbines are required to remain grid connected during voltage variations and to prevent high stator/rotor currents and power losses without losing the voltage stability of turbine. This condition is defined as low voltage ride through (LVRT) capability.

$$Magnitude \le 0.9\,pu \quad for\ sag\ condition \tag{2.1}$$

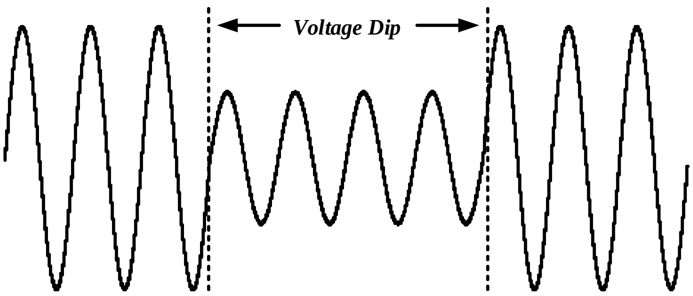

Figure 2.2 Voltage dip

2.2.1.2. Voltage Rise (Swell)

The second voltage variations are defined as voltage swells. These are determined as short duration rise in magnitude to 110% and 190% of its rated value, as shown in Figure 2.3. Grid voltage swell causes a transient dc flux component on generator stator winding even stronger than grid voltage dip, resulting in a much more serious stator, rotor current, and torque oscillation (Xie et al., 2015). In power electronics converter based wind energy generation systems, the reactive power will be absorbed by the power converter system from the grid during swell period (Ahmad and Loganathan, 2010). In order to prevent the negative influences of voltage swells, over voltage withstanding capability of wind turbine is defined as high voltage ride through (HVRT) capability (Zheng et al., 2013). The duration of voltage dip/swell varies from half-period to 1 minute in IEEE 519 standards (Sadigh and Smedley, 2016). In electrical systems, voltage swell is defined as according to (2.2):

$$Magnitude \geq 1.1\,pu \quad for \quad swell \quad condition \tag{2.2}$$

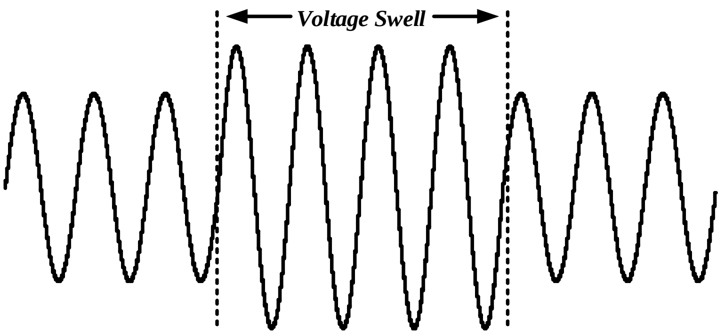

Figure 2.3 Voltage Swell

2.2.1.3. Voltage Interruption

Voltage interruption is defined as the completely loss of grid side voltage (Manoj Kumar Swain, 2013), as shown in Figure 2.4. According to its time interval, it can be classified as instantaneous, momentary, temporary and sustained (IEEE, 1995; IEEE, 2009).

- Instantaneous - 0.5 to 30 cycles
- Momentary - 30 cycles to 2 seconds
- Temporary - 2 seconds to 2 minutes
- Sustained - greater than 2 minutes

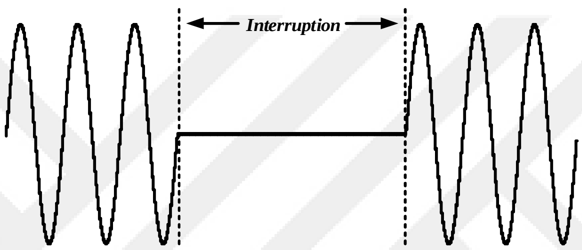

Figure 2.4 Interruption

2.2.1.4. Voltage Unbalances

In a three phase system, if the magnitudes of phase voltages and/or phase angles are different, this condition is called as voltage unbalance (Pillay and Manyage, 2001). The waveforms of voltage unbalance situation are shown in Figure 2.5. The main sources of this problem are high-rated unbalanced loads in electrical systems (Sugirtha and Latha, 2011). This unbalance condition creates negative sequence currents in electrical machines which cause unequal overheating and torque in stator windings of generator (Sugirtha and Latha, 2011; Raju et al., 2012).

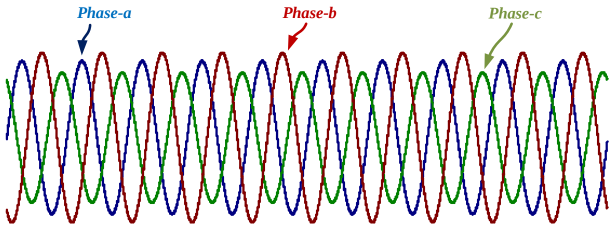

Figure 2.5 Voltage unbalances in a three phase system

2.2.1.5. Flicker

The voltage flickers are dynamic variations in the network caused by wind turbine or by varying load (Chen, 2005; Mohod and Aware, 2010). The voltage flickers are caused due to switching operation, pitch error, yaw error and fluctuation of wind speed (Sunil and Loganathan, 2012). The power fluctuations from wind turbine continuously occur in the course of operation. The amplitude of voltage fluctuation depends on grid strength, network impedance, phase-angle and power factor of the wind turbines, and the fluctuation of voltage flicker is in a frequency 10-35 Hz (Mohod and Aware, 2010). The measurement of PQ at GCWESs is defined by IEC 61400-21 and voltage fluctuation should be within +/-5% of nominal value in approximately 10 (ten) minutes (Emanuel et al., 2009; Sunil and Loganathan, 2012).

2.2.1.6. Harmonics

Voltage harmonics is defined as a distortion due to integer multiple components of the fundamental sinusoidal voltage waveform alternating at 50/60 Hz and repeats every cycle. Figure 2.6 shows a voltage waveform with harmonics which consists of fundamental and selective harmonics (3rd). Nonlinear loads, power electronic loads, rectifiers and inverters are well-known sources of harmonics (Larsson, 2000). These problems cause over heating of transformer/generators, fault operation of protective equipment and an increase in currents through shunt capacitors which lead to failure of such capacitors (Reid, 1994; Sugirtha and Latha, 2011).

The individual voltage components are used to calculate total harmonic distortion (THD) in percentage. THD limits are defined by using IEEE-519 standards (IEEE, 1993). The THD of a voltage (THD_V) is defined as:

$$THD_V = \frac{\sqrt{\sum_{h=2} V_h^2}}{V_1} \times 100\% \qquad (2.3)$$

Where, V_h is individual harmonic component of h^{th} component and V_1 is fundamental component of a voltage.

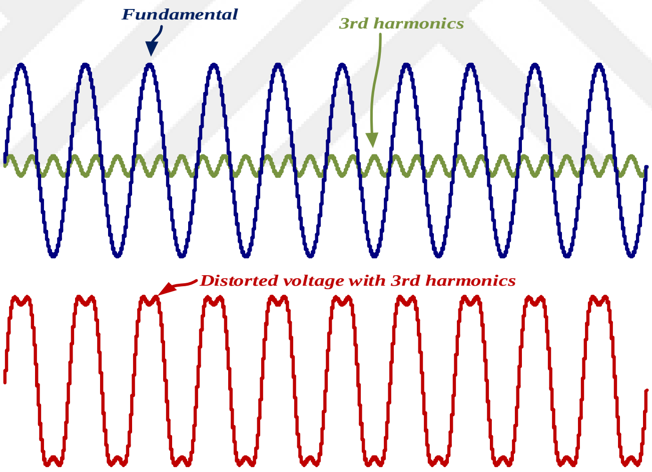

Figure 2.6 Waveforms of fundamental voltage, individual harmonics and distorted voltage with harmonics

2.2.1.7. Transients

Transients are known as sudden rises in voltage signals. Voltage Transients occur due to switching of capacitors using mechanical switches which provides reactive power compensation in wind energy generation systems (Larsson, 2000;

Sugirtha and Latha, 2011). These problems can damage to sensitive electronic devices in control systems of wind systems (Sugirtha and Latha, 2011).

2.2.2. Frequency Variations

Frequency variation can be expressed as a change in fundamental frequency of the utility from its defined nominal value (50 or 60 Hz) and the steady-state power system frequency is directly related to the rotational speed of the generators on the system (IEEE, 2009; IEEE, 2014). The frequency variations affects the power generation, non-optimal tip speed ratio and aerodynamic efficiency in a wind system (Sugirtha and Latha, 2011; S.Tripathi, 2014). This condition causes less energy capture and lower power output for wind generation (S.Tripathi, 2014).

2.3. PQ Standards

The development of wind energy requires to improve the PQ issue. The international standards specify the characteristics of PQ issue in GCWESs. These standards are defined by working group of Technical Committee-88 of the International Electro-technical Commission (IEC) (Mohod and Aware, 2010). These standards consist of the following parts under the general titled as IEC-61400 (IEC, 2005; Yuvaraj et al., 2011):

- Part 1: Design requirements
- Part 2: Design requirements for small wind turbines
- Part 11: Acoustic noise measurement techniques
- Part 12: Wind turbine power performance testing
- Part 13: Measurement of mechanical loads
- Part 14: Declaration of apparent sound power level and tonality values
- Part 21: Measurement and assessment of PQ characteristics of GCWESs

- Part 23: Full-scale structural testing of rotor blades
- Part 24: Lightning protection

3. GCWES: OVERVIEW, DFIG AND CONTROL

This section introduces the installed global wind power in World and Turkey. Also, it explains the fundamentals, overview and properties of wind turbine systems. At the end of chapter, the functions and control of DFIG are explained in detailed.

3.1. Wind Energy

Wind energy industry has become one of the most important renewable energy sources with the development of technology and reduction of fossil fuels. The wind power capacity in world has installed up to 432.9 GW (2016) from nearly 47.3 GW (2004) (Blaabjerg and Chen, 2006; Steve Sawyer and Rave, 2016). Wind energy systems are being connected to the electrical systems, called as grid connected wind energy systems, are utilized to reduce the demand of utility-fed electricity for machines, illumination, heating and refreshment. Besides, it is expected to increase the electricity-generation vie wind power plants in most industrialized countries in following years (Fortman, 2015).

3.1.1. Wind Energy in World

According to the report of GWEC, the installed global power reached to 432.9 GW at the end of 2015 (Steve Sawyer and Rave, 2016). In global installed wind power capacities, Asia region has the highest share compared to other regions. The global installed wind power capacities of continental regions in world are presented in Table 3.1.

In world, cumulative capacities of top 10 countries are presented in Table 3.2. Among cumulative capacities of countries in world, PR Chine has 145.3 GW electrical generation and shares 33.6% for total wind energy.

Table 3.1 Global installed wind power capacities

Region	Installed Power (2015)	Percent
Africa & Middle East	3,489 GW	0.806 %
Asia	175,831 GW	40.618 %
Europe	147,771 GW	34.137 %
Latin America & Caribbean	12,220 GW	2.823 %
North America	88,749 GW	20.502 %
Pacific Region	4,823 GW	1.114 %
World Total	**432 GW 883 MW**	**100%**

Table 3.2 Cumulative capacities of top 10 countries in world

	Country	GW	Share %		Country	GW	Share %
1.	PR China	145,36	33.6	6.	UK	13,60	3.1
2.	USA	74,47	17.2	7.	Canada	11,20	2.6
3.	Germany	44,94	10.4	8.	France	10,35	2.4
4.	India	25,08	5.8	9.	Italy	8,95	2.1
5.	Spain	23,02	5.3	10.	Brazil	8,71	2.0
					Total Top 10	365731	84.5

3.1.2. Wind Energy in Turkey

The installed global wind power capacity in Europe is 147 GW 771 MW according the ratings of 2015. The list for top ten countries is presented in Table 3.3 for wind power generation. According to table, In Europe, Germany is known as country which has the highest power ratings generated wind power. It has an approximately 45 GW installed power capacity. Turkey has an approximately 4.7 GW installed wind power capacity.

Table 3.3 Cumulative capacities of top 10 countries in Europe

	Country	MW		Country	MW
1.	Germany	44947	6.	Sweden	6025
2.	Spain	23025	7.	Poland	5100
3.	UK	13603	8.	Portugal	5079
4.	France	10358	9.	Denmark	5063
5.	Italy	8958	10.	Turkey	4694

The percentage values of cumulative values generated in Europe is shown in Figure 3.1. As shown in Figure, Turkey meets 4% of total wind power in Europe.

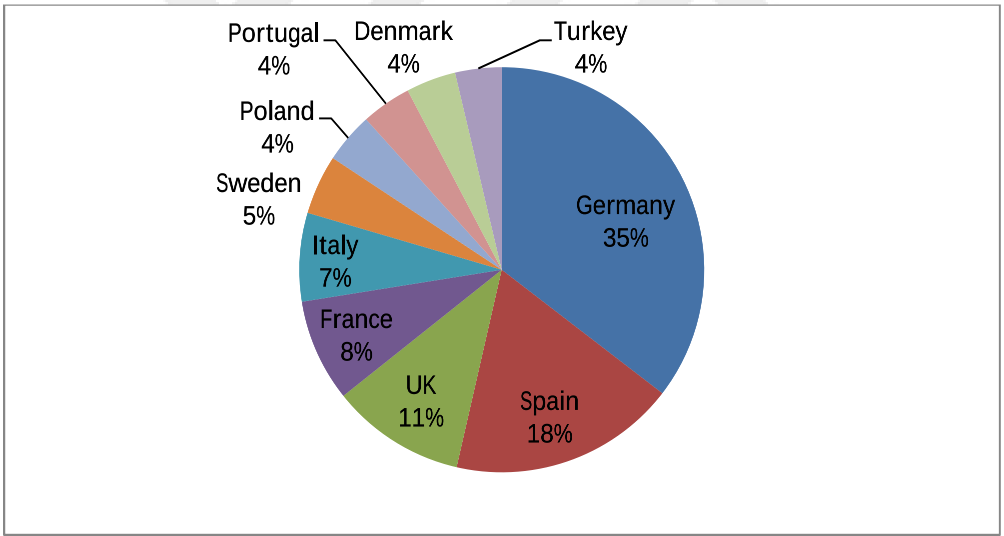

Figure 3.1 The percentage values of cumulative values in Europe (Steve Sawyer and Rave, 2016)

According to years, the installed power ratings in Turkey are presented in Figure 3.2. It shows a rapid increase from 2006 to 2015. The installed power increases from 51 MW to 4718 MW in this duration.

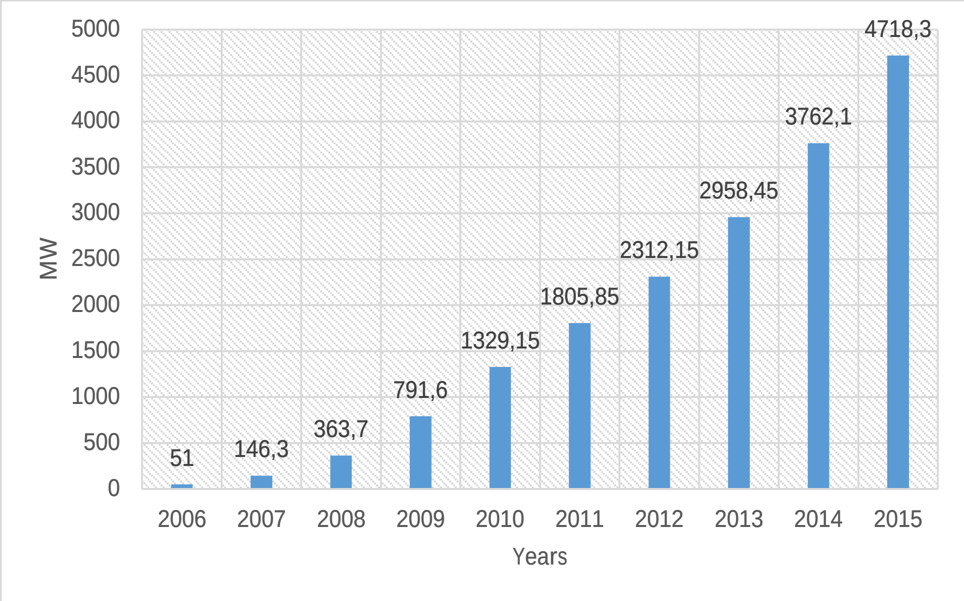

Figure 3.2 Cumulative wind power installations in Turkey (Konuray, 2016)

Figure 3.3 presents the installed power ratings according to regions in Turkey.

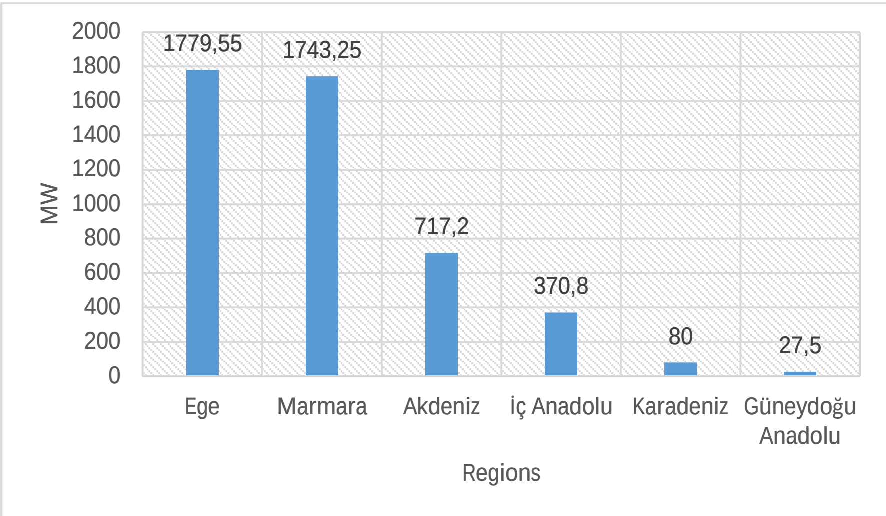

Figure 3.3 Regions according to operating wind power plants (Konuray, 2016)

According to cities of Turkey, the most installed wind power plants are located in Balıkesir. The power plants in Balıkesir generates nearly 923 MW. Figure 3.4 demonstrates the installed power ratings of top-18 cities in Turkey.

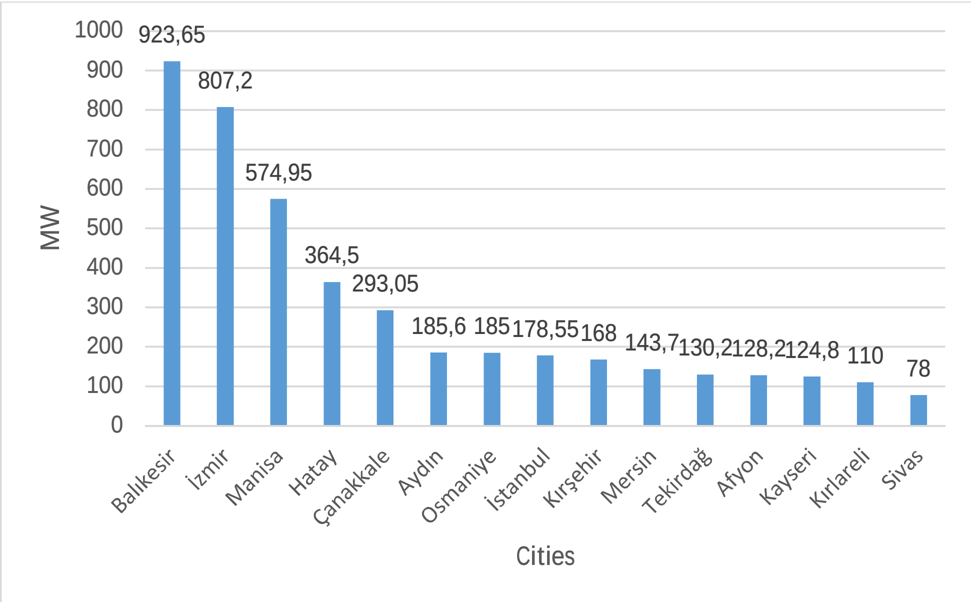

Figure 3.4 Cities according to operational power plants (Konuray, 2016)

3.2. Wind and Aerodynamic

In this part, wind modeling and aerodynamic model for a turbine system is introduced.

3.2.1. Wind Speed

In this section, the components and properties of a wind model are expressed. A wind speed consists of four main components (Koç, 2010). These components are called as:

- Fundamental wind velocity, $V_{w,\, fundamental}$ (m/s)
- Gust wind component, $V_{w,gust}$(m/s)
- Ramp wind component, $V_{w,ramp}$ (m/s)
- Noise wind component, $V_{w,noise}$ (m/s)

The total wind speed is written as the summation of four main components.

$$V_{wind} = V_{w,\, fundamental} + V_{w,gust} + V_{w,ramp} + V_{w,noise} \tag{3.1}$$

Fundamental wind velocity is a constant value which is essential for running of a wind system. In this study, fundamental wind velocity is assumed as input of wind turbine and gust, ramp and noise components don’t influence the analysis of proposed system.

3.2.2. Aerodynamic Model

In wind turbine systems, turbine rotor extracts the kinetic energy from the flow air in the wind and converts this energy into mechanical rotational energy (Koç, 2010). The power of the wind is expressed as (Chouhan, 2010):

$$P_{wind} = \frac{1}{2} \rho \pi r^2 V_{wind}^3 \tag{3.2}$$

Where, r is the radius of turbine blade and V_{wind} is speed of wind in m/s.

The mechanical power (P_{mech}) extracted from the wind power for a turbine system is a part of wind power which defined by Betz Constant (C_p). According to Betz theory, the maximum value is limited to 0.593 (Tao, 2004; Chandrasekaran, 2014).

$$C_p(\max) = 0.593 \tag{3.3}$$

$$P_{mech} = C_p P_{wind} = C_p \left(\frac{1}{2}\rho A V_{wind}^3\right) = \frac{1}{2}\rho R^2 V_{wind}^3 C_p(\lambda,\beta) \tag{3.4}$$

Where, R indicates the radius of a turbine blade in meters. V_{wind} is wind speed in m/sec and ρ is air density in kg/m3. C_p is a variable value and dependent to wind speed, rotational speed of turbine and turbine blade parameters (Koç, 2010). According to (8), C_p is calculated by using tip speed ratio (λ) and blade pitch angle (β in degrees) (Fortman, 2015).

$$C_p(\lambda,\beta) = c_1\left(\frac{c_2}{\lambda_i} - c_3\beta - c_4\beta^{c_5} - c_6\right)e^{-c_7/\lambda_i} \tag{3.5}$$

Where, c1, c2, c3, c4, c5, c6, c7, c8 and c9 are constant values characterized by turbine manufacturers (Koç, 2010). In C_p, λ_i is defined as (Fortman, 2015):

$$\lambda_i = \frac{1}{\dfrac{1}{\lambda + c_8\beta} + \dfrac{c_9}{\beta^3+1}} \tag{3.6}$$

In C_p function, tip speed ratio (λ) is expressed as (Jing, 2009; Tuscaloosa, 2009):

$$\lambda = \frac{\omega_{mech} R_{blade}}{V_{wind}} \tag{3.7}$$

Where, the mechanical angular velocity of turbine rotor is defined by ω_{mech} in rad/s. ω_{mech} is calculated by using n (rpm) in (3.8).

$$\omega_{mech} = \frac{2\pi n}{60} \tag{3.8}$$

The mechanical torque (T_{mech}) at rotor shaft is dependent to P_{mech} and w_{rotor} (Koç, 2010).

$$T_{mech} = \frac{P_{mech}}{w_{rotor}} \tag{3.9}$$

The maximum power is obtained with highest C_p value which is provided for optimum pitch angle and optimum tip speed ratio. 0° for pitch is optimum value for high wind speeds and transient conditions. Optimum tip speed ratio λ_{opt} is a proportion to obtain maximum amount power from the wind (Tao, 2004; Petersson, 2005; Chandrasekaran, 2014). The optimum rotor speed is:

$$\lambda_{opt} = \frac{w_{rotor,opt} \times r}{V_{wind}} \tag{3.10}$$

Where, r is rotor radius.

3.3. The Fundamentals and Main Components

In order to generate electricity through wind power plants, the fundamental components of wind system are a turbine rotor, gearbox (optional), generator, transformer and electronics converters (optional) (Blaabjerg and Chen, 2006), as shown in Figure 3.5.

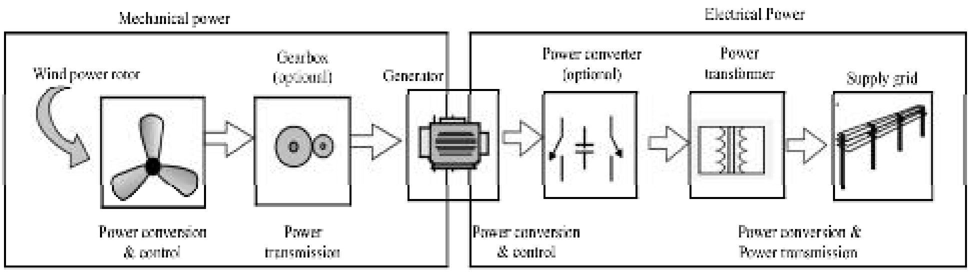

Figure 3.5 The main components of a wind turbine system (Blaabjerg and Chen, 2006).

In wind energy generation systems, wind power rotates the blades which consist of normally three blades, and it is converted to rotating mechanical power. The gearbox is optional and it is used to increase and stabilize the low speed of turbine rotor at generator-side. The generator transforms mechanical energy into electrical energy which supplies an electrical grid through power electronics converters and power transformers. In order to transform mechanical energy into electrical energy, both induction and synchronous generators are used in wind turbine systems. Induction generators are applied for both fixed-speed and variable-speed wind systems (Blaabjerg and Chen, 2006; Chen et al., 2009). Among wind energy generation systems, Doubly Fed Induction Generator is the most common type for wind farm applications because of its advantages such as variable speed operation, active/reactive power control and smaller rated power converters (Aga and Jadhav, 2013; Blaabjerg and Ma, 2013; Polinder et al., 2013).

3.4. The Classification of Wind Turbines

The classifications of wind turbines can be categorized according to speed control ability and concepts of power electronics converters.

3.4.1. Classification According to Speed Control

Wind turbines can be classified into two categories according to speed control ability. These are named as constant speed and variable speed wind turbines.

3.4.1.1. Constant speed

In the early 1990s, the most of installed wind turbines are operated at constant-speed (Hansen et al., 2004). This means that, the rotor speed of turbine is constant and defined by the grid-voltage frequency, gear ratio and generator design (Hansen et al., 2004; Ackermann, 2005). This type is designed to obtain maximum efficiency at specific wind speed (Blaabjerg and Chen, 2006). Constant speed wind turbines are based on squirrel cage induction generators and directly connected to grid with a soft starter and capacitor bank (Pan et al., 2013). The advantages of this type are simple, low-cost, robust and reliable (Ditkovich et al., 2012). The disadvantages are uncontrollable reactive power flow, mechanical stress and limited power quality control (Moursi et al., 2014). Due to constant speed operation, wind speed fluctuations create mechanical torque oscillations and electrical power fluctuations at grid-side (Ackermann, 2005).

3.4.1.2. Variable Speed

According to speed control ability, second type turbines are defined as variable speed. This type is designed to obtain maximum aerodynamic efficiency between a wide range of wind speeds (Hansen et al., 2004). These turbines continuously to adjust rotational speed (ω) of turbine at variable wind speeds

(Ackermann, 2005). For this purpose, tip speed ratio is kept constant at a defined value correspond to maximum power coefficient (Fortman, 2015). On the contrary of constant speed wind turbines, variable speed turbines keep the generator torque approximately constant.

Variable speed wind turbines are based on induction or synchronous generators. They are connected to grid via power electronics based converters. The speed of generator is controlled by power converters, thus, the power fluctuations are primarily eliminated by changes in the generator rotor speed (Fortman, 2015). These systems are more complex when compared to fixed speed wind systems (Blaabjerg and Chen, 2006). In this way, variable speed operation is performed via power electronics converters.

The advantages of these turbines can be explained as:

- Reduces the mechanical stress at the mechanical components (Hansen et al., 2004)
- Increases power capture capability (Hansen et al., 2004)
- Controls active reactive power flows (Ackermann, 2005)
- Fast response during transient situations (Sun et al., 2009)
- Improves power quality (Hansen et al., 2004; Sun et al., 2009)

The disadvantages of these turbines are more complex, more expensive and maintenance in comparison with constant speed turbines.

3.4.2. Classification According to Concepts of Power Converters

There are four types according to concepts of power converters in wind turbines. These are called as Type 1, Type 2, Type 3 and Type 4, as shown in Figure 3.6.

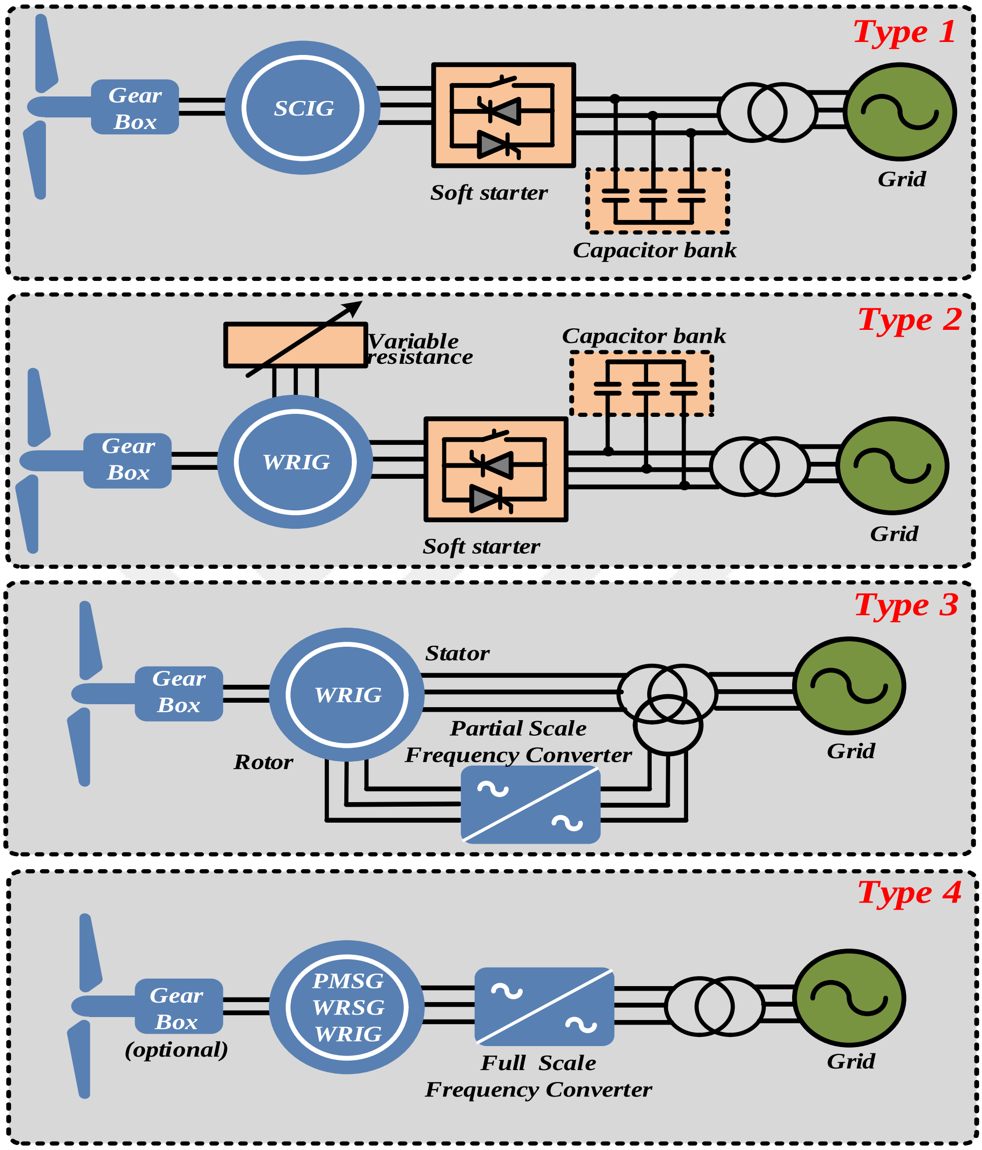

Figure 3.6 The classification of wind turbines according to concepts of power converters

3.4.2.1. Type 1

This type is known as constant speed wind turbine with asynchronous squirrel cage induction generators (SCIG) (Ackermann, 2005; Polinder et al., 2013). In this type, it is connected directly to grid without power electronic converters. SCIG continuously absorbs reactive power from grid (Fortman, 2015). In order to compensate partial reactive power, capacitor banks are used in Type 1 (Sun et al., 2009). Soft starter is used to improve grid connection and control startup (Blaabjerg and Chen, 2006).

3.4.2.2. Type 2

This structure achieves limited variable speed control for wind turbines with rotor resistance (Chaudhary et al., 2013). This type is based on wound rotor induction generator (WRIG) and directly tied to grid. A controlled resistance is connected in series to rotor winding which determine the range of variable speed. The range is typically between 0% and 10% for synchronous generators (Ackermann, 2005).

3.4.2.3. Type 3

This construction is known as doubly fed induction generator (DFIG) concept (Polinder et al., 2013; Fortman, 2015). In this concept, the stator of DFIG type wind turbine is directly tied to the grid, while the rotor is connected to grid via partially back-to-back converters called as Rotor Side Converter (RSC) and Grid Side Converter (GSC) which have partial rating (nearly 30%) of power generator by wind turbine (Blaabjerg and Chen, 2006; Sun et al., 2009). RSC is used to control active/reactive power and speed of machine under normal conditions, while GSC is used to keep dc-link voltage constant and reactive power exchange with the grid (Polinder et al., 2013).

3.4.2.4. Type 4

This structure allows to full variable speed control for wind systems (Ackermann, 2005; Kim and Lu, 2010). In this structure, the stator of generator is directly tied to grid via full –scale frequency converter (Ackermann, 2005). Wound rotor synchronous generator (WRSG) or WRIG or permanent magnet synchronous generator (PMSG) can be selected as generator in Type 4 (Hansen et al., 2004). Full scale frequency converter is used for reactive power compensation and smooth grid connection (Ackermann, 2005).

3.5. DFIG

Doubly fed induction generator is the most widely used generator type in wind energy systems. The following subjects about DFIG are clarified in this topic.

- The functions
- Equivalent circuit and mathematical modeling
- RSC and GSC control

3.5.1. The Functions

The schematic diagram of grid connected wind system based on DFIG is presented in Figure 3.7. It includes two converters called as rotor side converter (RSC) and grid side converter (GSC), respectively. These are linked back-to-back with common a dc-link capacitor. Basically, the stator of DFIG type wind turbine is directly tied to the grid, while the rotor is connected to grid via partially back-to-back converters called as Rotor Side Converter (RSC) and Grid Side Converter (GSC) which have partial rating (nearly 30%) of power generator by wind turbine. RSC is used to control active/reactive power and speed of machine under normal conditions, while GSC is used to keep dc-link voltage constant and reactive power exchange with the grid (Edrah et al., 2015; Karaipoom and Ngamroo, 2015; Xiong and Sun, 2016; Zhu et al., 2016).

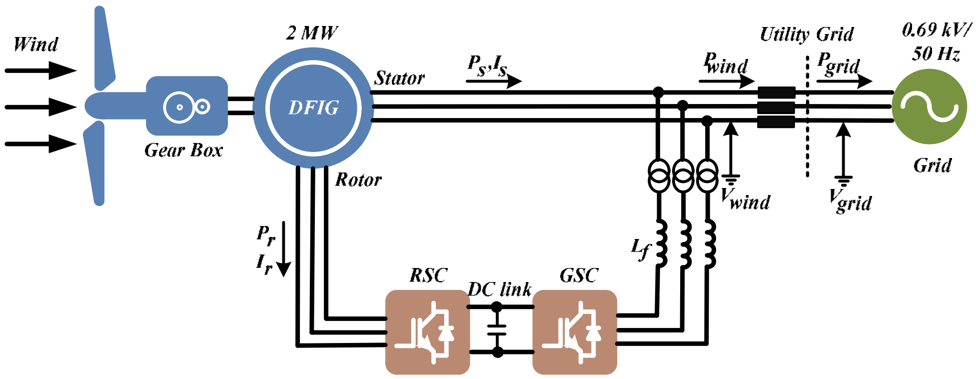

Figure 3.7 Grid connected wind energy system based on DFIG

3.5.2. Equivalent Circuit and Mathematical Modeling

The equivalent circuit of DFIG is illustrated in Figure 3.8.

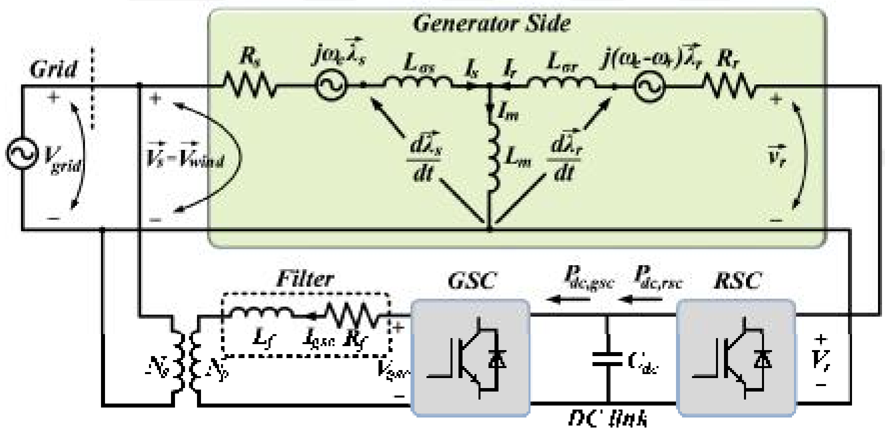

Figure 3.8 The equivalent circuit of grid connected wind energy system

$$\vec{V}_s = R_s \vec{i}_s + j\omega_e \vec{\lambda}_s + \frac{d\vec{\lambda}_s}{dt} \quad (3.11)$$

$$\vec{V}_r = R_r \vec{i}_r + j(\omega_e - \omega_r)\vec{\lambda}_r + \frac{d\vec{\lambda}_r}{dt} \quad (3.12)$$

$$\lambda_s = L_s \vec{i}_s + L_m \vec{i}_r \qquad (3.13)$$

$$\lambda_r = L_r \vec{i}_r + L_m \vec{i}_s \qquad (3.14)$$

In (3.11)-(3.14), $\vec{\lambda}$, $\vec{v}$ and $\vec{i}$ indicates flux, voltage and current in equivalent circuit of DFIG . $L_s = L_{\sigma s} + L_m$ and $L_r = L_{\sigma r} + L_m$ formulate the inductances of stator and rotor, respectively (Fortman, 2015). Also, electrical stator angular velocity is defined as $\omega_e = \omega_s$. L_m , R_s and R_r are symbols of mutual inductance, stator resistance and rotor resistance (Wessels et al., 2011; Almoataz Y. Abdelaziz, 2013).

Total power of a grid connected DFIG are dependent to phase current flowing in all three phases.

$$P_{wind} = Re\left(V_a i_a^* + V_b i_b^* + V_c i_c^*\right) \qquad (3.15)$$

$$Q_{wind} = Im\left(V_a i_a^* + V_b i_b^* + V_c i_c^*\right) \qquad (3.16)$$

The control of real and reactive power is performed in dq frame rather than phase frame.

$$P_{wind} = P_s + P_r = \frac{3}{2}\left(V_{d,s} i_{d,s} + V_{q,s} i_{q,s}\right) + \frac{3}{2}\left(V_{d,r} i_{d,r} + V_{q,r} i_{q,r}\right) \qquad (3.17)$$

$$Q_{wind} == Q_s + Q_r = \frac{3}{2}\left(V_{q,s} i_{d,s} - V_{d,s} i_{q,s}\right) + \frac{3}{2}\left(V_{q,s} i_{d,r} - V_{d,s} i_{q,r}\right) \qquad (3.18)$$

In order to control the real and reactive power, independent control must be provided for (3.17) and (3.18). It can be observed in (3.17-18), P and Q can be independent if Vd or Vq is zero. According to Clarke's transformation, three phase signals are converted to dq components. In order to realize this process, three phase signals are first converted to αβ components. After this process, αβ components are transformed to dq components. Figure 3.9 presents vector diagram for stator voltage oriented control in dq frame.

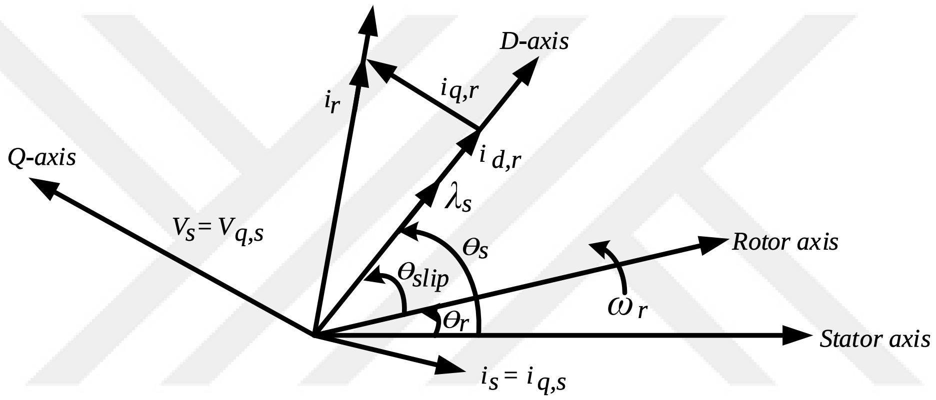

Figure 3.9. Transfomation from phase frame to dq frame (Aggarwal Archna et al., 2014)

3.5.3. Rotor Side Converter (RSC) Control

The controller of stator real power and stator reactive power flow is realized by using the control of rotor side converter (RSC) in DFIG based wind systems. The relation of real and reactive power between stator and grid side is defined as:

$$P_s = \frac{3}{2}(V_{d,s} i_{d,s} + V_{q,s} i_{q,s}) \tag{3.19}$$

$$Q_s = \frac{3}{2}(V_{q,s}i_{d,s} - V_{d,s}i_{q,s}) \tag{3.20}$$

It is clear from (3.19) and (3.20) that the real and reactive power flows cannot be controlled independently using the d and q axis currents. Thus, the rotor side converter is controlled in the stator flux oriented reference frame in order to decouple the control of real and reactive power flows associated with the stator (Saraf, 2012).

In order to achieve a decouple control of active and reactive power, stator flux oriented vector control scheme is adopted. Based on the previous research the following assumptions are considered (Md. ARIFUJJAMAN et al., 2009):

- Stator voltage drop across resistance has been neglected as the effect of stator resistance is quite low compared to the grid voltage (Mohamed et al., 2004).
- The DFIG is connected to a stiff grid, i.e., the frequency and amplitude of the stator or grid voltage is assumed constant (He et al., 2005).
- Magnetizing current of the stator is assumed to be determined by the grid (He et al., 2005).
- The q-axis is 90^o ahead of the d-axis and rotating at synchronous speed in the direction of rotation (Holdsworth et al., 2003).
- The stator flux vector is aligned with the d-axis of the stator (Holdsworth et al., 2003).

$$I_{d,s} = I_s \tag{3.21}$$

$$I_{q,s} = 0 \tag{3.22}$$

By ignoring the resistance of windings,

$$V_{d,s} = 0 \tag{3.23}$$

$$V_{q,s} = V_s \tag{3.24}$$

Readjusting the (3.19) and (3.20) by using (3.23) and (3.24), the new values of P_s and Q_s are:

$$P_s = \frac{3}{2} V_{q,s} i_{q,s} = \frac{3}{2} V_s i_{q,s} \tag{3.25}$$

$$Q_s = \frac{3}{2} V_{q,s} i_{d,s} = \frac{3}{2} V_s i_{d,s} \tag{3.26}$$

Since the stator active and reactive powers have to be controlled using the rotor currents, the above relationships have to be modified to include rotor d and q axes currents in the active and reactive power relationships (Koç, 2010; Saraf, 2012; Shafiei, 2012).

The flux linkages for d and q components are given in (3.27) and (3.28).

$$\lambda_{d,s} = L_s i_{d,s} + L_m i_{d,r} \tag{3.27}$$

$$\lambda_{q,s} = L_s i_{q,s} + L_m i_{q,r} \tag{3.28}$$

In the stator flux oriented frame, $i_{d,s}$ and $i_{q,s}$ be expressed in terms of $i_{d,r}$ and $i_{q,r}$, respectively as:

$$i_{d,s} = \frac{\lambda_{d,s} - L_m i_{d,r}}{L_s} \tag{3.29}$$

$$i_{q,s} = -\frac{L_m}{L_s} i_{q,r} \tag{3.30}$$

In the stator flux oriented frame, the d - axis stator flux is constant and equal to λ_s. By using (3.29) and (3.30), the real and reactive power flows are extracted in (3.31) and (3.32) due to stator voltage and rotor currents in dq components (Pena et al., 1996).

$$P_s = \frac{3}{2} V_s \left[-\frac{L_m}{L_s} i_{q,r} \right] = -\frac{3}{2} \frac{L_m}{L_s} V_s i_{q,r} \tag{3.31}$$

$$Q_s = \frac{3}{2} V_s i_{d,s} = \frac{3}{2} V_s \frac{(\lambda_{d,s} - L_m i_{d,r})}{L_s} \tag{3.32}$$

According to (3.31) and (3.32), power flows in RSC can be controlled by using d and q components of rotor current. The controller scheme of RSC is illustrated in Figure 3.10. According to controller scheme, instantaneous real and reactive powers of stator is calculated and subtracted from reference signals. By using PI controllers, $i^*_{d,r}$ and $i^*_{q,r}$ are generated and these signals are converted into phase reference rotor currents ($i^*_{r,n}$) via inverse dq transform at θ_{slip}. The difference between actual rotor and reference rotor currents are used in hysteresis band to generate gate signals in RSC (Shafiei, 2012). This method is also called as current reference pwm method.

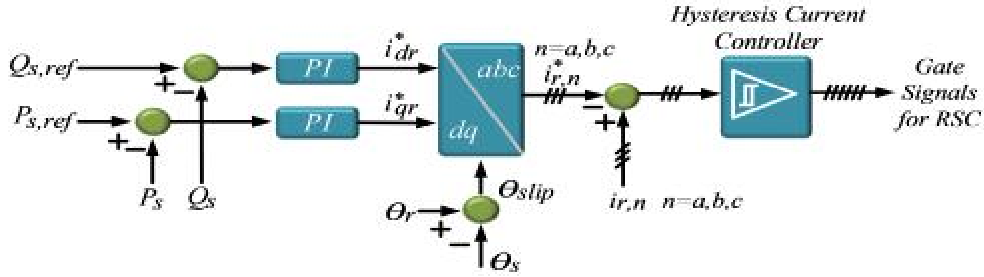

Figure 3.10 Vector control based RSC control

In controller, θ_r and θ_s indicate rotor angular position and the angle of stator flux, respectively. The stator flux angle is calculated as (Tao, 2004; Romlie, 2014):

$$\frac{d}{dt}\lambda_{\alpha,\beta s} = V_{\alpha,\beta s} - r_s i_{\alpha,\beta s} \tag{3.33}$$

$$\lambda_{\alpha,\beta s} = \int (V_{\alpha,\beta s} - r_s i_{\alpha,\beta s})dt \tag{3.34}$$

$$\phi_s = \tan^{-1}(\frac{\lambda_{\beta s}}{\lambda_{\alpha s}}) \tag{3.35}$$

3.5.4. Grid-Side Converter (GSC) Control

Grid-side converter (GSC) is used to stabilize DC link capacitor voltage constant and control the reactive power flow between GSC and grid. The value of reactive power is adjusted to zero in order to maintain zero reactive power flow between grid and GSC. In grid side control, d-component is oriented in dq frame to control dc link voltage and power flow.

$$V_{d,s} = V_s \tag{3.36}$$

$$V_{q,s} = 0 \tag{3.37}$$

Therefore, the grid side power magnitudes in dq frame are:

$$P_{gsc} = \frac{3}{2}\left(V_{d,s}i_{d,gsc} + V_{q,s}i_{q,gsc}\right) = \frac{3}{2}V_{d,s}i_{d,gsc} \tag{3.38}$$

$$Q_{gsc} = \frac{3}{2}\left(V_{q,s}i_{d,gsc} - V_{d,s}i_{q,gsc}\right) = -\frac{3}{2}V_{d,s}i_{q,gsc} \tag{3.39}$$

According to (3.38) and (3.39), the real power is controlled by using only d component of grid current, and q component of grid current is applied in reactive power control between GSC and grid (Aggarwal Archna et al., 2014).

The scheme of equivalent circuit between GSC and grid is presented in Figure 3.11.

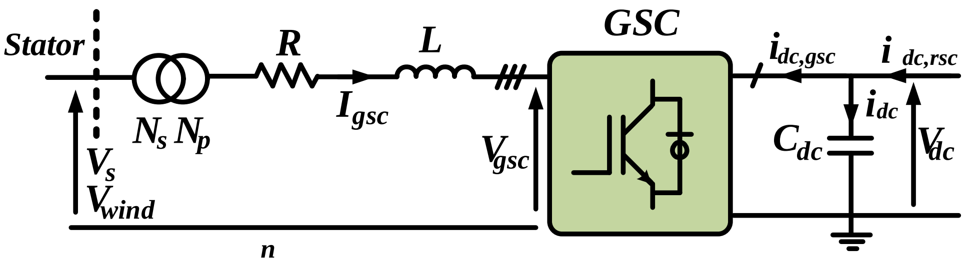

Figure 3.11 The connection of GSC to stator

Using circuit theory for Ns=Np:

$$V_s = Ri_{gsc} + L\frac{di_{gsc}}{dt} + V_{gsc} \tag{3.40}$$

According to relationship of GSC and grid, grid side voltages are rewritten in dq frame with a frequency w_e (Romlie, 2014).

$$V_{d,s} = Ri_{d,gsc} + L\frac{di_{d,gsc}}{dt} - w_e L i_{q,gsc} + V_{d,gsc} \tag{3.41}$$

$$V_{q,s} = Ri_{q,gsc} + L\frac{di_{q,gsc}}{dt} + w_e L i_{q,gsc} + V_{q,gsc} \tag{3.42}$$

The switching signals can be generated due to grid side converter voltage. In dq frame, $v_{d,gsc}$ and $v_{q,gsc}$ are dependent to both d and q components of grid current. This condition makes the controllability difficult and complex (Pena et al., 1996). In order to simplify the equivalents, $V'_{d,gsc}$ and $V'_{q,gsc}$ are defined as:

$$V'_{d,gsc} = Ri_{d,gsc} + L\frac{di_{d,gsc}}{dt} \tag{3.43}$$

$$V'_{q,gsc} = Ri_{q,gsc} + L\frac{di_{q,gsc}}{dt} \tag{3.44}$$

By substituting:

$$V^*_{d,gsc} = -V'_{d,gsc} + w_e L i_{q,gsc} + V_{d,s} \tag{3.45}$$

$$V^*_{q,gsc} = -V'_{q,gsc} - w_e L i_{q,gsc} + V_{q,s} \tag{3.46}$$

$V^*_{d,gsc}$ and $V^*_{q,gsc}$ indicates the reference GSC voltages in dq frame. It means that the transfer function between current and voltage is (Romlie, 2014):

$$\frac{i_{d,gsc}(s)}{V'_{d,gsc}(s)} = \frac{i_{q,gsc}(s)}{V'_{q,gsc}(s)} = \frac{1}{Ls+R} \tag{3.47}$$

It expresses that PI controllers are used in linear plant defined by (3.47) shown in Figure 3.12.

For three phase system, the relationship of power of dc link capacitor and grid is defined as (Romlie, 2014):

$$V_{dc} i_{dc,gsc} = \frac{3}{2} V_{d,s} i_{d,gsc} \tag{3.48}$$

$$V_{d,gsc} = \frac{m}{2} V_{dc} \tag{3.49}$$

$$i_{dc,gsc} = \frac{3}{4} m i_{d,s} \tag{3.50}$$

$$C \frac{dV_{dc}}{dt} = i_{dc,gsc} - i_{dc,rsc} \tag{3.51}$$

Where, m is modulation index of inverter in GSC.

DC link control is realized in continuous domain and assume that for ideal case $i_{dc,rsc} = 0$, the effective transfer function is (Tao, 2004; Romlie, 2014) :

$$\frac{V_{dc}(s)}{i_{d,gsc}(s)} = \frac{3m}{4Cs} \tag{3.52}$$

In control, d component of GSC current ($i_{d,gsc}$) controls the dc link voltage. In addition, reactive power is controlled by using q component of GSC current ($i_{q,gsc}$) (Aggarwal Archna et al., 2014). Also, reference of reactive power is adjusted to zero for providing unity power factor.

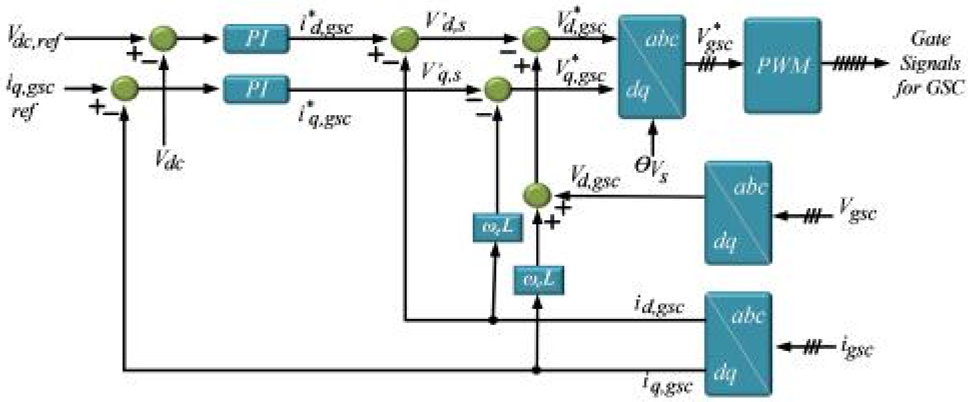

Figure 3.12 Vector control based GSC controller

4. DVR FOR FAULT RIDE-THROUGH

Voltage dip/swell and harmonics are defined as the most hazardous disturbances in distribution systems. These disturbances cause several serious problems such as equipment failure and economical loss in critical loads. Voltage disturbances can disturb the operation of sensitive loads like regulation devices, computer hardwares and monitoring devices. To compensate these voltage quality problems, inverter based Custom Power Devices (CPDs) are applied in distribution systems, where Series Active Power Filter, Dynamic Voltage Restorer (DVR) and Static Compensator (Statcom) are the most widespread used CPDs. DVR is the most effective inverter based device which eliminates voltage disturbances among CPDs.

4.1. Fault Ride Through (FRT) Capability

In grid connected wind energy systems, there are two different fault ride through capabilities. These are known as:

- Low-Voltage Ride Through (LVRT) Capability
- High-Voltage Ride Through (HVRT) Capability

4.1.1. Low Voltage Ride Through

Voltage problems at grid-side significantly affect power system stability of wind energy systems during the interaction with grid. Voltage dips, swells and harmonics are the most significant issues which affects energy quality in grid connected wind systems (Kyaw and Ramachandaramurthy, 2011; Sugirtha and Latha, 2011; Tourou and Sourkounis, 2014). Voltage dips (sags) are known as voltage variations which cause power losses resulting in damage of power equipments. Furthermore, generator current and electrical torque reaches to higher values by losing voltage stability (Hansen and Michalke, 2007; Chouhan, 2010). After occurrence of grid faults, wind turbines are required to remain grid connected during voltage variations and to prevent high stator/rotor currents and power losses without losing the voltage stability of turbine (Mohammadpour et al., 2015). This condition is defined as low voltage ride through (LVRT) capability.

4.1.2. High Voltage Ride Through

Voltage swell at grid-side causes a transient dc flux component on doubly fed induction generator (DFIG) stator winding even stronger than grid voltage dip, resulting in a much more serious stator, rotor current, and torque oscillation (Xie et al., 2015). Also, swells may lead to the reversal of the power flow in the back-back converter, and current may flow from the grid into the DC-link which results voltage rise in dc link voltage (Feltes et al., 2008). In electrical networks, high voltage ride through (HVRT) is defined as the capability to stay connected in short durations of voltage swells in order to prevent the negative effects (Boukhris et al., 2015; Xie et al., 2015).

4.2. FRT Requirements

Wind energy generation systems have to fulfill international standards and grid codes to be connected to the energy network (Wessels et al., 2010). Grid codes for wind turbines cover the steady-state and transient state operation as well as the communication and power dispatch (Wessels et al., 2010). The main dynamic requirements concern the FRT capability of wind turbines. Transmission system operators have specified their recent requirements, so that wind turbines must offer ride through capability from the grid turbines have to stay connected and supply reactive power to the grid continuously to support the voltage level (Abbey et al., 2006; Shin et al., 2011). LVRT requirement from the german transmission code is introduced in Figure 4.1 (Wessels et al., 2010).

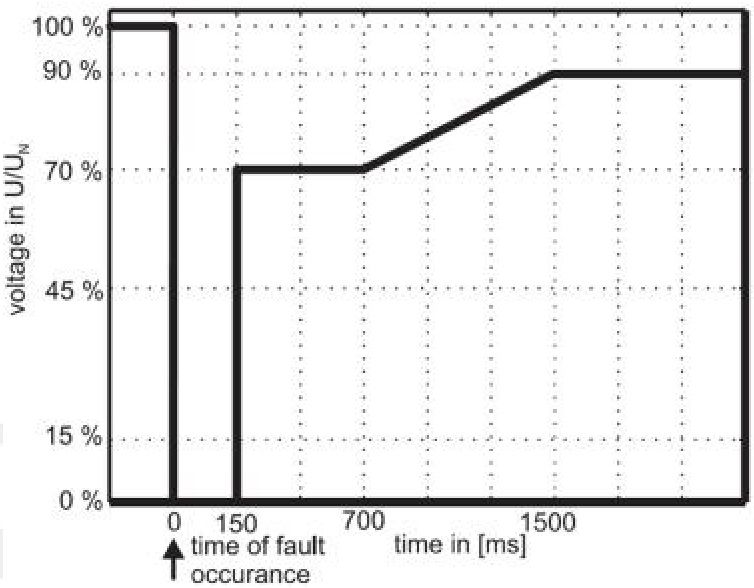

Figure 4.1 LVRT requirement in german VDN transmission code T11-8 (Wessels et al., 2010)

The International Electro-technical Commission (IEC) developed and released the IEC standard 61400-21 for testing and accessing power quality characteristics of grid-connected wind energy converters (Emanuel et al., 2009). The standards specifiy the measurement of the turbine electrical behavior under symmetrical/asymmetrical voltage dips of different amplitudes (90%, 50% and 20%) and duration (200 ms to 500 ms) (Wessels et al., 2010).

The effects of grid voltage swell on wind turbine and corresponding high-voltage ride-through (HVRT) strategy have not been given sufficient attention (Xie et al., 2015). HVRT capabilities are expected to gradually become a requirement for wind farms with the continuous improvement of wind power capacity and grid connection standards (Boukhris et al., 2015). Australia initially formulated the HVRT guideline for grid-connection wind turbines [12]. In the HVRT guideline, when the grid voltage swells to 1.3pu, the wind turbine should stay connected for 60ms to provide reactive recovery current as shown in Figure 4.2 (Boukhris et al., 2015; Xie et al., 2015).

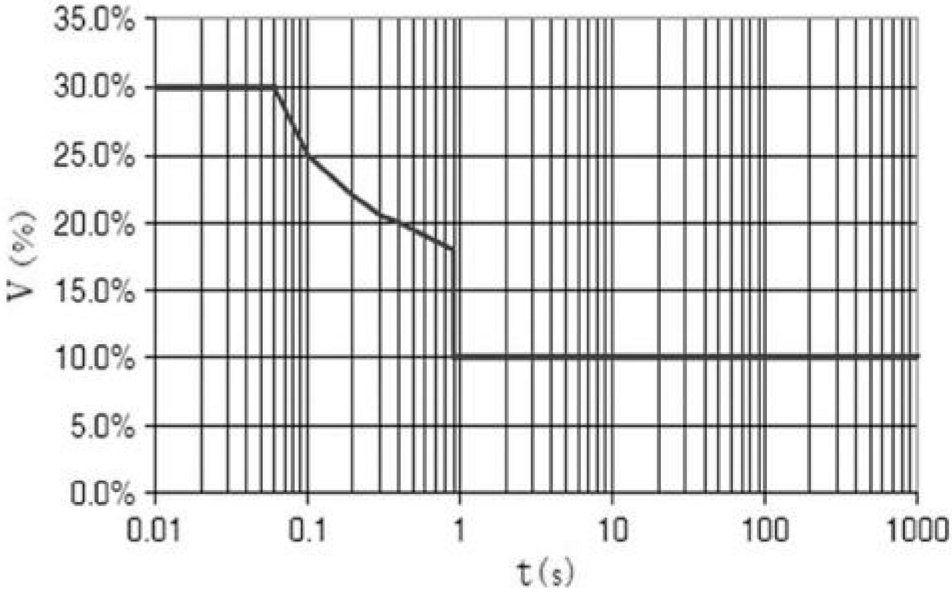

Figure 4.2 HVRT requirements (Xie et al., 2015)

4.3. DVR for FRT Capability

In this section, the most popular solutions for FRT capability and the advantages/disadvantages of solution techniques are given. Also, conventional DVR based systems and capabilities of DVRs in wind systems are explained in this part.

4.3.1. DVR vs Statcom & Crowbar for FRT

Voltage variations on grid-side voltage such as balanced/unbalanced faults cause high stator currents due to the direct connection of stator to the grid. Because of magnetic coupling between stator and rotor, high transient currents occur in rotor-side of system. The DFIG does have the disadvantage of a direct grid connection so that voltage dips on the grid can cause significant flux transients and high rotor current to flow (Romlie, 2014). High transient currents damage solid-state devices and increase dc-link voltage of back-to-back converters in DFIG. To prevent these harmful conditions under unstable conditions, protection devices are applied in grid connected wind energy systems to support LVRT. The most popular solutions for DFIG are crowbar (Pannell et al., 2010; Chen et al., 2016; Wenjie et al., 2016), STATCOM (Qiao et al., 2009; Wang and Truong, 2013), and Dynamic Voltage Restorer (DVR) (Ibrahim et al., 2011; Wessels et al., 2011; Alaraifi et al., 2013). Among these topologies, crowbar is a resistive network which is connected to rotor winding in DFIG. In fault conditions, crowbar is short-circuited and DFIG behaves like an induction generator. But, high short current flows when the crowbar is active. In this situation, it absorbs a large amount of reactive power from grid, which is not applicable for grid code requirements (Ibrahim et al., 2011). Other methods called as STATCOM and DVR are power electronics based devices to support reactive power at point common of coupling. DVR injects less reactive current to provide voltage stability compared with STATCOM.

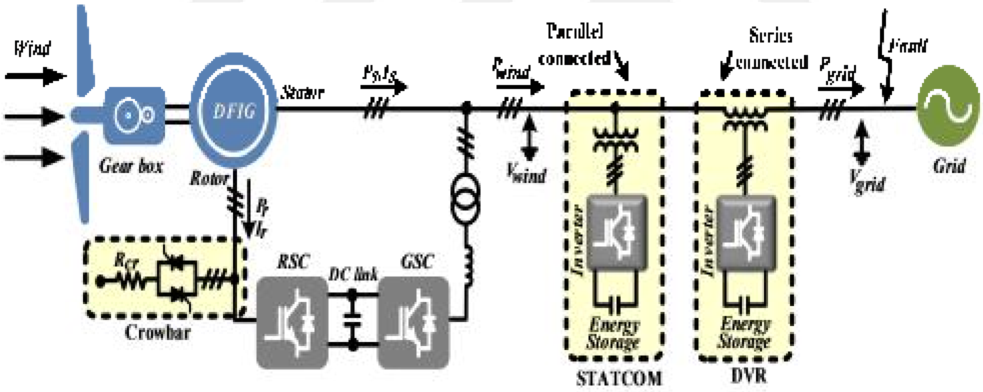

Figure 4.3 The locations and structures of crowbar, statcom and dvr in grid connected DFIG wind systems

4.3.2. Advantages/Disadvantages of Crowbar, Statcom and DVR

Table 4.1 provides a brief comparison of the advantages and disadvantages of each technique. The system properties and functional capabilities show that DVR is a very effective solution to provide voltage stability during voltage dip situations.

Table 4.1 Comparison of Crowbar, Statcom and DVR

Type	Advantage	Disadvantage
Crowbar	*Decrease rotor over current, dc-link over voltage and torque oscillations *Simple *Low-cost	*During faults, DFIG behaves like an IG. It reduces the power rating generated system. *High short currents when the crowbar is active. *Absorption of large amount of reactive power from grid
STATCOM	* Reactive Power Support * Voltage Stability Improvement * Phase Jump Compensation	*Large Current Injection to Compensate Voltage Disturbances *Complex * More Expensive
DVR	*Small Current Injection for compensation * Voltage Stability Improvement * Phase Jump Compensation *Active/Reactive Power Control *Voltage Controlled	*Complex * Expensive than crowbar

4.3.3. Conventional DVR Based Systems

DVR is located in series between wind turbine and electrical grid (Gkavanoudis and Demoulias, 2015). A conventional DVR consists of an inverter, filter, energy storage unit and a series transformer (Leon et al., 2011). Inverter generates controlled voltage from energy storage unit to compensate voltage dips occurred at grid-side. Then, generated voltage is filtered through LC filter (Guo and Liu, 2011), and injected to system via series transformer (İnci et al., 2016).

4.3.4. Capabilities of DVRs in Wind Systems

This paper investigates DVR based on grid connected wind turbine to fulfill simultaneous FRT capability and harmonics compensation. Traditional DVRs used with GCWS are used to compensation for only voltage dips or unbalances during symmetrical and/or asymmetrical grid faults in (Flannery and Venkataramanan, 2009; Abdel-Baqi and Nasiri, 2011; Ibrahim et al., 2011; Leon et al., 2011; Ramirez et al., 2011; Wessels et al., 2011; Zhang et al., 2012; Alaraifi et al., 2013; Amutha and Kumar, 2013; Yao et al., 2013; Chen and Wang, 2014; Gkavanoudis and Demoulias, 2015) . The compensation capabilities of the systems are introduced in Table 4.2. However, voltage harmonics cause overheating of transformers and generators, losses in transmission lines/cables in GCWES. In traditional DVR based systems, only voltage dips are compensated in (Flannery and Venkataramanan, 2009; Abdel-Baqi and Nasiri, 2011; Ibrahim et al., 2011; Ramirez et al., 2011; Wessels et al., 2011; Zhang et al., 2012; Alaraifi et al., 2013; Amutha and Kumar, 2013; Chen and Wang, 2014; Gkavanoudis and Demoulias, 2015) for FRT. Compensation of only voltage unbalances is performed in (Leon et al., 2011) and (Yao et al., 2013) in order to prevent negative sequence currents in electrical machines which cause unequal overheating and torque in stator windings of generator.

Table 4.2 Generator types, properties and compensation capabilities of DVR connected wind energy generation systems in studies

Reference	Type	P, V/f	Functions
(Ibrahim et al., 2011) (Wessels et al., 2011) (Ramirez et al., 2011)	DFIG	2 MW 0.69 kV/60Hz	LVRT
(Leon et al., 2011)	SCIG	24 MW 0.69 kV/50 Hz	Voltage Unbalances
(Zhang et al., 2012)	DFIG	1.5 MW 0.575 kV/50 Hz	LVRT
(Amutha and Kumar, 2013)	SCIG	- -/50Hz	LVRT
(Alaraifi et al., 2013) (Hussein and Ali, 2016)	DFIG	1.5 MVA 0.575 kV/ 60 Hz	LVRT
(Sivasankar and Kumar, 2014)	IG	3 MVA 0.69 kV/ 50 Hz	LVRT
(Gkavanoudis and Demoulias, 2015)	DFIG	25 kVA 0.4 kV/50 Hz	LVRT
(Jiang et al., 2016)	SCIG	2 MW 0.4 kV/50 Hz	LVRT
(Zhu et al., 2016)	DFIG	2 MW 380 V/50 Hz	LVRT

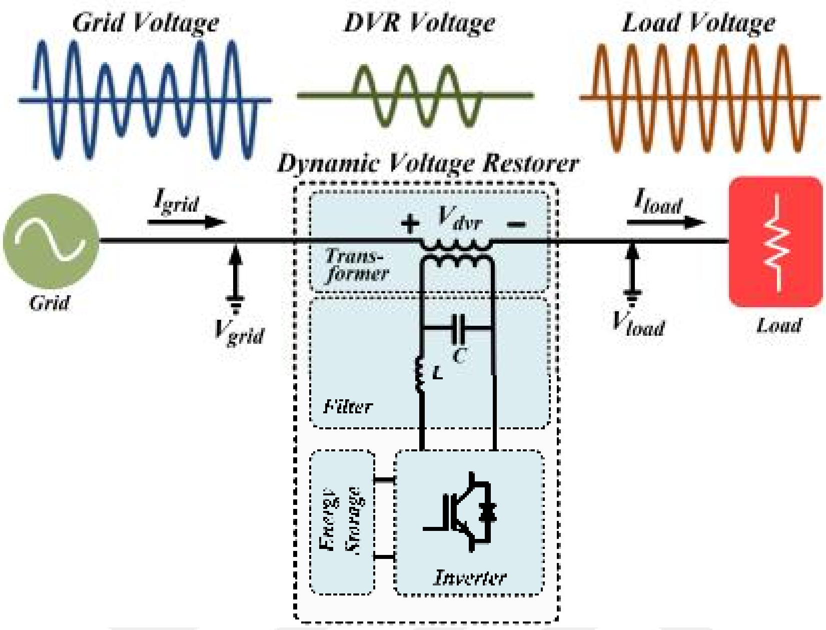

Figure 4.4 Conventional DVR

4.4. DVR Structure

A conventional DVR system consists of

- an inverter
- injection transformer
- energy storage unit
- output filter

4.4.1. Inverter Topologies

Inverter is one of the most important components in dynamic voltage restorer. Inverter generates controlled voltage to compensate voltage sag/swell and harmonics. There are several inverter topologies to compensate voltage problems in DVR systems.

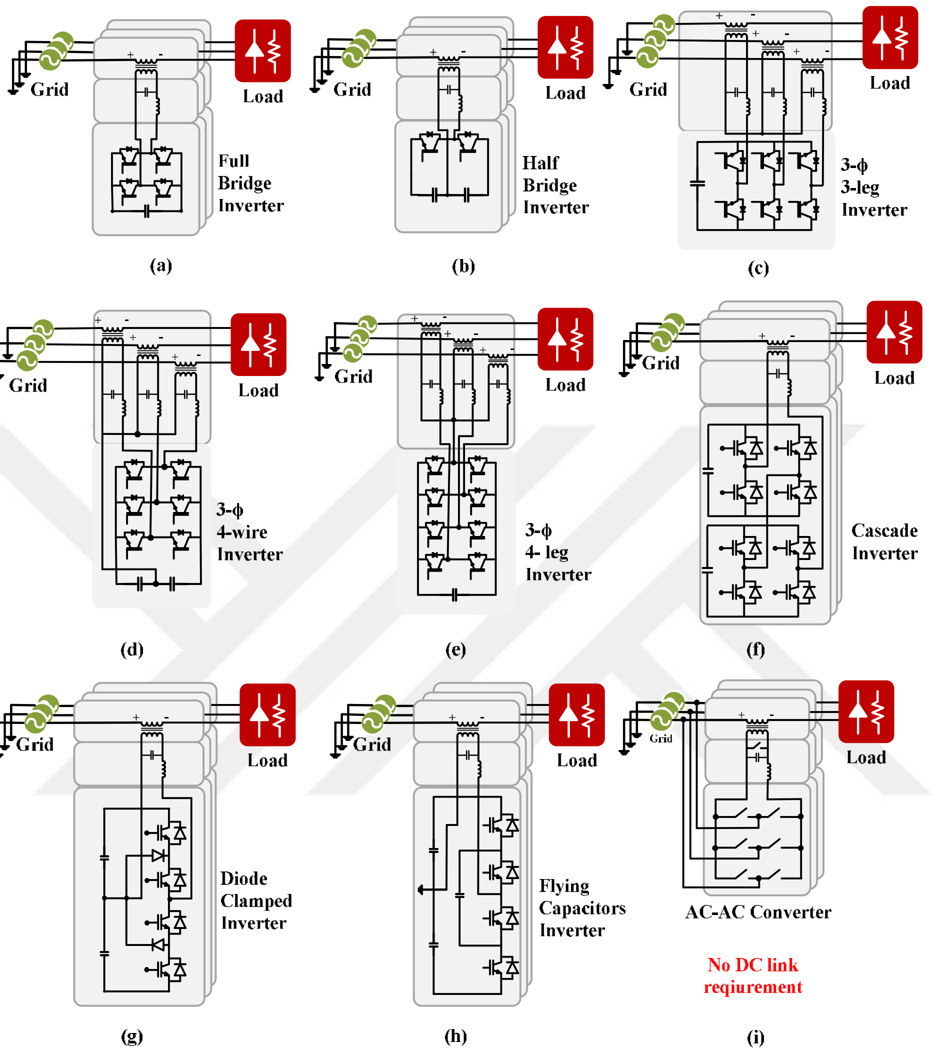

Figure 4.5 The most common converter topologies used in dynamic voltage restorers

The most common inverter topology is known as three phase three wire inverters (Zhan et al., 2001; Vilathgamuwa et al., 2006; Shi et al., 2010; Islam and Pota, 2013; Rauf and Khadkikar, 2015). These inverters are used to compensate only balanced problems. In order to eliminate the disadvantages of three phase three wire inverters, there are generally two alternative types: split-capacitor and four leg inverters. In split capacitor inverter based DVRs, the neutral point is connected directly to the midpoint of the dc link capacitors. In Figure 4.5, the neutral of the injection transformer is connected with the inverter ground in order to provide a zero-sequence current path for a system to operate under unbalanced conditions (Vilathgamuwa et al., 2002; Li et al., 2007; Omar and Rahim, 2012). The four leg topology which requires additional power switches (Naidu and Fernandes, 2009; Ebrahimzadeh et al., 2015), also needs a more complex control strategy compared to split capacitor inverters. But it provides several advantages such as a reduction of neutral currents and the possibility of neutral point voltage control. In both single phase systems and three phase balanced/unbalanced systems, H-bridge (Newman et al., 2003; Ghosh et al., 2004; Li et al., 2006; Ramasamy and Thangavel, 2012; Gonzalez et al., 2014) and half-bridge (Silva et al., 2005; Ho and Chung, 2010) inverters are used to generate pwm signals for DVRs. Two-level voltage source inverters are inadequate for high power applications due to their voltage rating. Multilevel inverters allow high voltage levels instead of these inverters. The most popular topologies among multilevel inverters implemented in DVR are Cascade (Wang et al., 2006; Al-Hadidi et al., 2008; Al-Hadidi et al., 2008; Massoud et al., 2010; Marei et al., 2012; Babaei et al., 2014), Diode Clamped (Barros and Silva, 2010; Leon et al., 2011; Bhumkittipich et al., 2013) and Flying Capacitors (Roncero-Sanchez and Acha, 2009). Recently, AC-AC converters which don't need an energy storage unit, are alternative topologies to compensate voltage disturbances in utility systems instead of inverters (Sree and Mohan, 2000; Sree and Mohan, 2000; Wang and Venkataramanan, 2009; Babaei et al., 2010; Babaei et al., 2010; Babaei and Kangarlu, 2011; Babaei and Kangarlu, 2012).

4.4.2. Energy Storage Components

Conventional DVRs stand an energy storage unit which supplies active power for compensation of voltage dips and harmonics. The voltage of energy storage unit is in dc form, and inverter converts this energy into ac form. The most used energy storage units are lead-acid batteries (Zhan et al., 2003), capacitors (Li et al., 2002; Ghosh et al., 2004), super capacitors (Omar and Rahim, 2012), flywheels (Wang and Venkataramanan, 2009), superconducting magnetic energy storage (SMES) (Shi et al., 2010).

4.4.3. Output Filter

Solid-state devices are implemented in different areas with nonlinear loads. The nonlinear characteristics of these switching devices cause distorted voltage waveforms with high-order harmonics. In order to mitigate the high order harmonics of switching, LC filters are commonly used in DVR structures (Choi et al., 2000). These filters also have following issues:

- The first is parameter design of components in LC filter. The filter is designed to prevent the passing of high frequency harmonics, and voltage drop should be fairly small on filter. Also, inductance value should be as small as possible for low-cost (Guo and Liu, 2011).
- Another important issue for LC filter is the resonance problem. In resonance condition, the control system may have transient distortions and affect the overall system stability (Li, 2009).

4.4.4. Injection Transformer

The injection or series transformers are located in series to inject controlled voltages to system. The power rating of injection transformer is adjusted to compensation level of voltage dip/swell. The main functions of series transformer are explained as:

- It also provides electrical isolation (Li et al., 2007).
- It reduces the voltage magnitude at input of inverter (Perera et al., 2006).
- It can also achieve to prevent noise and transients from the primary side to secondary side (Zhan et al., 2001).

5. THE PROPOSED SYSTEM AND CONTROL

In this chapter, the modeled system topologies called as Topology I and Topology II, power flow in DVR tied GCWES, design of DVR and proposed reference generation methods for multifunctional compensation are explained. Proposed study is briefly explained in the following topics.

- In this section, two DVR topologies called as Topology I and Topology II are presented. Topology I ensures dc energy from a battery. In Topology II, it shares the dc-link capacitors of back-back converters in DFIG.
- The power flow is analyzed under voltage dips and swells.
- Five level H-bridge diode clamped multilevel inverter (H-DCMI) is selected due to generated low THD values at injected voltages. Five level H-DCMI based DVR system is designed to generate controlled voltages for compensation operation.
- The switching of H-DCMI, voltage ratings at the dc-link capacitors, filter design and transformer design for proposed study is explained in detailed.
- In control part of DVR, different reference generation methods are proposed. The system is designed and simulated to compensate voltage dips/swells and voltage harmonics occurred at grid-side. The common property of these methods are that they can generate reference signals for voltage dips/swell and harmonics. Also, they are applicable for each phase, separately.
- The proposed DVR tied GCWES is implemented in PSCAD/EMDTC program. The implementation of modeled system in PSCAD is presented at the end of this section.

5.1. The Proposed Topologies

The structures of Topology I and Topology II are detailed in 5.1.1 and 5.1.2, respectively.

5.1.1. Topology-I

In first topology called as Topology-I, DVR is tied between grid and DFIG and wind system. In topology I, the structure consists of three single-phase series transformers, a DC/AC converter and a DC-link energy storage (battery). The DVR is controlled in order to keep stator terminal voltages of the DFIG at desired (pre-fault) magnitude. The equivalent circuit of Topology-I is shown in Figure 5.1.

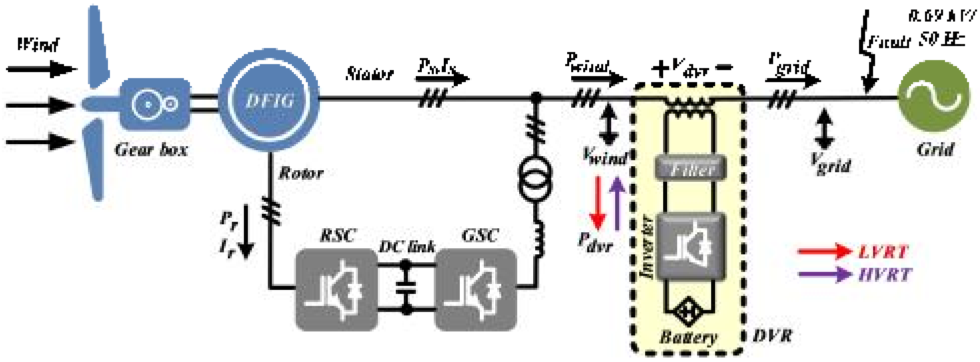

Figure 5.1 The power flow of Topology-I for LVRT and HVRT

5.1.2. Topology-II

In Topology-II, DVR is tied between grid and DFIG and wind system. The main difference of Topology-II is that it provides energy from dc link capacitor of back-back converter. The equivalent circuit of Topology-II is shown in Figure 5.2.

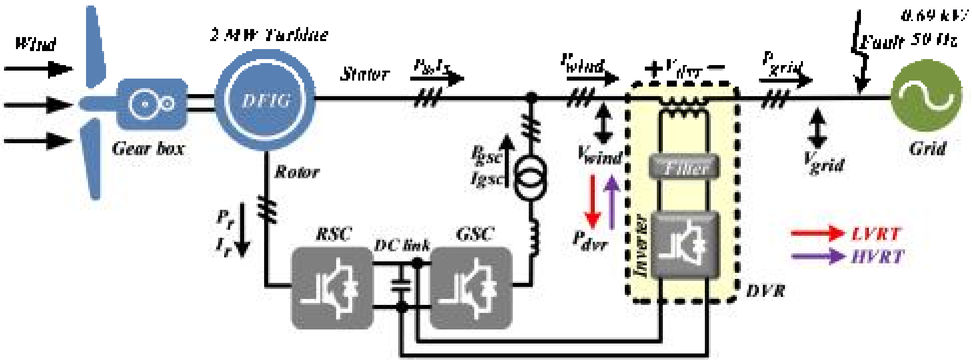

Figure 5.2 The power flow of Topology-II for LVRT and HVRT

5.2. Power Flow in DVR tied GCWES

The single line circuit diagram of power flow for DVR tied GCWES is shown in Figure 5.3. In GCWES, the current flows from wind system to grid. The power flow in these systems are contrary to conventional DVR systems based on sensitive loads.

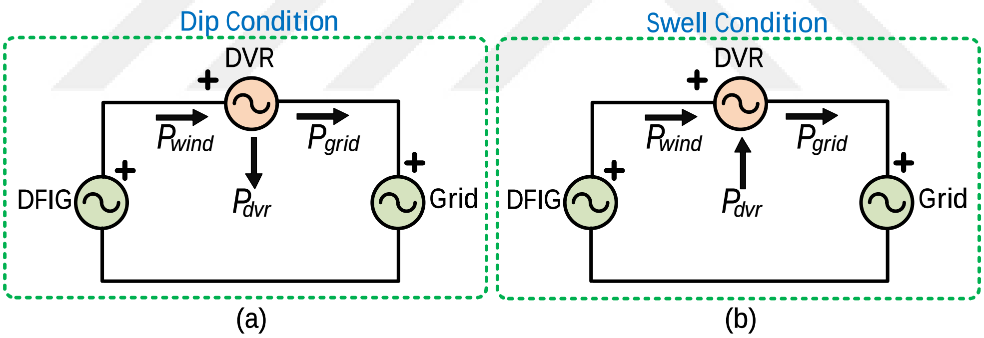

Figure 5.3 The power flow during (a) dip condition, (b) swell condition

According to the power flow, DVR is used to provide LVRT capability under voltage dip (sag) conditions. In this condition, active power flow is absorbed from inverter to dc-link (battery). As a result, the power exchange (P_{dvr}) during voltage dips is negative.

$$P_{dvr} = P_{wind} - P_{grid} < 0 \tag{5.1}$$

In swell conditions, power flow is realized from battery to inverter. Active power is injected to compensate voltage swell problem and provide HVRT capability, and the value of P_{dvr} is positive.

$$P_{dvr} = P_{wind} - P_{grid} > 0 \tag{5.2}$$

5.3. Design of DVR

In this part, the following subjects which are the main components of DVR will be detailed:

- Inverter design
- Energy Unit
- Filter Design
- Transformer Design

5.3.1. Inverter Design

In this thesis, five level H-DCMI topology ise used and tested in inverter part of DVR. The inverter consists of three legs for each phase with common-dc link (Wang et al., 2006) and it is applicable for compensation of both symmetrical and asymmetrical problems.

The five level H-DCMI is composed by the H-bridge connection of two traditional three-level diode clamped legs (Rojas et al., 2014), as shown in Figure 5.4. A single leg of three level DCMI generates three voltage levels (-Vdc/2, 0, +Vdc/2). By combination of two legs in H-bridge structure, five different voltages (-Vdc, -Vdc/2, 0, +Vdc/2, +Vdc) are generated at the output-side voltage of five level H-DCMI (Nami et al., 2011).

Five level HDCMI based DVR structure is shown in Figure 5.4. The switching states of a single phase five level H-DCMI are presented in Table 5.1.

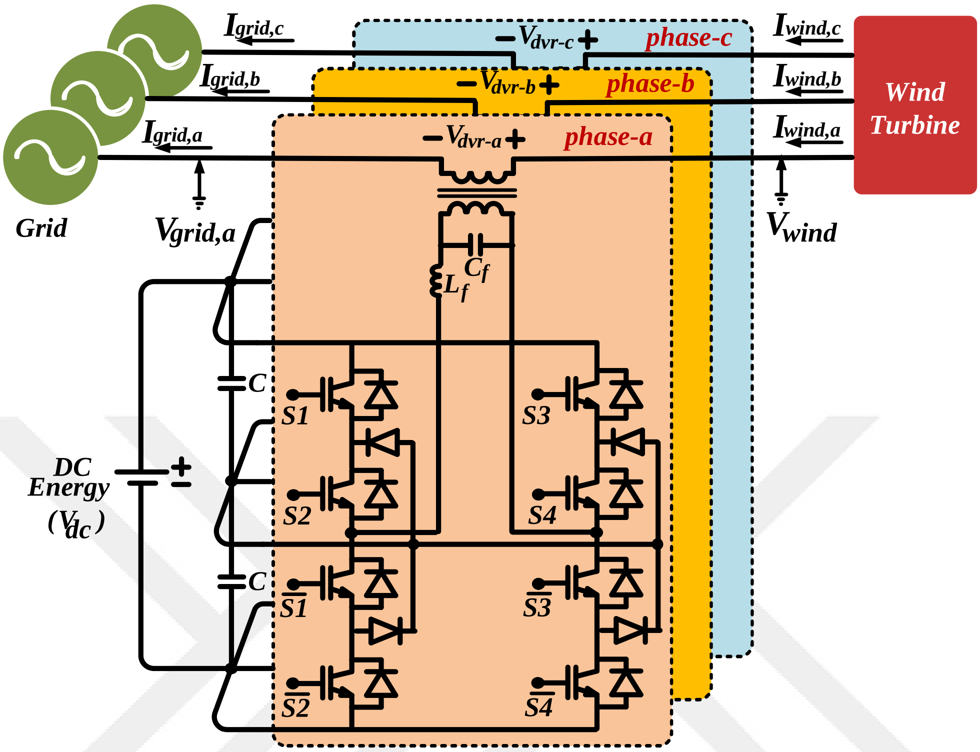

Figure 5.4 Five-level H-DCMI based DVR system

Table 5.1 Switching states of five level H-DCMI (Rojas et al., 2014)

State	S1	S2	S3	S4	Vout
1	0	0	1	1	+Vdc
2	0	1	1	1	+Vdc/2
3	0	0	0	1	+Vdc/2
4	1	1	1	1	0
5	0	1	0	0	0
6	0	0	0	0	0
7	1	1	0	1	-Vdc/2
8	0	1	0	0	-Vdc/2
9	1	1	0	0	-Vdc

(S_1, S_2, S_3, S_4) are the fundamental switching components. $(\overline{S_1}, \overline{S_2}, \overline{S_3}, \overline{S_4})$ are triggered by the inverse switching signals of (S_1, S_2, S_3, S_4).

5.3.2. Energy Storage

In Topology I, battery is selected as energy storage unit to provide dc energy for inverter, as presented in Figure 5.5. In Topology II, the dc-link capacitors of back-to-back converter in DFIG based wind system are shared with DVR, as illustrated in Figure 5.6. For this reason, the dc-link voltage of DVR is arranged to dc-link voltages of back-back converters.

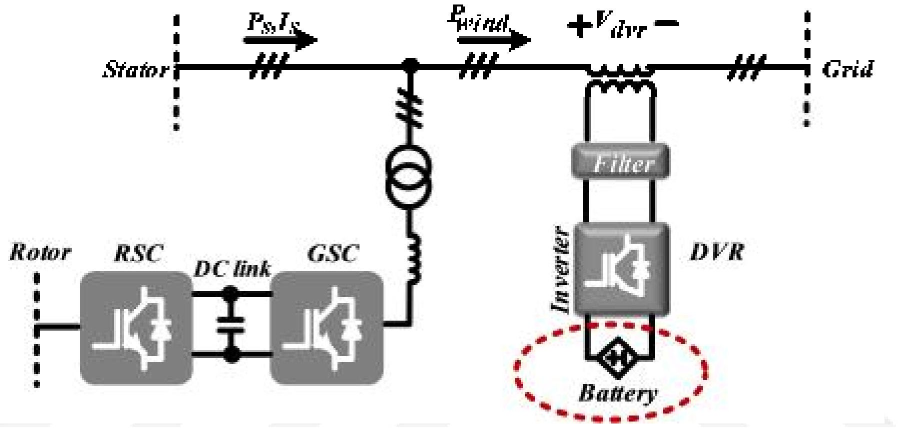

Figure 5.5 The scheme of battery based DVR called as Topology I

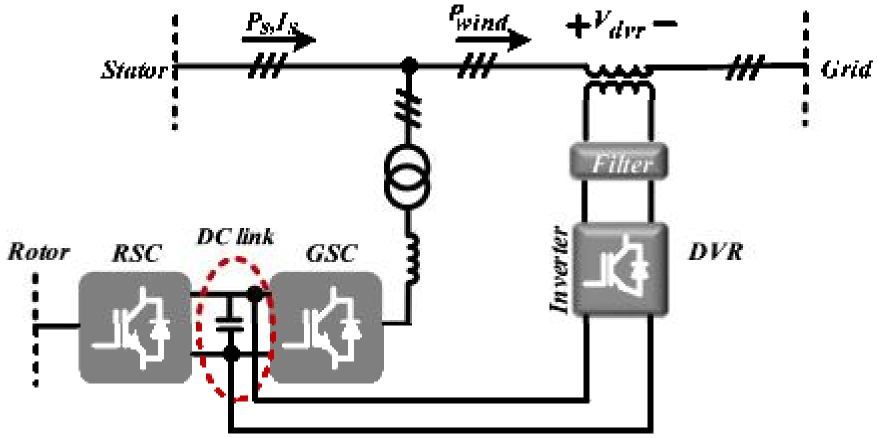

Figure 5.6 The scheme of Topology II with common dc-link capacitor

5.3.3. Filter Design

In this part, the filter design is explained for suitable inductor and capacitor values which are based on the fundamental voltage drop, cut-off frequency and small inductance for low-cost. The equivalent circuit for design of LC filter is shown in Figure 5.7.

In DVR structure, the series transformer has a leakage inductor which analyzed in filter design (Guo and Liu, 2011). Actually, the output LC filter consists a LCL filter with leakage inductor. In order to design output filter, leakage inductance is firstly calculated. In order to estimate the actual values of leakage inductance, base values of resistance and inductance are calculated by using (5.3-6).

$$R_{base} = \frac{V_{base}^{2}}{S_{base}} \tag{5.3}$$

$$L_{base} = \frac{R_{base}}{2\pi f} \tag{5.4}$$

$$L_{leak} = L_{leak,pu} \times L_{base} \tag{5.5}$$

$$Z_{eq} = 2\pi f L_{leak} \tag{5.6}$$

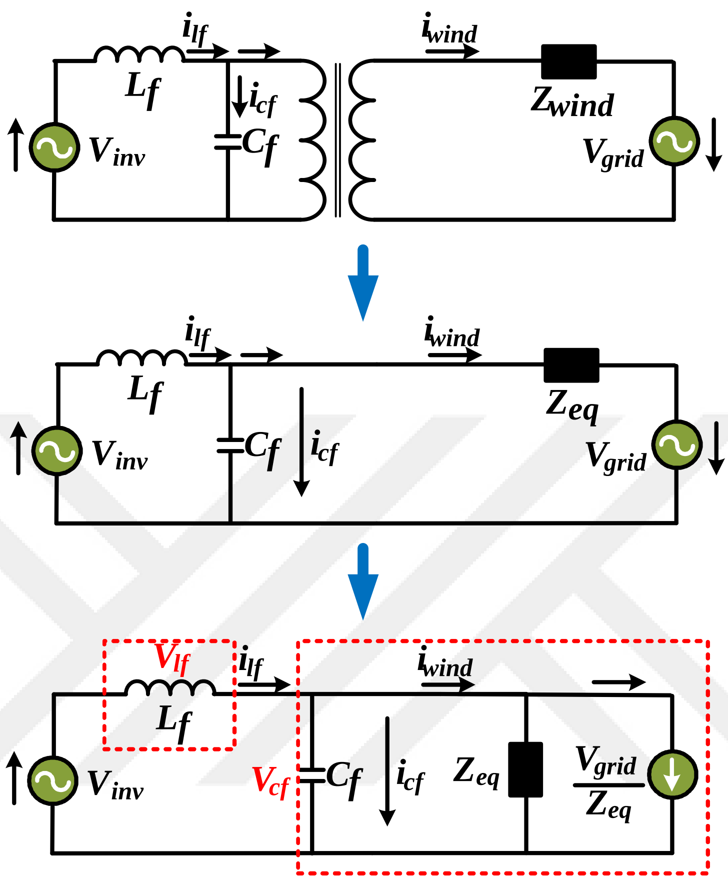

Figure 5.7 The equivalent circuit of system

LC filter is used to prevent the harmonic components occurring in the filter output voltage. The fundamental principle in the filter design is to provide a shunt way for the harmonic current and a series impedance to carry the harmonic voltages (Choi et al., 2002). To perform this aim, the fundamental current flowing through capacitor should be far less than the transformer current.

$$i_{lf} = i_{cf} + i_{wind} \tag{5.7}$$

Assume that i_{cf} is very smaller than i_{wind} (Guo and Liu, 2011). So,

$$\frac{x_1}{100}\frac{1}{Zeq} \le \frac{1}{Z_{cf}} \le \frac{x_2}{100}\frac{1}{Z_{eq}} \tag{5.8}$$

x_1 and x_2 are real numbers.

Secondly, the inductor value is calculated for LC filter design. The fundamental voltage in inductor should be far less than the injected voltage value (Guo and Liu, 2011). The equivalent inductance of transformer is relatively small than the voltage across Z_{eq}.

$$V_{lf} << V_{cf} \tag{5.9}$$

$$\frac{y_1}{100}(Z_{eq} // Z_{cf}) \le Z_{cf} \le \frac{y_2}{100}(Z_{eq} // Z_{cf}) \tag{5.10}$$

In third step, the cut-off frequency of the filter is designed. The cut-off frequency of LC filter could be designed according to the following equations (Guo and Liu, 2011):

$$\frac{f_{sw}}{3} \le f_{cut-off} \le \frac{f_{sw}}{2} \tag{5.11}$$

$$f_{cut-off} = \frac{1}{2\pi\sqrt{L_f C_f}} \tag{5.12}$$

$f_{cut-off}$ and f_{sw} are cut off frequency and switching frequency, respectively.

5.3.4. Transformer Design

There are some significant issues in order to make an appropriate series transformer design (Li et al., 2000). In transformer based DVRs, power rating and the turn ratio of series transformer is designed dependent to single phase grid-side peak voltage ($V_{s,peak}$), dip/swell depth ($Mag_{dip,swell}$) and inverter output peak voltage ($V_{inv,peak}$) (Jimichi et al., 2008). The peak value of inverter voltage is also equal to dc link voltage. The power rating of a single phase is selected as dependent to depth of dip/swell ($Mag_{dip,swell}$) and system power. The power of a system (P_{system}) is the sum of phase a, phase b and phase c. The power rating of a single phase transformer is defined as:

$$P_{transformer} = \frac{Mag_{dip,swell} \times P_{system}}{3} \tag{5.13}$$

Injected voltage must be:

$$V_{inj,peak} = Mag_{dip,swell} \ V_{s,peak} \tag{5.14}$$

The generated inverter output peak voltage is:

$$V_{inv,peak} = V_{dc,link} \tag{5.15}$$

The inverter voltage is transformed into suitable value via transformer. By using V_{in} and $V_{inv,peak}$, turn ratio is calculated as (Jimichi et al., 2008):

$$\frac{n_2}{n_1} = \frac{V_{inj,\,peak}}{V_{inv,\,peak}} = \frac{Mag_{dip,swell}V_{s,\,peak}}{V_{dc,link}} \qquad (5.16)$$

Where, n_1 and n_2 indicates the windings of transformer.

5.4. Proposed Controller Scheme for DVR

Several controller methods are presented in literature in order to compensate voltage problems. In proposed controller method, it includes five main steps to generate injected voltages for dip/swell and harmonics compensation.

The general scheme of proposed controller methods is introduced in Figure 5.8. According to flowchart:

- Firstly, grid-side voltages are converted into per unit values.
- Secondly, the voltage magnitude and harmonics of grid-side voltages are extracted by using detection methods.
- Then, reference signals for dip/swell and harmonics are calculated, separately.
- In next process, final reference signal is determined by using $Ref_{dip-swell}$ and $Ref_{harmonics}$
- And finally, reference signals are compared with carrier signals in order to generate pwm signals.

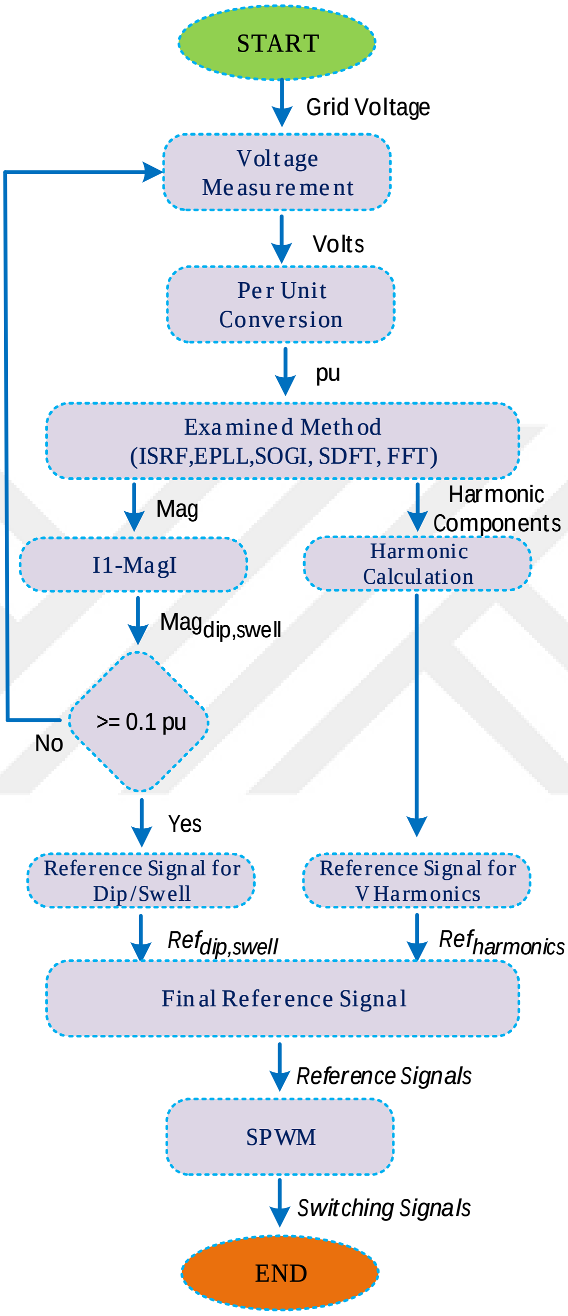

Figure 5.8. The flowchart of reference signal generation for voltage dips/swells and voltage harmonics

5.4.1. Per Unit Transform

According to the control scheme, grid voltages are firstly converted to per unit (pu) values. Then, pu values of grid-side voltage signals are used as inputs of detection or extraction method to generate voltage magnitudes at grid-side. This process is explained in (5.17):

$$V_{grid-n,pu} = \frac{V_{grid-n}}{the\ \ peak\ \ value\ \ of\ \ nth\ \ phase} \qquad n = a,b,c \tag{5.17}$$

5.4.2. Used Methods for Dip/Swell Detection and Harmonic Extraction

In this section, different multi-output methods are explained to detect voltage dips/swell and extract voltage harmonics at grid-side voltages. The examined methods are ISRF, EPLL, SOGI-PLL, FFT and SDFT in order to generate signals of dips/swells and harmonics.

5.4.2.1. ISRF

SRF theory or dq transform is the most common method to extract the components of three phase voltage signals. In SRF theory, three phase voltages (V_a , V_b and V_c) are converted to d and q components (Al-Hadidi et al., 2008; Ezoji et al., 2010; Jayaprakash et al., 2014; Rauf and Khadkikar, 2015; Sadigh and Smedley, 2016). The square root of sum of square of d and q components defines the average magnitude of input voltages. Due to average value at the output of dq transform, this method can detect the magnitudes of balanced voltages. But it cannot achieve the detection of voltage disturbances in unbalanced conditions. In order to eliminate the disadvantage of dq transform, Improved SRF (ISRF) is used for unbalanced situations by applying for each phase, separately (İnci et al., 2016). The transformation in ISRF is made by using balanced system theory. According to balanced three phase system, phase difference of 120^o is available between phases.

Relationship in balanced three phase voltages is presented in (5.18-20) (İnci et al., 2016).

$$input\_1 = V_{sa}\angle(0) \tag{5.18}$$

$$input\_2 = V_{sa}\angle\left(-\frac{2\pi}{3}\right) \tag{5.19}$$

$$input\_3 = V_{sa}\angle\left(\frac{2\pi}{3}\right) \tag{5.20}$$

ISRF detects voltages and extracts the components of voltages for each phase, separately (İnci et al., 2016). In addition, it can generates phase information for each input voltage, separately. In reference frame, the inputs of dq transform must be in identical magnitude value and phase difference of 120^{o} between phases to calculate the voltage magnitude accurately. In ISRF method, reference inputs are constructed using only single-voltage information for each phase (Wang et al., 2012), as shown in Figure 5.9. In dq-transform, virtual signals for input_2 and input_3 are derived using mathematical expressions. Therefore, input_2 and input_3 are again derived using Vsa. According to (1-3), reference signals for input_2 and input_3 are derived in phasor form. Because of $\angle\pi = -1$, the value of input_2 is to be delay π/3 multiplying by (-1) (İnci et al., 2016). In a balanced system, the sum of phasor voltages is zero ($input\_1 + input\_2 + input\_3 = 0$). As a result, the value of input_3 becomes the negative of the sum of input_1 and input_2 due to ($input\_3 = -(input\_1 + input\_2)$) (İnci et al., 2016). Phasor presentations of input_2 and input_3 are given in (5.21) and (5.22).

$$input\_2 = V_{sa}\angle(-\frac{2\pi}{3}) == -V_{sa}\angle(\frac{\pi}{3}) \quad (5.21)$$

$$input\_3 = -(input\_1 + input\_2) = -V_{sa} + V_{sa}\angle(\frac{\pi}{3}) \quad (5.22)$$

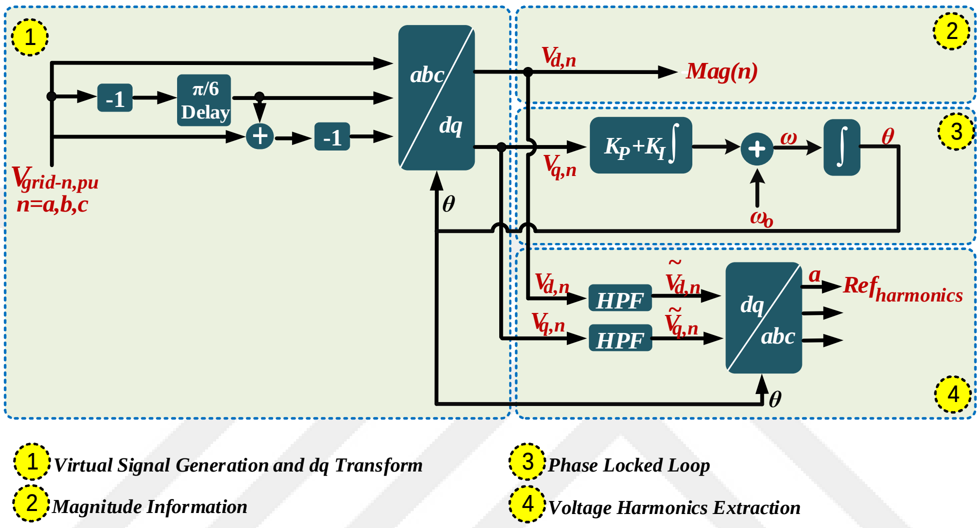

Figure 5.9 ISRF

dq transformation in multiple frame is applied for each phase, separately. In d-q transform process of controller method as shown, phase voltage and its symmetric reference signals are firstly transformed to d and q components for phase-a, phase-b and phase c, separately (İnci et al., 2016). Sine based Park transformation is used to generate d- and q- components of input voltage.

$$\begin{bmatrix} V_{d,n} \\ V_{q,n} \\ V_{0,n} \end{bmatrix} = \frac{2}{3} \begin{bmatrix} \sin(\omega t) & \sin(\omega t - 2\pi/3) & \sin(\omega t + 2\pi/3) \\ \cos(\omega t) & \cos(\omega t - 2\pi/3) & \cos(\omega t + 2\pi/3) \\ 1/2 & 1/2 & 1/2 \end{bmatrix} \begin{bmatrix} V_{s,n} \\ -V_{s,n}\angle(\pi/3) \\ -V_{s,n} + V_{sn}\angle(\pi/3) \end{bmatrix} \quad (5.23)$$

Where n=a, b and c.

The magnitude of a single phase voltage (Vd,n) is equal to d- component in pu (İnci et al., 2016). Then, Vd,n is subtracted from 1 pu to calculate the depth of voltage dip/swell. The magnitude of phase voltage is expressed in (5.24).

$$Mag = V_{d,n} \qquad n = a,b,c \tag{5.24}$$

In harmonic signal generation, high pass filter (HPF) is used to extract the harmonic components in dq coordinates (İnci et al., 2016). As a result of this process, the harmonic components are separated from fundamental component. Then, these signals are again applied for dq-abc transformation, and harmonics reference signals are generated for each phase.

Vd,n and Vq,n consist of fundamental and harmonic components. In dq frame, harmonics components behave as AC components while the fundamental component is in DC form. The equations to define these terms in dq frame:

$$\begin{bmatrix} V_{d,n} \\ V_{q,n} \end{bmatrix} = \begin{bmatrix} \bar{V}_{d,n} + \tilde{V}_{d,n} \\ \bar{V}_{q,n} + \tilde{V}_{q,n} \end{bmatrix} \qquad n = a,b,c \tag{5.25}$$

Where $\bar{V}_{d,n}$, $\bar{V}_{q,n}$ are dc components and $\tilde{V}_{d,n}$, $\tilde{V}_{q,n}$ are AC components. $\tilde{V}_{d,n}$, $\tilde{V}_{q,n}$ are separated from $V_{d,n}$ and $V_{q,n}$ using HPF. Following, $\tilde{V}_{d,n}$, $\tilde{V}_{q,n}$ are converted to a components expressed in (5.26) by using inverse dq transform.

$$\left[\tilde{V}_{a,n}\right] = \left[\cos(wt) \quad \sin(wt)\right] \begin{bmatrix} \tilde{V}_{d,n} \\ \tilde{V}_{q,n} \end{bmatrix} \tag{5.26}$$

Finally, the output of inverse dq transform is used to generate reference harmonics voltage. But, single reference signal is necessary, and generated in ISRF. Only first output signal of inverse dq transform process is used in reference generation (İnci et al., 2016). According to inverse Clarke transformation, harmonics components are obtained as (5.27) (İnci et al., 2016).

$$Ref_{harmonics}(n) = \tilde{V}_{a,n} \qquad n = a, b, c \tag{5.27}$$

After the extraction of the dq components of input voltage in reference frame, a simple structure PLL generates phase information which contains a PI regulator in synchronous dq reference frame applied to Vq component. When the angle traced by PLL is close to the actual voltage vector angle (ω*t- θ) is small or close to zero then sin(ωt- θ)≈ (ωt- θ) (Karimi-Ghartemani et al., 2004). Therefore, it can be observed that for a balanced three- phase system, the q-axis component in the rotating reference frame reduces to zero when PLL is locked, and it has small error when it is not locked (Karimi-Ghartemani et al., 2004). So, it can be defined as:

$$V_q \approx (\omega t - \theta) \tag{5.28}$$

The phase angle generated by ISRF is defined in (5.29).

$$\theta = \int \left[V_q(t) K_P + \Delta\omega t + \omega_0 \right] dt \tag{5.29}$$

Where

$$\Delta\omega t = \int V_q(t) K_I \, dt \tag{5.30}$$

5.4.2.2. EPLL

Enhanced phase locked loop (EPLL) is a non-linear adaptive filter in terms of its structure, which can generate from the input signal its magnitude, phase and frequency. The block diagram of EPLL is shown in Figure 5.10. EPLL is able to get the fundamental component of its input that contains power quality problems (Karimi-Ghartemani and Iravani, 2002; Karimi-Ghartemani et al., 2005). Besides, it is not affected from other disturbances (Karimi-Ghartemani, 2014). EPLL consists of phase detection (PD), low pass filter (LPF) and voltage controlled oscillator (VCO).

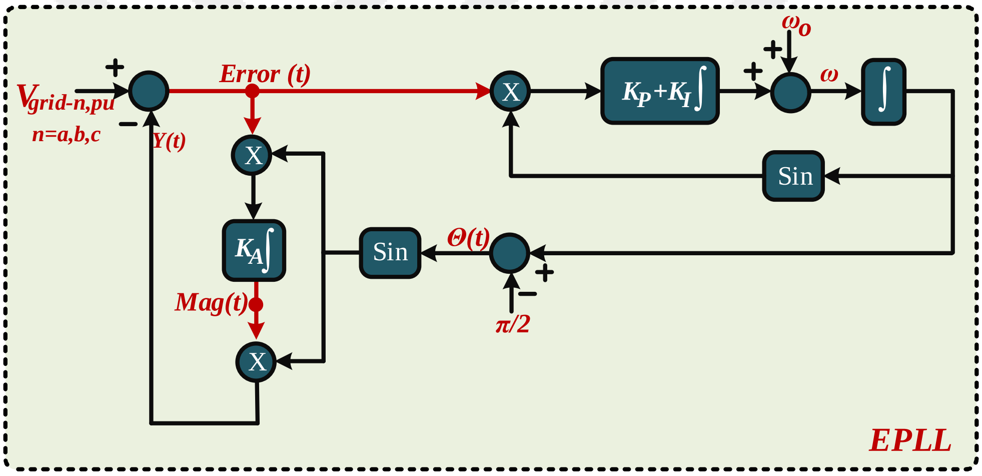

Figure 5.10 EPLL

The voltage magnitude of the input signal which is given in (5.31).

$$Mag(t) = \int Error(t).\sin\theta(t).K_A.dt \qquad (5.31)$$

And the error and phase angle equations are obtained from its block diagram as:

$$\mathrm{Ref}_{harmonics} = Error(t) = V_{grid-n,pu}(t) - Y(t) \quad (5.32)$$

$$Y(t) = \sin\theta(t)\int Error(t).\sin\theta(t).K_A.dt \quad (5.33)$$

$$\theta(t) = -\pi/2 + \int[Error(t).\cos\theta(t).K_P + \Delta\omega t + \omega_0]\,\mathrm{dt} \quad (5.34)$$

$$\Delta\omega t = \int \mathrm{Error}(t).\sin(\theta + \pi/2)(t).Ki.dt \quad (5.35)$$

The error signal is the total distortion in input signal defined in time-domain as (5.32). The error signal is used as reference harmonics signal in controller scheme. Where, KA, KI, KP are gains and integral constants which affect determination of magnitude and phase of the input signal. Thus, the speed and performance of EPLL are determined by these parameters (Karimi-Ghartemani et al., 2004).

5.4.2.3. SOGI-PLL

SOGI-PLL is a phase locked-loop which can be applied in both single phase and three phase systems, as shown in Figure 5.11. In addition to obtain phase information of a signal, it achieves the generation of amplitude of measured signal. It can also extract the amplitudes of asymmetrical voltage signals due to implementation for each phase, separately (İnci et al., 2016).

Electrical signals are usually distorted by harmonics. Adaptive filters are better way in order to be avoided from the harmonics since they are not affected too much from the harmonic characteristics and automatically adapt their parameters according to harmonic characteristics (İnci et al., 2016). They are also applicable under three-phase asymmetrical conditions.

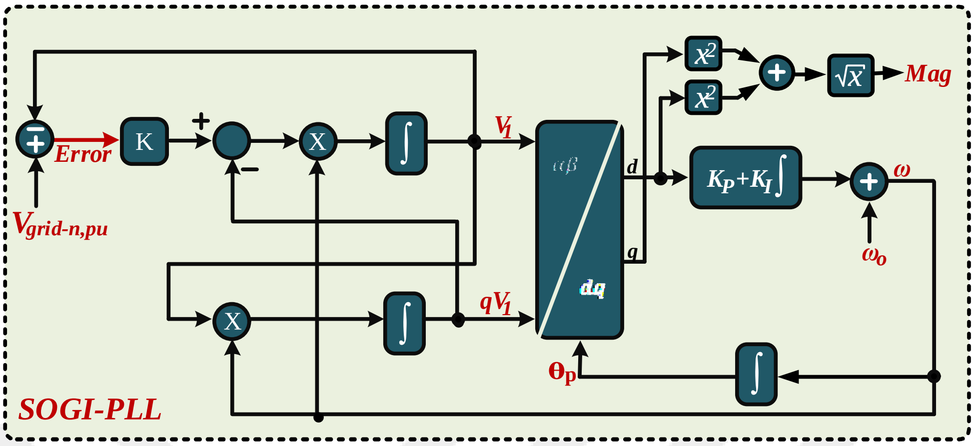

Figure 5.11 SOGI-PLL

The characteristic functions of SOGI, in-phase signal and quadrature signal can be derived as (İnci et al., 2016):

$$SOGI(s) = \frac{V_1}{K\ Error} = \frac{s\omega}{(s^2+\omega^2)} \tag{5.36}$$

$$D(s) = \frac{V_1}{V_{grid-n}}(s) = \frac{Error\,\omega\, s}{(s^2 + Error\,\omega\, s + \omega^2)} \tag{5.37}$$

$$Q(s) = \frac{qV_1}{V_{grid-n}}(s) = \frac{Error\,\omega^2}{(s^2 + Error\,\omega\, s + \omega^2)} \tag{5.38}$$

Then, α-β to dq transform is realized in (5.39).

$$\begin{bmatrix} V_{d,n} \\ V_{q,n} \end{bmatrix} = \begin{bmatrix} cos(\omega t) & sin(\omega t) \\ -sin(\omega t) & cos(\omega t) \end{bmatrix} \begin{bmatrix} V_1 \\ qV_1 \end{bmatrix} \quad n = a,b,c \tag{5.39}$$

Magnitude of a single phase voltage is calculated by using $V_{d,n}$ and $V_{q,n}$ components of SOGI-PLL. The magnitude of a voltage signal is equal to the square root of sum of squares of d- and q- components in pu (İnci et al., 2016).

$$Mag = V_{dq,n} = \sqrt{V_{d,n}^2 + V_{q,n}^2} \qquad n = a,b,c \tag{5.40}$$

Error signal indicates total distortion in input voltage. The error signal is used as reference harmonics signal in controller scheme for SOGI-PLL based controller.

$$\mathrm{Re}\,f_{harmonics} = Error \tag{5.41}$$

5.4.2.4. FFT

In this study, FFT based harmonic detection technique in (Wang et al., 2012) is used to obtain the components of the grid voltage. FFT which consists of small discrete fourier transform (DFT) pieces has a rapid response due to less complex calculations. Among FFT techniques, Cooley-Tukey is the most commonly applied algorithm (Asiminoaei et al., 2005; Lütfü Sarıbulut et al., 2013), as illustrated in Figure 5.12.

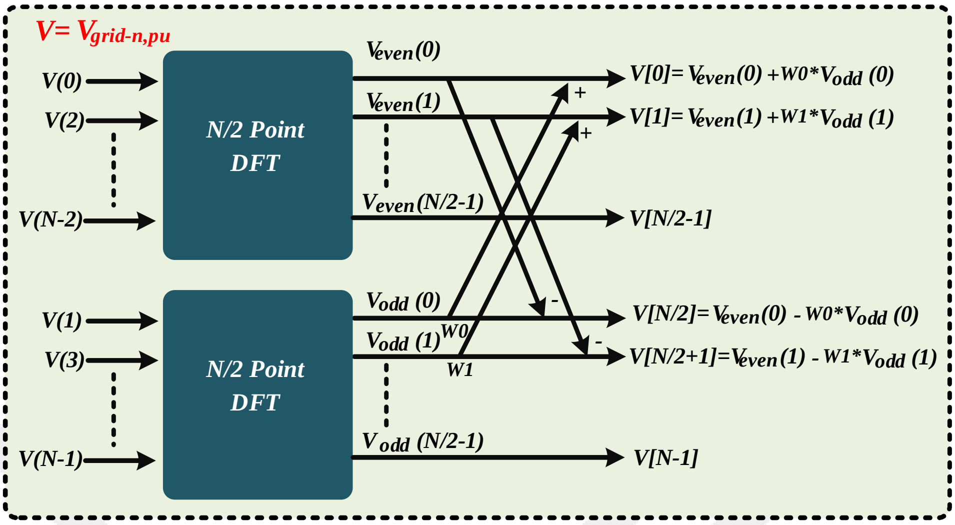

Figure 5.12 N/2-point DFTs approach of FFT

The DFT form of the grid voltage is,

$$V[k]=\sum_{n=0}^{N-1} v(n)W^{nk} \quad k=0,1,2,.......N-1 \tag{5.42}$$

Where

k: harmonic frequency index

N: number of sampling points

$W^k=e^{-j2\pi k/N}$

(5.42) can be written in polar form as,

$$V[k]=V_m(k)e^{j\theta(k)} \tag{5.43}$$

Where, V_m and θ indicate the magnitude and phase angle of kth harmonic.

In Cooley-Tukey algorithm, the voltage samples are categorized as odd samples (2n+1) and even samples (2n) (Lütfü Sarıbulut et al., 2013). Thus, (5.42) is rewritten as,

$$V[k]=\sum_{n=0}^{\frac{N}{2}-1} v(2n)W^{2nk}+W^{k}\sum_{n=0}^{\frac{N}{2}-1} v(2n+1)W^{2nk} \tag{5.44}$$

Where $W_N^{2nk}=e^{-j\frac{2\pi}{N}2nk}=e^{-j\frac{2\pi}{N/2}nk}=W_{N/2}^{nk}$

The equation (5.44) becomes as (5.45) through writing $W_{N/2}^{nk}$ instead of W_N^{2nk}

$$V[k]=\underbrace{\sum_{n=0}^{\frac{N}{2}-1} v(2n)W_{\frac{N}{2}}^{nk}}_{V_{even}(k)}+W^{k}\underbrace{\sum_{n=0}^{\frac{N}{2}-1} v(2n+1)W_{\frac{N}{2}}^{nk}}_{V_{odd}(k)} \tag{5.45}$$

$$V[k]=V_{even}(k)+W^{k}V_{odd}(k) \tag{5.46}$$

By using symmetric ($W_N^{k+\frac{N}{2}}=-W_N^{k}$) and periodic ($W_{N/2}^{k+\frac{N}{2}}=W_{N/2}^{k}$) properties, (5.45) is written as

$$V[k+\frac{N}{2}] = \underbrace{\sum_{n=0}^{\frac{N}{2}-1} v(2n)W_{\frac{N}{2}}^{nk}}_{V_{even}(k)} - W^{k}\underbrace{\sum_{n=0}^{\frac{N}{2}-1} v(2n+1)W_{\frac{N}{2}}^{nk}}_{V_{odd}(k)} \tag{5.47}$$

$$V[k+\frac{N}{2}] = V_{even}(k) - W^{k}V_{odd}(k) \tag{5.48}$$

N/2-point DFTs can be reduced by half DFTs in order to decrease calculations further. If the sample number is selected the power of 2 (N=2r), then it can be degraded until 2-point DFTs which is known as radix-2 FFT algorithm. Therefore, the calculations are decreased, and FFT becomes faster. In this study, 1024 points are exploited in 1-period. As a result, radix-2 FFT algorithm is applied as illustrated in Figure 5.13.

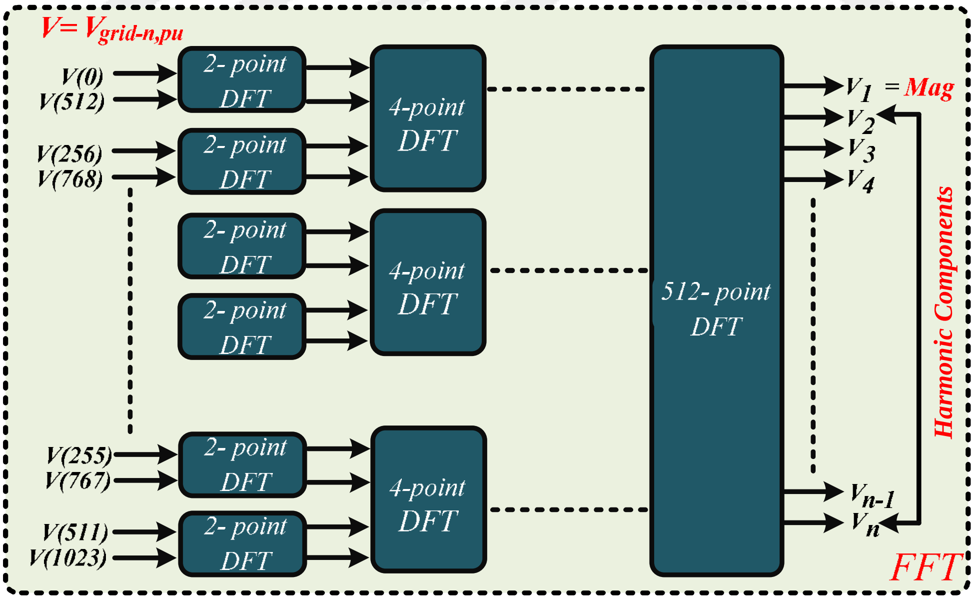

Figure 5.13 Radix-2 FFT with 1024 samples of the grid voltage

The magnitude of a fundamental signal is defined as:

$$Mag = V[1] \tag{5.49}$$

To generate reference signal of voltage harmonics, FFT extracts the selective components (kth) of voltage harmonics for each phase, separately.

$$Harmonic\,(k) = V[k]Sin(wt + \theta_k) \tag{5.50}$$

In proposed system, 5th, 7th, 11th and 13th components of voltage harmonics are compensated. Therefore, $\mathrm{Re}f_{har}(n)$ is rewritten as:

$$Ref_{har}(n) = \sum_{k \in M} Harmonic\,(k) \qquad M = \{5, 7, 11, 13\} \tag{5.51}$$

5.4.2.5. SDFT

The sliding DFT (SDFT) or Recursive DFT algorithm performs an N - point DFT on time samples within a sliding-window (Jacobsen and Lyons, 2003). The principle used for the SDFT is known as the DFT shifting theorem or the circular shift property (Springer, 1988).

A single DFT output (the kth bin of an N-point DFT) is defined by (Limin et al., 2007):

$$V_o(k) = \sum_{n=0}^{N-1} V(n) W^{-nk}, \qquad W = e^{j2\pi/N} \tag{5.52}$$

Where $V_o(k)$ represents the kth order harmonic component of the N-point sequence. When the rectangular window of N- point data moves one step forward, the kth order harmonic component is updated by (Limin et al., 2007):

$$V_1(k) = \sum_{n=0}^{N-1} V(n+1)W^{-nk} \tag{5.53}$$

From (5.52) and (5.53), a recursive way of computing DFT is obtained as:

$$V_1(k) = W^k \left[V_{i-1}(k) + V(i) - V(i-N)\right] \tag{5.54}$$

Calculating DFT in this way is called a recursive DFT. RDFT updates the specific kth order harmonic component each sampling time with one complex multiply and two real adds (Limin et al., 2007). If the input signal V(n) is real sequence, then:

$$\mathrm{Re}\, V_i(k) = \mathrm{Re}\, V_i(N-k) \tag{5.55}$$

$$\mathrm{Im}\, V_i(k) = -\,\mathrm{Im}\, V_i(N-k) \tag{5.56}$$

Thus, to calculate M (M≤N/2) harmonic components, RDFT requires M complex multiply and 2*M real adds (Limin et al., 2007).

Due to the narrowband nature of the estimated spectrum coefficients, update of harmonic components calculation at each sampling period is not necessarily required. Consider an N-point wide sliding window move forward through the signal every p step forward (1≤p≤N) (Limin et al., 2007).

$$V_p(k) = \sum_{n=0}^{N-1} V(n+p)W^{-nk} \qquad (5.57)$$

From (5.52) and (56), the recursive way of calculating the kth harmonic component at the pth sampling time can be got as (Limin et al., 2007):

$$V_p(k) = \left\{ V_o(k) + \sum_{n=0}^{p-1} V(n+N) - V(n)W^{-nk} \right\} W^{pk} \qquad (5.58)$$

The magnitude of a fundamental signal is defined as:

$$Mag = V_p[1] \qquad (5.59)$$

To generate reference signal of voltage harmonics, FFT extracts the selective components (nth) of voltage harmonics for each phase, separately.

$$Harmonic\,(n) = V_p\,[k]\,Sin\,(wt + \theta_N) \qquad (5.60)$$

In proposed system, 5th, 7th, 11th and 13th components of voltage harmonics are compensated by using SDFT. Therefore, $Ref_{har}(n)$ is rewritten as:

$$Ref_{har}(n) = \sum_{k \in M} Harmonic(n) \qquad k = \{5,7,11,13\} \qquad (5.61)$$

5.4.3. Reference Signal Generation

The depth of dip/swell ($Mag_{dip,swell}$) is in pu:

$$Mag_{dip,swell}(n) = \left|1 - Mag(n)\right| \qquad n = a,b,c \tag{5.62}$$

Then, reference signal of voltage dip/swell is determined multiplying by sine function in same phase. Reference signal for voltage dip/swell is calculated as:

$$Reference_{dip,swell}(n) = Mag_{dip,swell}(n).\angle(\theta_n - \pi/2) \qquad n = a,b,c \tag{5.63}$$

where, θ_n is instantaneous phase angle.

Reference signal in multifunctional compensation consists of harmonics and dip/swell components. The compensation of harmonics is achieved with injection of inverse voltage in addition to dip/swell compensation. Therefore, reference signal is the sum of $Ref_{dip,swelll}(n)$ and inverse of $Ref_{harmonics}(n)$.

$$Reference(n) = Reference_{dip,swell}(n) - Reference_{harmonics}(n) \tag{5.64}$$

Where, $n = a,b,c$.

The reference signals (Reference (n)) for each phase are compared with carrier signals to generate injected controlled voltages.

5.4.4. Generation of Switching Signals

Reference signals are used to generate controlled voltages at the output of inverters. In order to perform these process, references are compared with carrier signals in pulse width modulation (PWM) and switching signals are generated, as shown in Figure 5.14. In this thesis study, Sinusoidal PWM is used to generate the switching signals of multilevel inverter topologies.

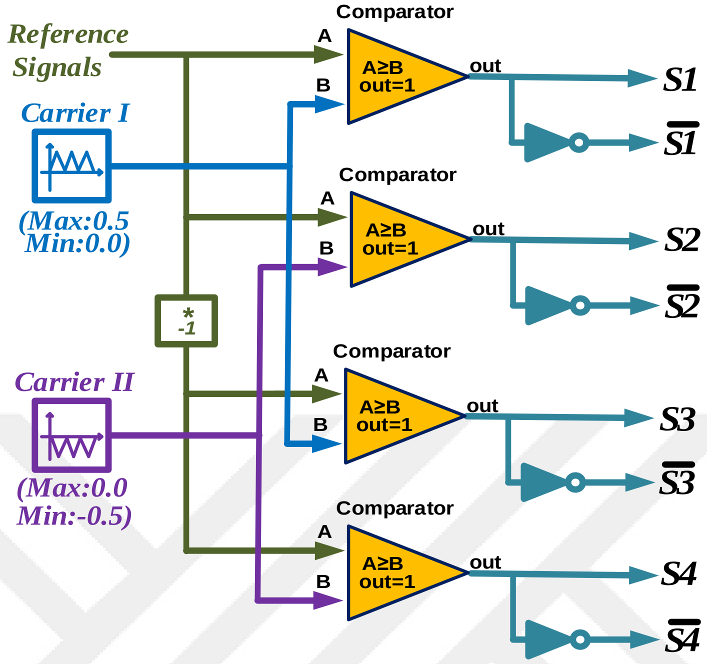

Figure 5.14 Pulse width modulation for five level HDCMI

In generation of switching signals, (S_1, S_2, S_3, S_4) are the fundamental switching signals. $(\overline{S_1}, \overline{S_2}, \overline{S_3}, \overline{S_4})$ are obtained by the inverse switching signals of (S_1, S_2, S_3, S_4) in five level H-DCMI.

5.5. The Implementation in PSCAD

In this part, PSCAD models of the system model, turbine and DVR are presented.

5.5.1. The System Model

In order to present the performance results for DVR tied DFIG wind turbine, simulation of modelled controller system has been performed by using PSCAD/EMDTC. The performance results are tested to fulfill FRT under grid voltages with harmonics up to 9% THD. The voltage and frequency of grid are selected as 0.69 kV and 50 Hz. DVR is used to protect approximately 1 MVA DFIG from symmetrical/asymmetrical faults in addition to voltage harmonics. The schemes of DVRs tied grid connected DFIG wind systems for Topology I and Topology II are shown in Figure 5.15 and Figure 5.16, respectively.

Simulation parameters used in PSCAD/EMTDC are given in Table 5.2. Parameters of grid voltages are presented in Table 5.3.

Table 5.2 PSCAD/EMTDC simulation parameters

Parameter	Value
Solution Time Step	20 μs
Channel Plot Step	50 μs
Duration of Simulation Run	10 s

Table 5.3 Grid parameters

Parameter	Value
Fundamental Frequency	50 Hz
Voltage Source	0.69 kV (line-line, rms), phase angle 0^o

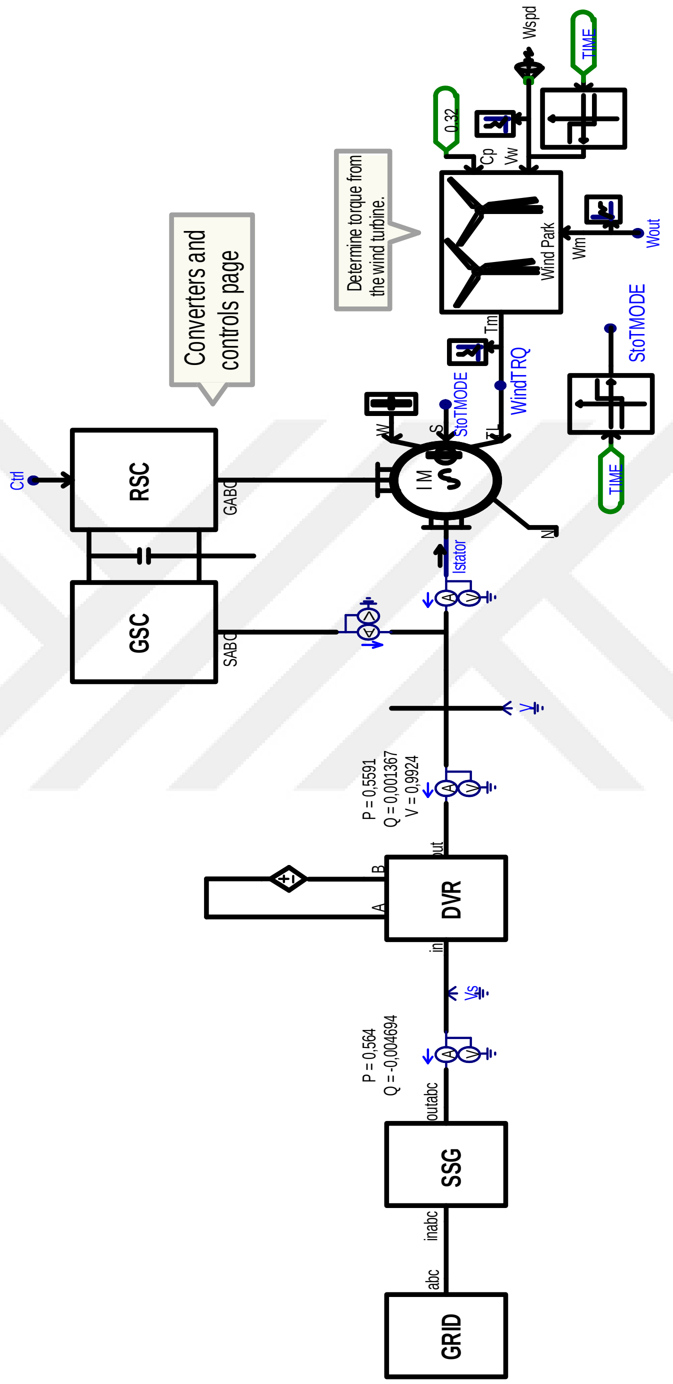

Figure 5.15 The implementation of Topology I in PSCAD

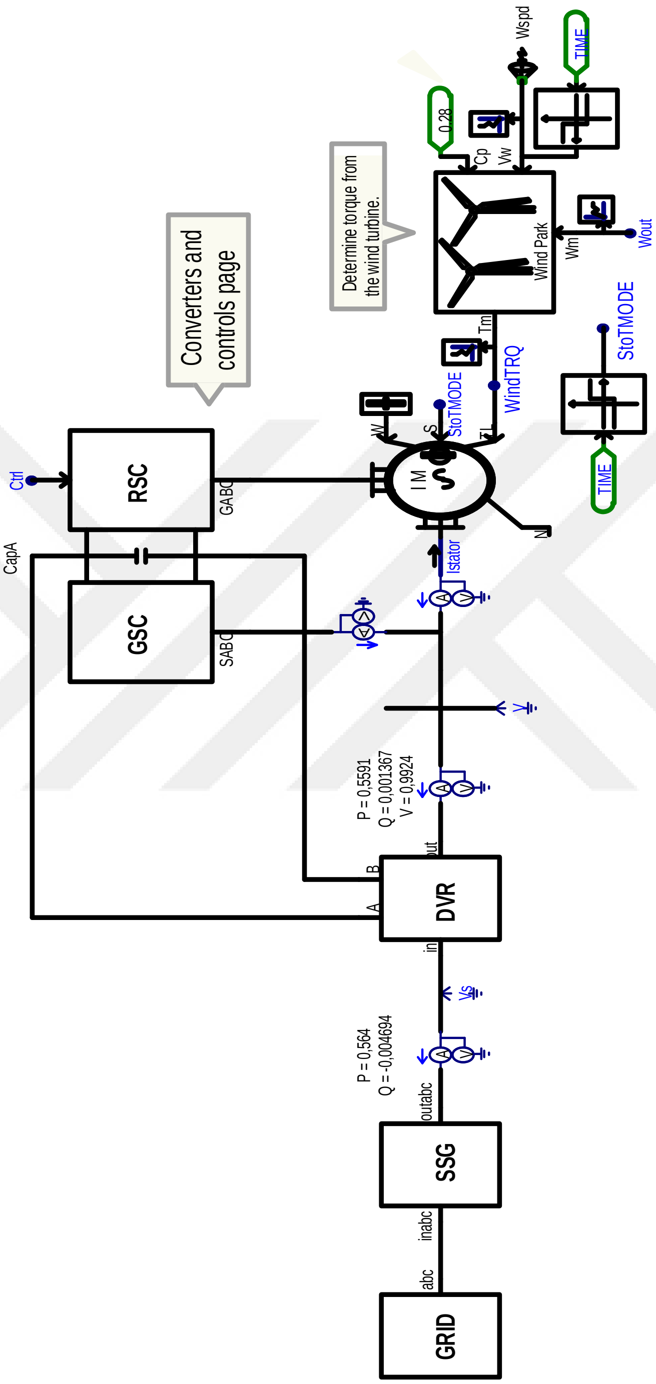

Figure 5.16 The implementation of Topology II in PSCAD

5.5.2. Turbine Modeling

The structure of doubly fed induction generator implemented in PSCAD/EMDTC is presented in Figure 5.17. As shown in structure, DFIG model in PSCAD includes three inputs called as initial machine angular speed (W), machine control mode (S) and input torque (TL). In torque control mode, it requires too interval to initialize the system. In starting of the machine, the speed mode control is used and then it is passed to torque control mode in order to enable it to generate power based on the existing wind conditions. The importance of the initial machine speed is set to a suitable value which reduces the machine transients caused shifting from speed control to torque control. In this way, the starting duration and performance of simulation is accelerated compared to the starting of torque control mode. After the starting of simulation, the machine controller passes from speed control to torque control mode within 0.5 seconds. Input torque from wind turbine must be negative in generation mode of DFIG. In PSCAD, MOD-2 and MOD-5 are two models designed for wind turbines. In modeling studies, MOD-2 is selected because of suitable for three blades based wind turbines.

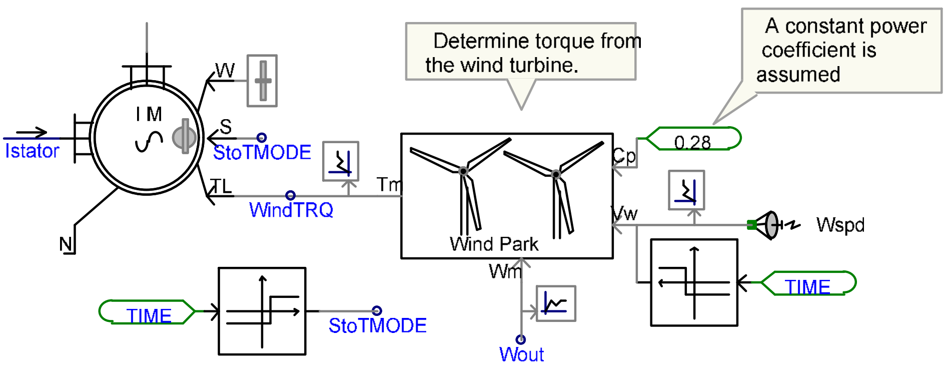

Figure 5.17 DFIG system in PSCAD

DFIG systems use back-to-back bidirectional converters at the rotor end of the machine. Figure 5.18 shows the scheme of bidirectional converter modeled in

PSCAD program. The system parameters of designed DFIG are given in Table 5.4.

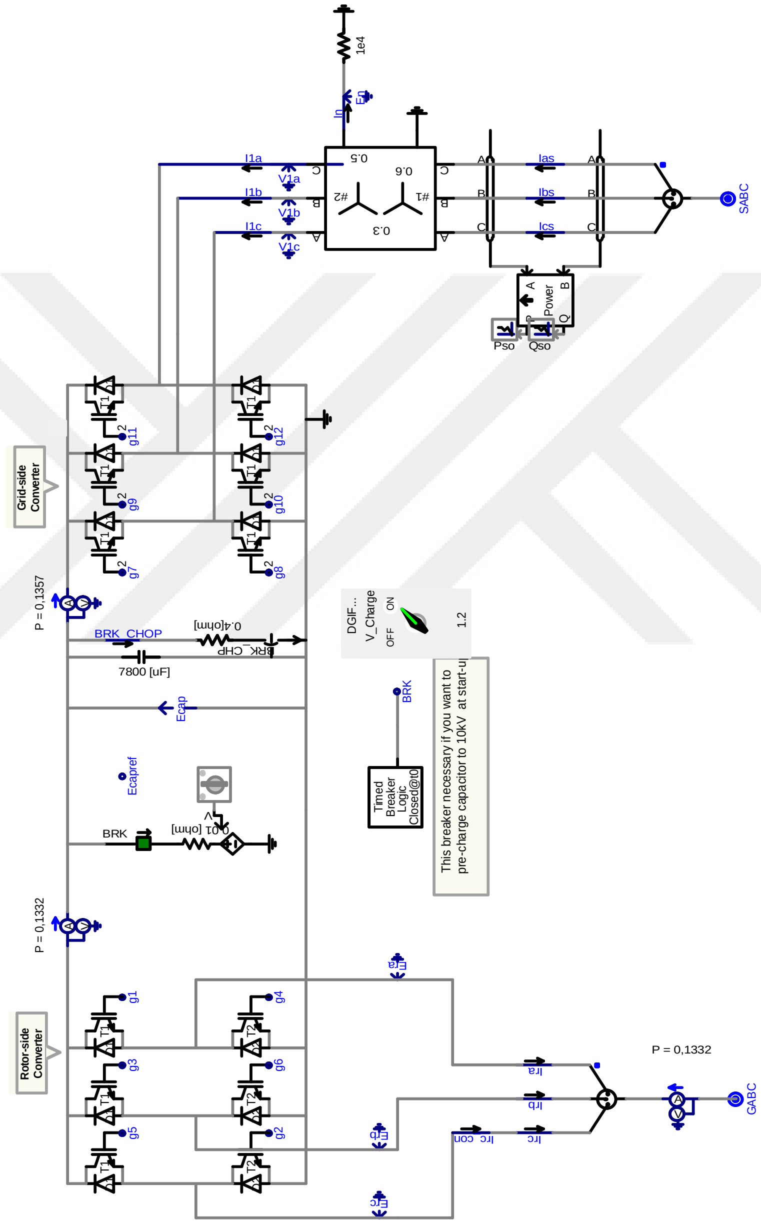

Figure 5.18 Stator and rotor side converters in PSCAD

Table 5.4. The system parameters of the DFIG

Input parameters	**Values**
Rated power	0.9 MVA
Rated voltage (L-L)	0.69 kV
Base angular frequency	50 Hz
Stator/rotor turns ratio	0.3
Angular moment of inertia	0.85 s
Mechanical damping	0.0001 pu
Stator resistance	0.0054 pu
Wound rotor resistance	0.00607 pu
Magnetizing inductance	4.5 pu
Stator leakage inductance	0.01 pu
Wound rotor leakage resistance	0.01 pu

5.5.2.1. RSC Controller

The control of real and reactive power is dependent to d and q components of rotor current. In order to realize this process, d and q components of rotor current are generated by using PI controllers which is dependent to error between reference and actual stator real and reactive powers. These reference d and q axis currents are again used to generate the reference phase currents through the inverse dq transformation (Saraf, 2012). These reference currents for each phase are used to generate switching signals of rotor side converter by using hysteresis controller.

The active power exchange between rotor and grid is measured via angular speed of the rotor. The reference angular speed is based on a fixed tip speed ratio calculated using the initial wind speed and angular speed ‘W’ (when the machine is in speed control mode). The reference angular speed signal is generated by using wind speed signal (V_w), as shown in Figure 5.19. In study, initial wind speed is 12 m/s and the initial speed of the machine is 1.2 pu. In this way, constant tip speed ratio is calculated as 9.6 (12/1.2).

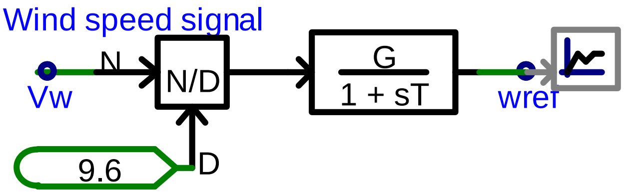

Figure 5.19 Generation of reference angular speed

The calculation of stator flux angle information is presented in Figure 5.20.

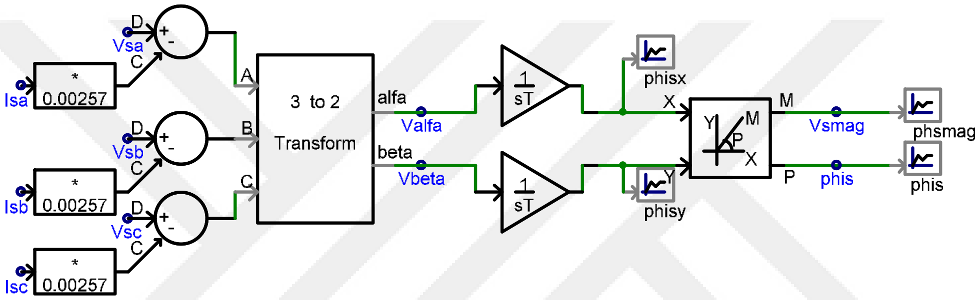

Figure 5.20 The calculation of stator flux angle

The block diagrams to generate the references of d and q axis rotor currents are illustrated in Figure 5.21. The signal “StoTMODE” in Figure 5.21 is provided as a control signal to a two input selector. This signal controls the inputs to the two proportional integral controllers meant for stator active and reactive powers. When the machine is operated in the speed control mode, the input to the both the proportional - integral controllers is zero and as soon as the machine is switched to torque control mode, the inputs change from zero to the respective error signals (Saraf, 2012). The PI parameters of reference dq components for rotor current are given in Table 5.5 and Table 5.6.

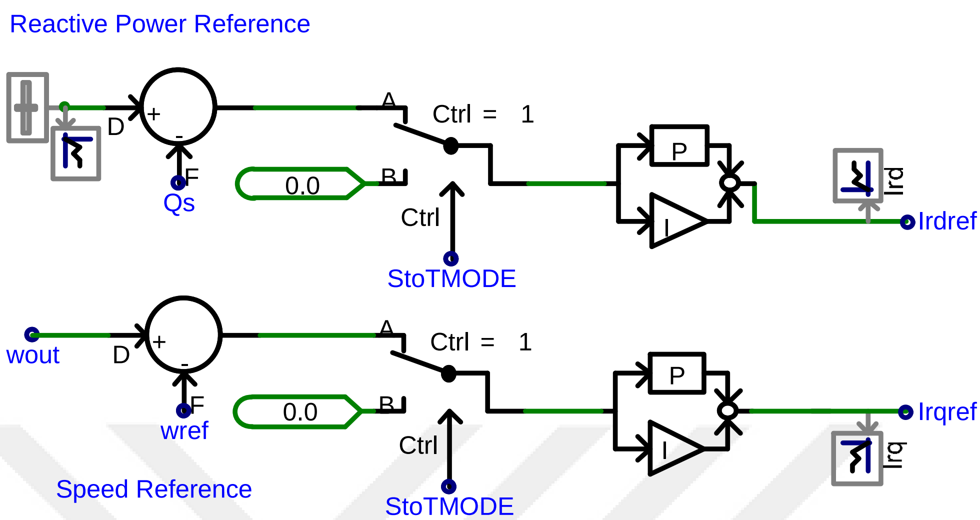

Figure 5.21 Generation of reference d and q components for rotor-side current (Hosseini et al., 2005)

Table 5.5 Parameters of the PI controller for generating $I_{rq,ref}$

Input parameters	**Values**
Proportional gain (Kp)	0.5
Integral time constant (Kp/Ki)	1
Maximum limit	5
Minimum limit	0
Initial output of the integrator	0.207

Table 5.6 Parameters of the PI controller for generating $I_{rd,ref}$

Input parameters	**Values**
Proportional gain (Kp)	0.25
Integral time constant (Kp/Ki)	0.5
Maximum limit	3
Minimum limit	0
Initial output of the integrator	0.075

The switching of solid state devices (IGBTs) in rotor side converter is achieved by using dq components of rotor currents in hysteresis current controller.

The scheme of hysteresis controller is presented in Figure 5.22. In order to generate reference rotor current signals, d and q components are firstly transformed into three phase signals by using inverse dq transform. The angle called as slpang is difference between the stator flux angle and the rotor angle. This angle is used to transform reference rotor currents in dq frame into three phase reference currents in phase frame (Saraf, 2012). Table 6.6 has the values for the hysteresis band selected for the controller.

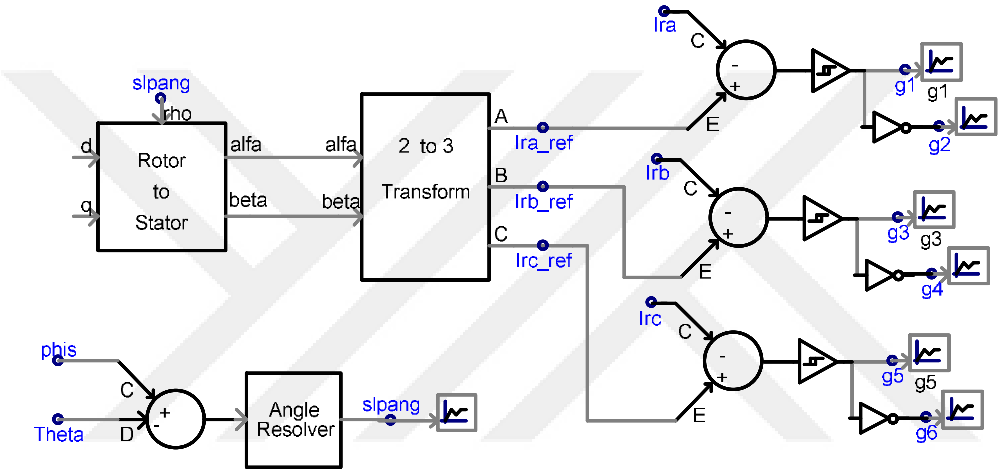

Figure 5.22 Generation of switching signals using hysteresis control (Hosseini et al., 2005)

Table 5.7 Hysteresis controller bandwidth in PSCAD

Parameter	Range
Hysteresis band	0.001 to -0.001

5.5.2.2. GSC Controller

A significant part in GSC control is generation supply side voltage angle information. In order to calculate this information, α and β components of supply side voltage angle information are used in calculation given in (5.65) (Koç, 2010).

$$\theta_{v_s} = \tan^{-1}\left(\frac{V_b}{V_a}\right) \quad (5.65)$$

In PSCAD, voltage signals of supply side are firstly transformed to α and β signals. After this process, phase information is obtained by using polar rectangular coordinate conversion module, as shown in Figure 5.23.

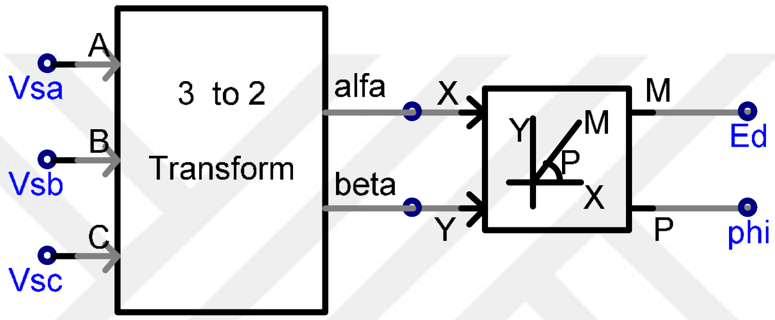

Figure 5.23 Supply side voltage angle determination in PSCAD [12]

After obtaining the stator voltage angle, the three phase currents flowing between the GSC and grid are transformed to the grid-side voltage oriented frame using the supply voltage angle. The block diagram in PSCAD has been shown in Figure 5.24 (Saraf, 2012).

In next process, three phase currents in GSC and grid are converted to dq components by using supply side voltage phase angle information. Figure 5.24 illustrates the modules of dq transformation constructed in PSCAD.

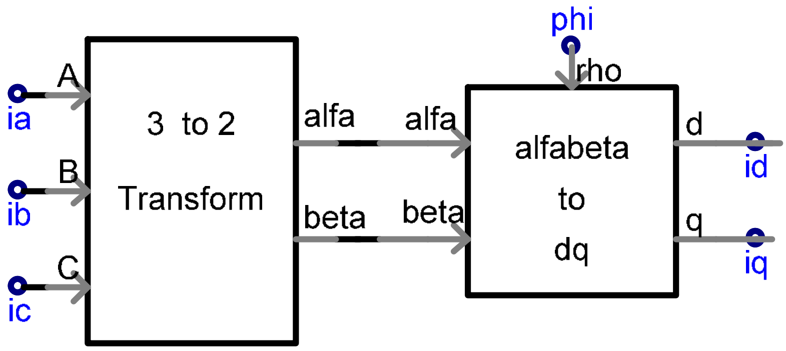

Figure 5.24 abc to dq conversion of currents

Thus, PI controllers are used to reflect the error in i_d on $V'_{d,grid}$ and i_q on $V'_{q,grid}$ respectively (Saraf, 2012). In PSCAD, the control system is built as shown in Figure 5.25.

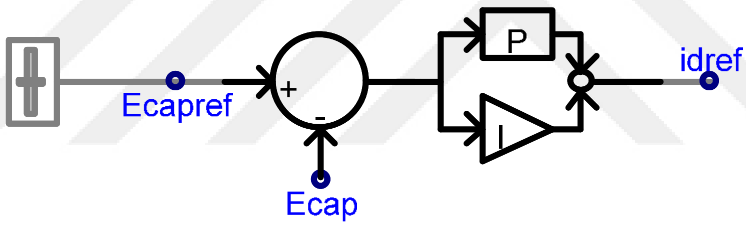

Figure 5.25 Generation of i_{dref} based on the error in capacitor voltage

The PI parameters to generate i_{dref} for GSC are given in Table 5.8.

Table 5.8 Parameters of the PI controller for capacitor voltage

Input parameters	**Values**
Reference capacitor voltage, Ecapref	0.8 kV
Proportional gain, Kp	5
Integral time constant, Ti	0.01
Maximum limit	2
Minimum limit	-2
Initial output of integrator	0

In Figure 5.26, the modeling scheme is presented to generate d component of reference GSC voltage.

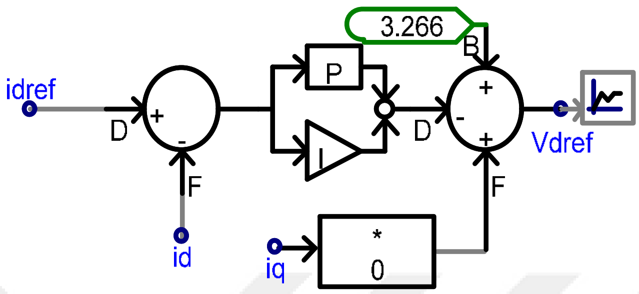

Figure 5.26 Generation of d-axis reference for grid side converter output voltage

The PI parameters to generate $V'_{d,grid}$ are given in Table 5.9.

Table 5.9 Parameters of the PI controller for generation $V'_{d,grid}$

Input parameters	**Values**
Proportional gain, Kp	10
Integral time constant, Ti	0.01
Maximum limit	15
Minimum limit	-15
Initial output of integrator	0

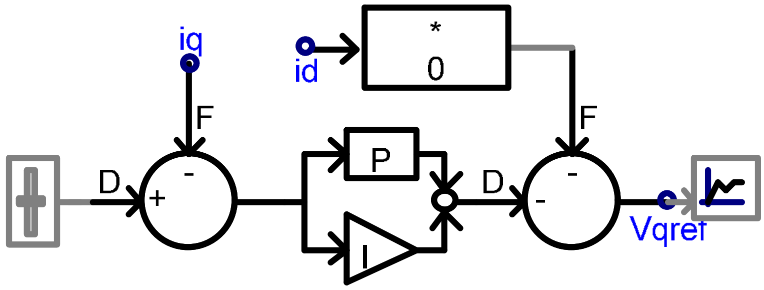

Figure 5.27 Generation of q- axis reference for grid side converter output voltage

The reference value selected for i_{qref} is zero since the wind generator is made to operate at a power factor close to unity (Saraf, 2012). The PI parameters to generate $V'_{q,grid}$ are given in Table 5.10.

Table 5.10 Parameters of the PI controller for generation $V'_{q,grid}$

Input parameters	**Values**
Proportional gain, Kp	10
Integral time constant, Ti	0.01
Maximum limit	15
Minimum limit	-15
Initial output of integrator	0

The reference signal generation of GSC voltages is realized using inverse dq transform, as shown in Figure 5.28.

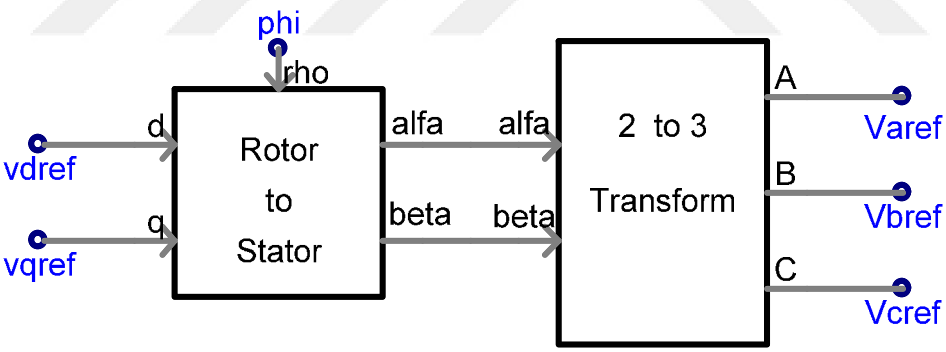

Figure 5.28 Conversion of reference voltages from d- q to phase frame

In PWM process, switching signals are generated by using the reference voltage signals compared with carrier signals. Figure 5.29 shows the construction of PWM structure in PSCAD.

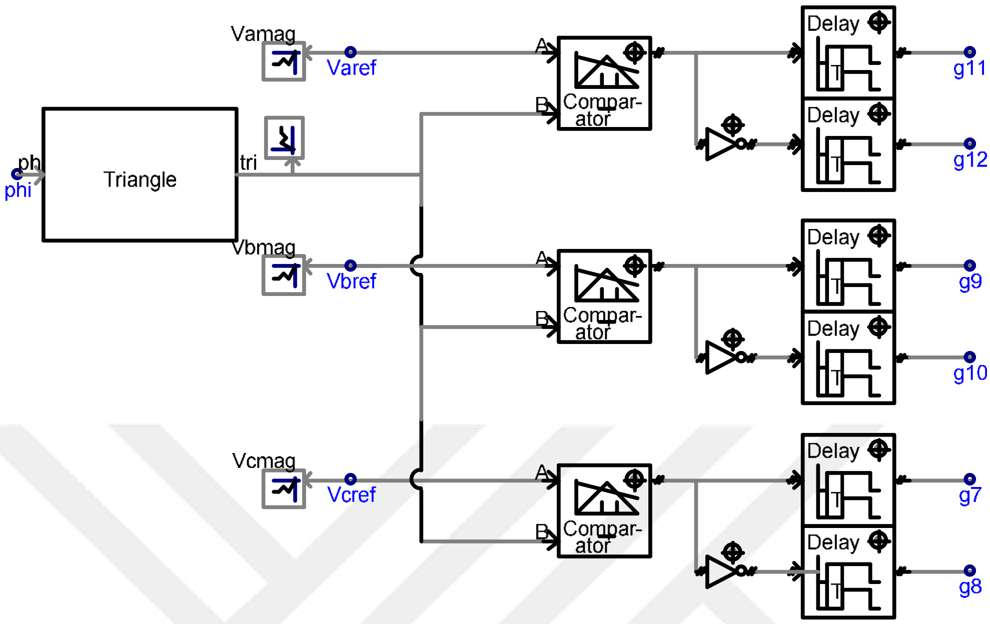

Figure 5.29 PWM for GSC

5.5.3. DVR Modeling

The power circuit of DVR constructed in PSCAD/EMTDC is shown in Figure 5.30. It consists of an inverter, dc-link capacitors and LC filter and injection transformers. The parameters of LC filters and injection transformers are introduced in Table 5.11.

Table 5.11 The values of inductor and capacitor in output filter

Parameter	Value
Filter inductor (L_f)	0.1 mH
Filter Capacitor (C_f)	50 µF

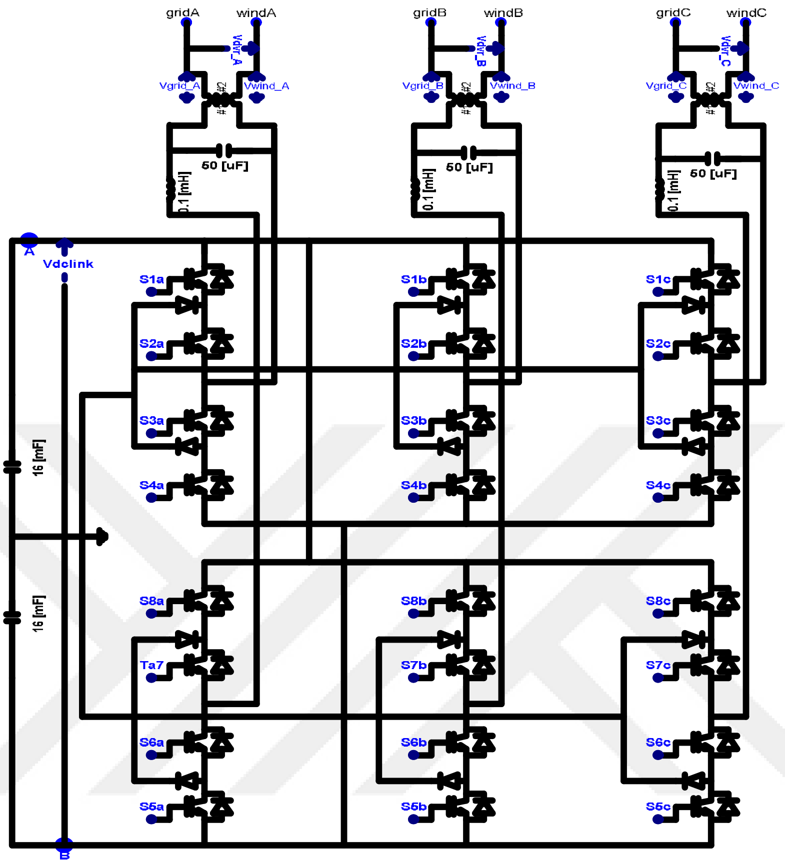

Figure 5.30 DVR Model in PSCAD

Table 5.12 The parameters of injection transformers

Parameter	Value
Transformer MVA	200 kVA
Base Operation Frequency	50 Hz
Leakage reactance	0.1 pu
No load losses	0.1 pu
Winding Voltages (RMS)	800 V/280 V

Grid-side voltages are firstly converted to per unit (pu) values, as shown in Figure 5.31. Then, the converted values of grid-side voltage signals are used as inputs of detection or extraction method to generate voltage magnitudes in the page module of reference signal generation.

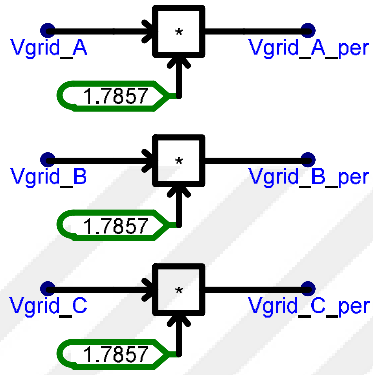

Figure 5.31 Per unit transformation in PSCAD

By using pu grid-side voltages, reference signals of voltage dips/swells and harmonics are generated as shown in Figure 5.32. According to reference generation block, magnitude information, references and dip/swell detection signals are generated through different methods. In proposed study, ISRF, EPLL, SDFT, SDFT and FFT are separately tested in reference signal generation process.

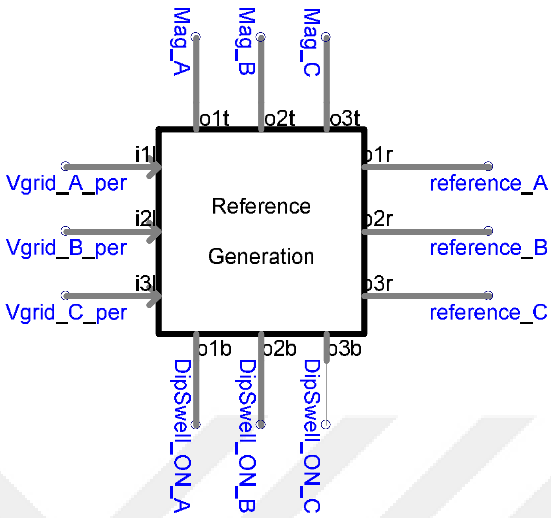

Figure 5.32 Block (page module) of reference signal generation in PSCAD

The generated reference signals are compared with carrier signals in order to generate switching signals for five level H-DCMI, as shown in Figure 5.33.

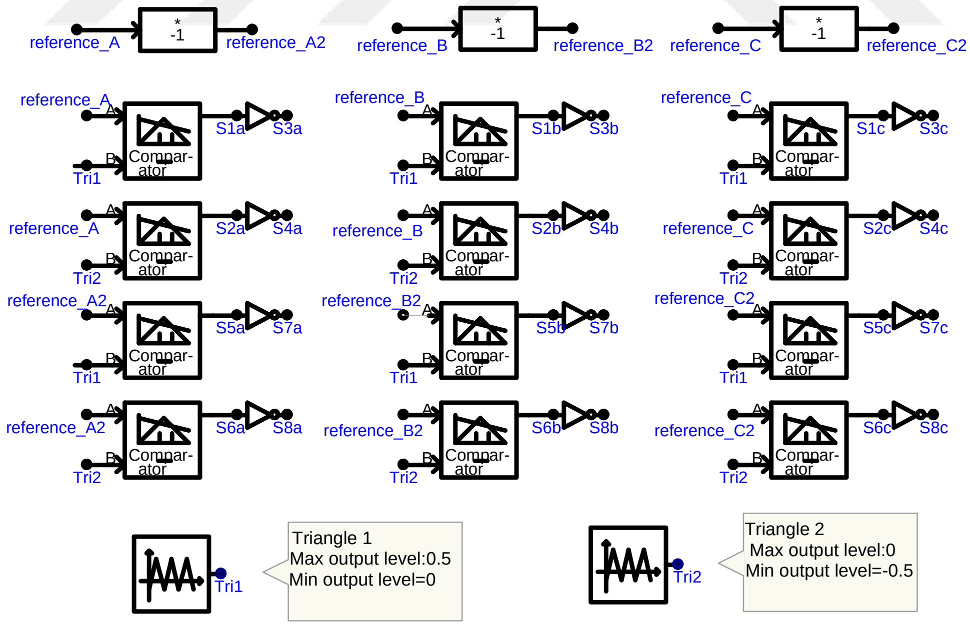

Figure 5.33 PWM of DVR in PSCAD

6. PERFORMANCE COMPARISON OF METHODS

In this section, the performance results of different reference signal generation method based DVR are presented. In order to compare the performance results of reference generation methods, Topology I is used to compensate voltage problems at grid-side voltages. The single line scheme of Topology I with controlled different reference generation methods is introduced in Figure 6.1.

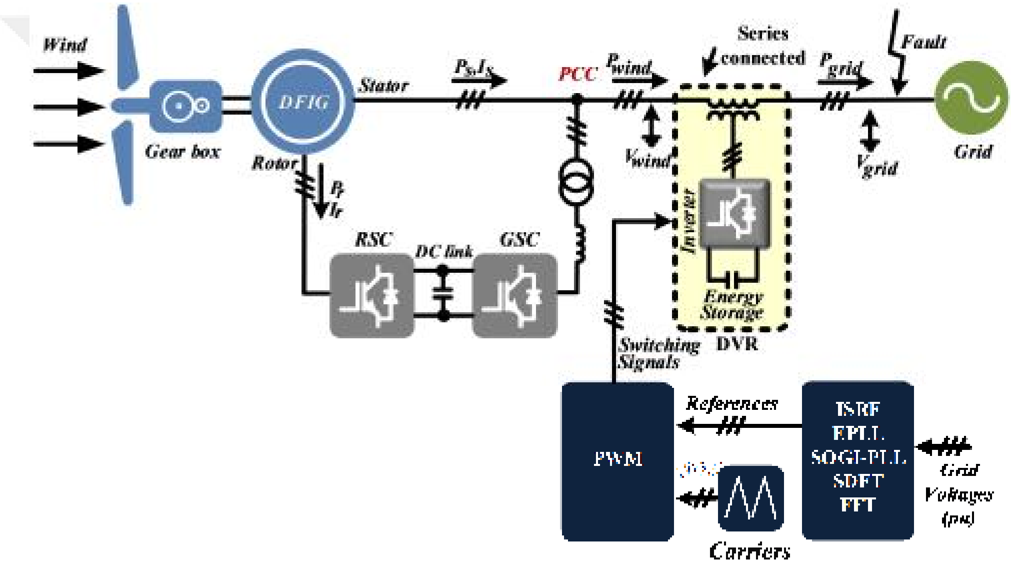

Figure 6.1 Single line scheme of Topology I with controlled different reference generation methods

In this section, these topics will be analyzed:

- Three phase asymmetrical dips and its affects in DFIG
- Performance analysis for voltage compensation by using EPLL, ISRF, SOGI-PLL, FFT and SDFT reference methods
- Detection speeds of examined methods for starting time and ending time
- THD values according to controller methods

6.1. 3-ϕ Asymmetrical Dips and Its Affects

Three phase asymmetrical voltage dips occur at grid-side voltages between t=3.0 s and t=3.2 s. Voltage dip magnitudes of phases are 0.3 pu, 0.5 pu and 0.4 pu for phase-a, phase-b and phase-c, respectively. Voltage magnitudes reduce to 278.6 Vrms, 199 Vrms and 238.8 Vrms from 398 Vrms phase-neutral voltage. In the absence of voltage dip compensation, the fault at grid-side induces higher rotor/stator currents and torque oscillations during fault and immediately after the fault as shown in Figure 6.2.

Table 6.1 introduces the values of nth components of grid-side phase peak voltages. As presented in values, the harmonic components are balanced for 3-ϕ grid voltages.

Table 6.1 The components of distorted grid-side voltages with selective harmonic components for performance comparison study

		Phase A	Phase B	Phase C
Dip Depth		0.3 pu	0.5 pu	0.4 pu
THD at grid-side		7.45%	7.45%	7.45%
The components of Grid-side Voltages	f1=50 Hz	560 V	560 V	560 V
	f5=250 Hz	30 V	30 V	30 V
	f7=350 Hz	25 V	25 V	25 V
	f11=550 Hz	13 V	13 V	13 V
	f13=650 Hz	9 V	9 V	9 V

THD values of three phase voltages are identical and equal to 7.45%. The waveforms of grid-side voltages and THD values are presented in Figure 6.3 and Figure 6.4, respectively.

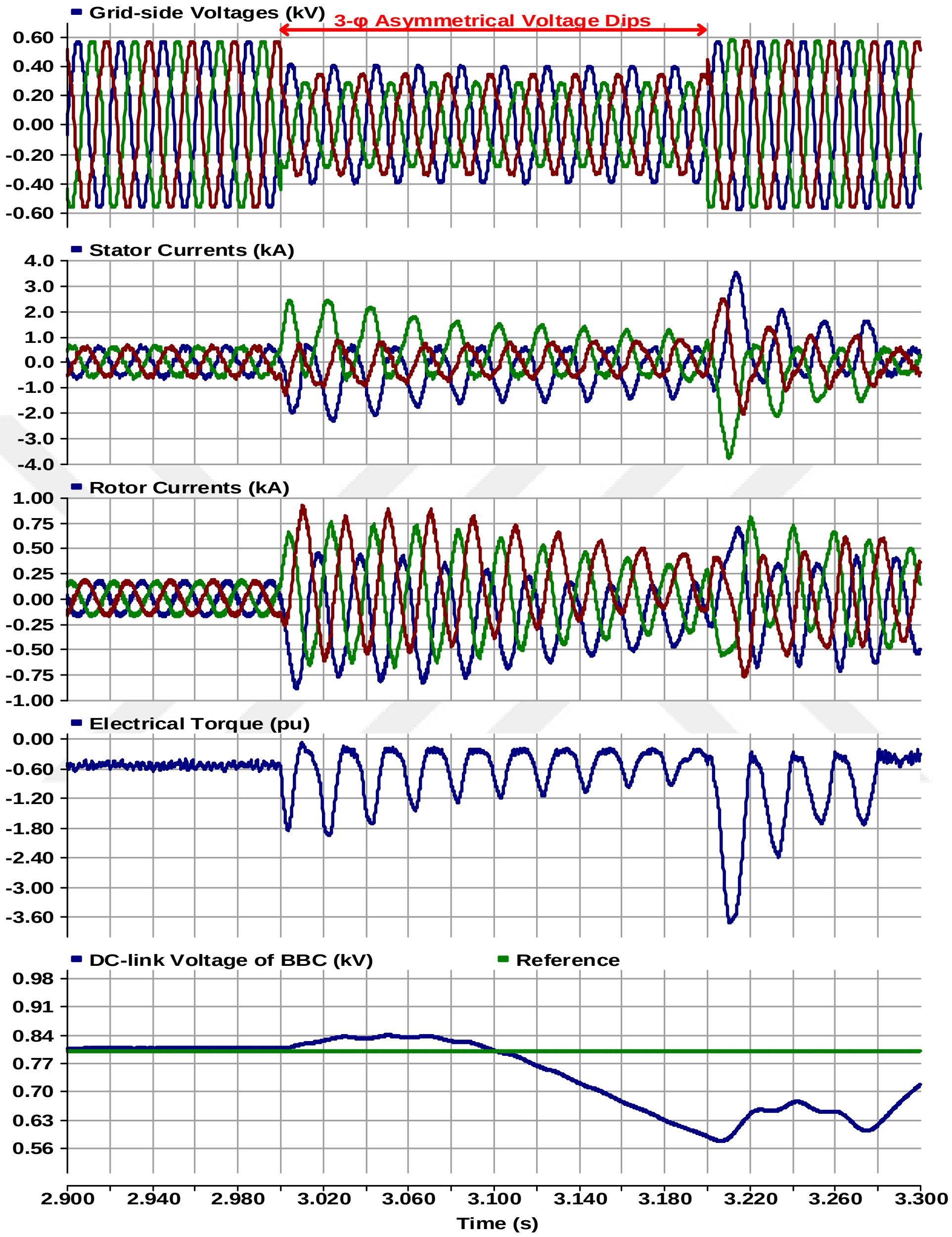

Figure 6.2 The waveforms of grid-side voltages, stator/rotor currents, electrical torque and dc-link voltage during 3-ϕ asymmetrical voltage dips

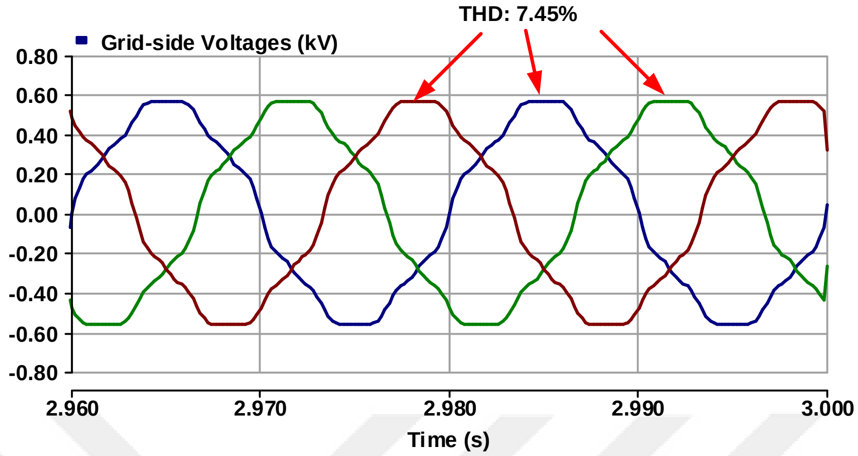

Figure 6.3 Grid-side voltages with harmonics (THD:7.45%)

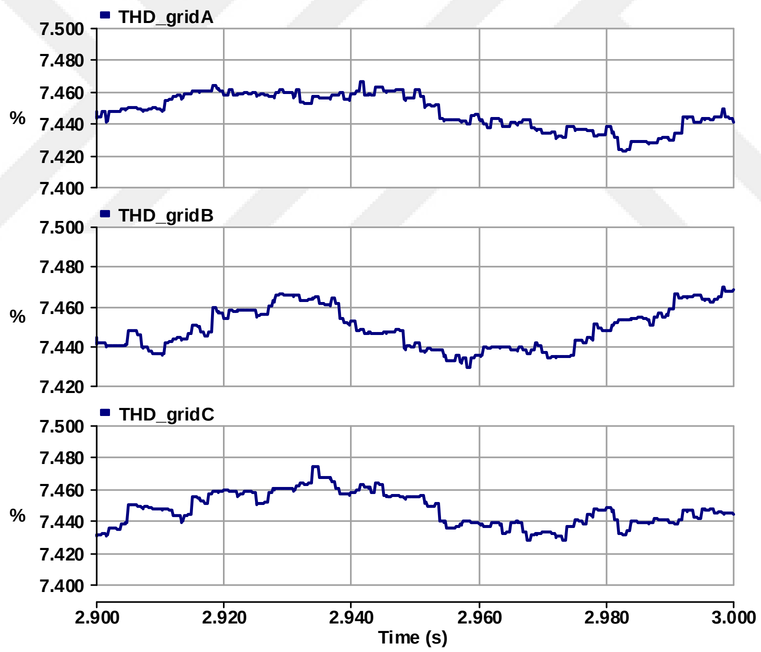

Figure 6.4 THD values for phase-a, phase-b and phase-c, respectively

After the occurrence of voltage dips, transient THD values appear in three phase voltages of grid side voltages. THD values in these phases are nearly 16 %

for phase a, 36% for phase b and 25.5 % for phase c. The THD values belong to phases are shown in Figure 6.5.

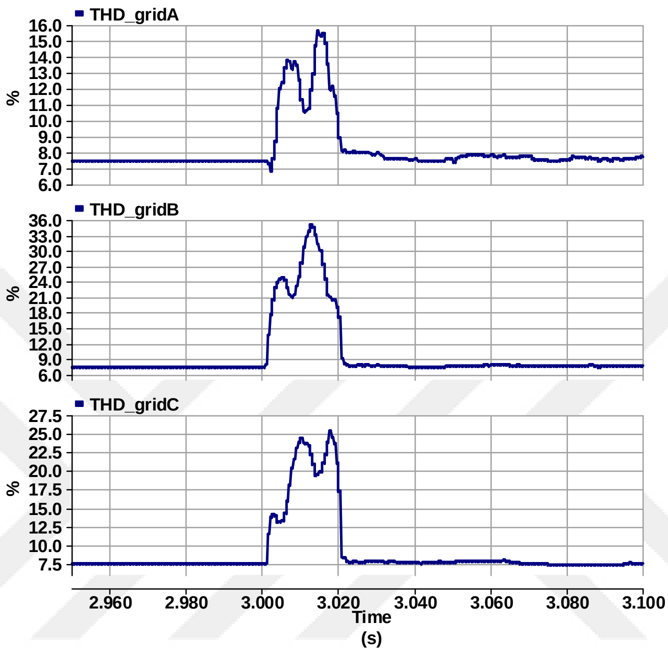

Figure 6.5 THD values under transient conditions

6.2. Comparison Results of Examined Methods for Determination of Starting-time/Ending-time of Voltage Dips

Figure 6.6 presents the amplitude information of 3-ϕ grid-side voltages by using ISRF, EPLL, SOGI, SDFT and FFT methods.

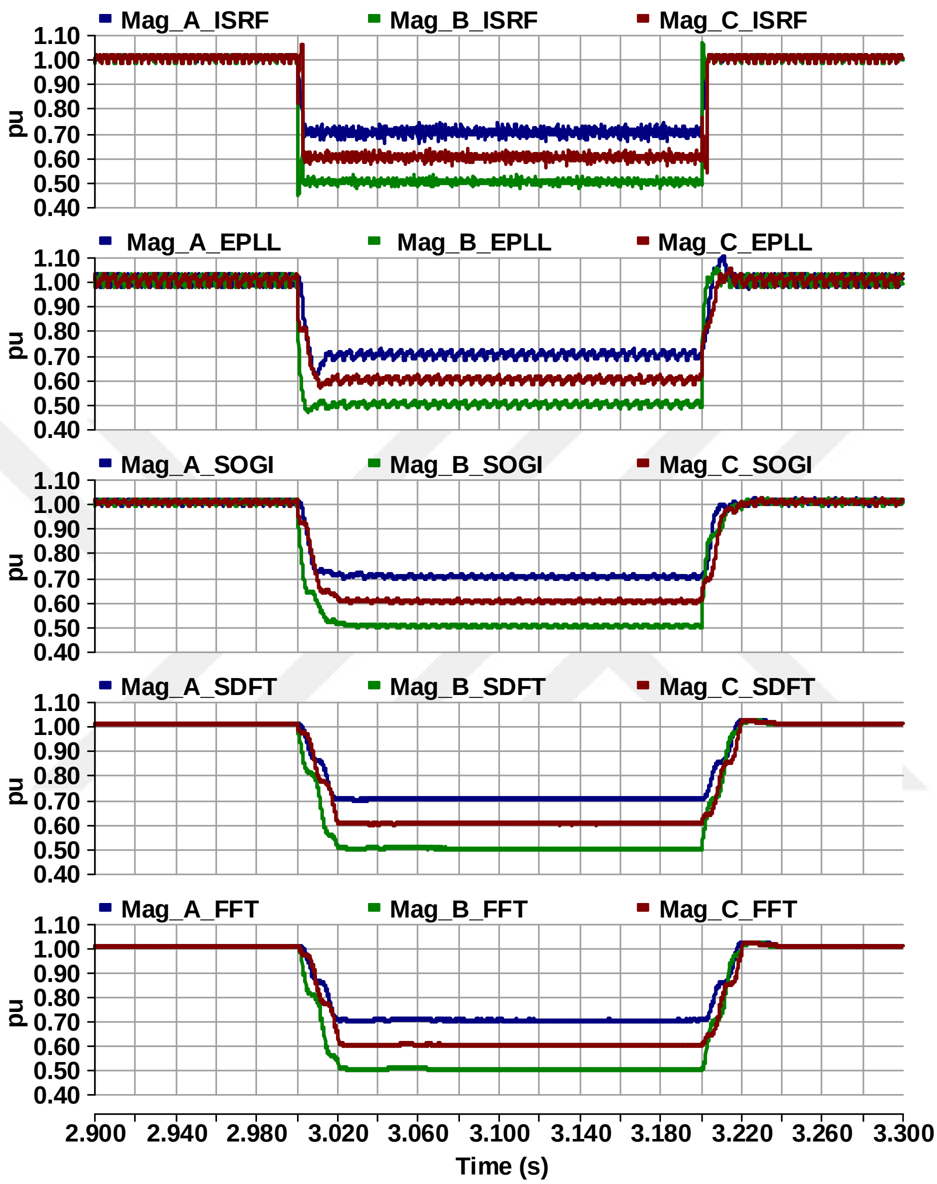

Figure 6.6 Magnitude waveforms in pu for performance comparison results

Figure 6.7 presents the detection speed of 3-ϕ asymmetrical voltage dips at grid-side voltages by using ISRF, EPLL, SOGI, SDFT and FFT methods for starting times of voltage dips.

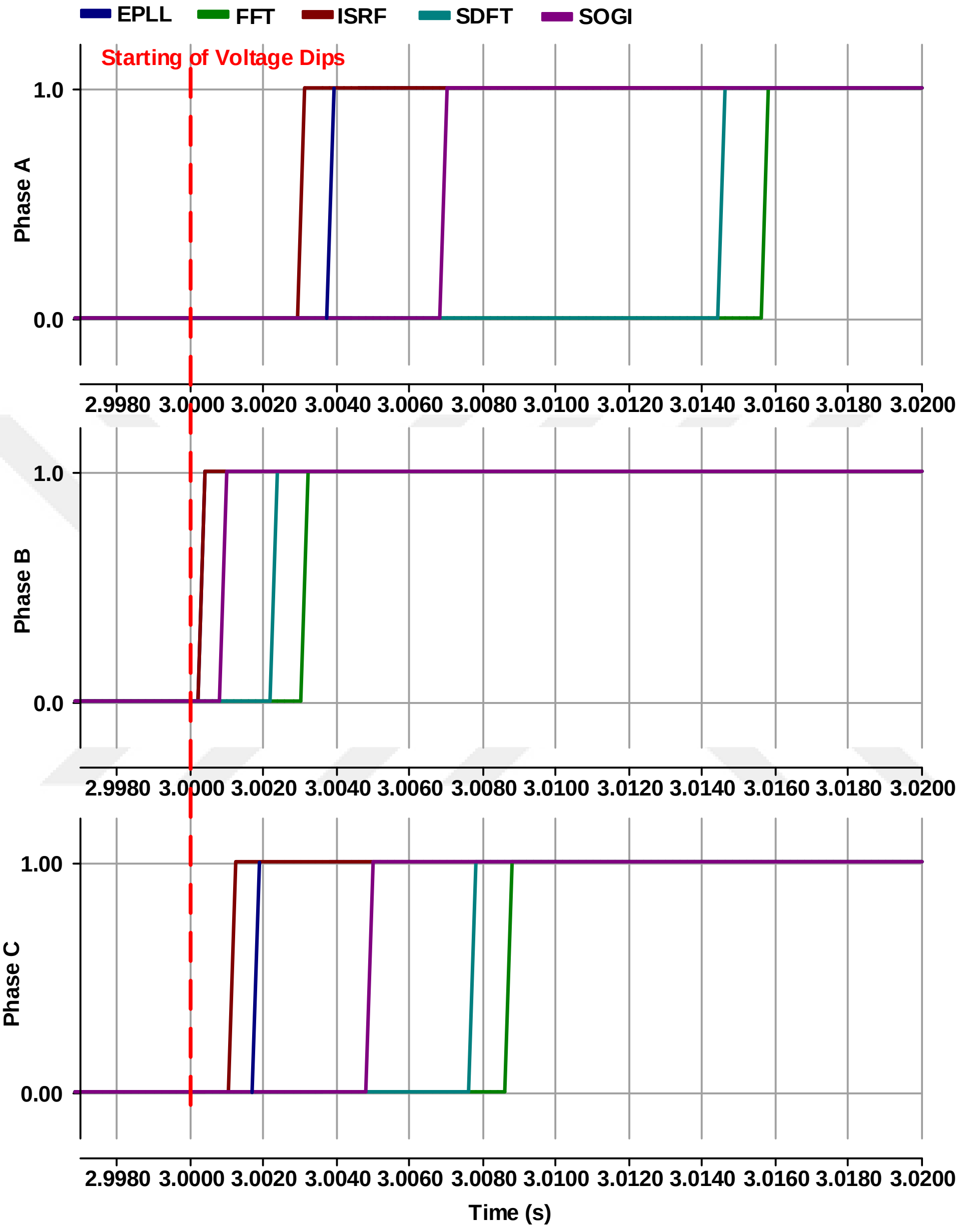

Figure 6.7 Detection speed of starting of voltage dips for different methods

Figure 6.8 presents the detection speed of 3-ϕ asymmetrical voltage dips at grid-side voltages by using ISRF, EPLL, SOGI, SDFT and FFT methods for ending times of voltage dips.

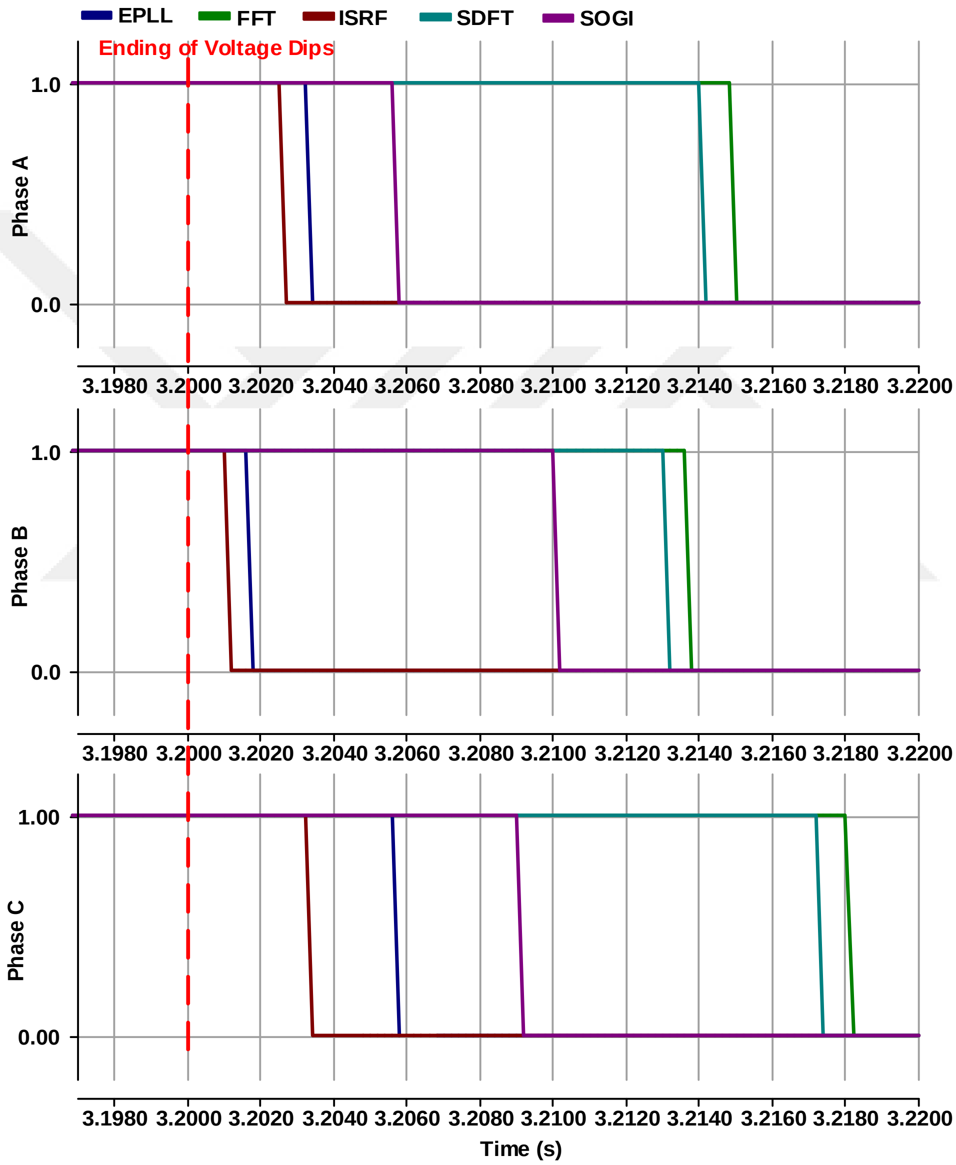

Figure 6.8 Detection speed of ending of voltage dips for different methods

Figure 6.9 presents the generated reference signals by using ISRF, EPLL, SOGI, SDFT and FFT methods for 3-ϕ asymmetrical voltage dips at grid-side voltages.

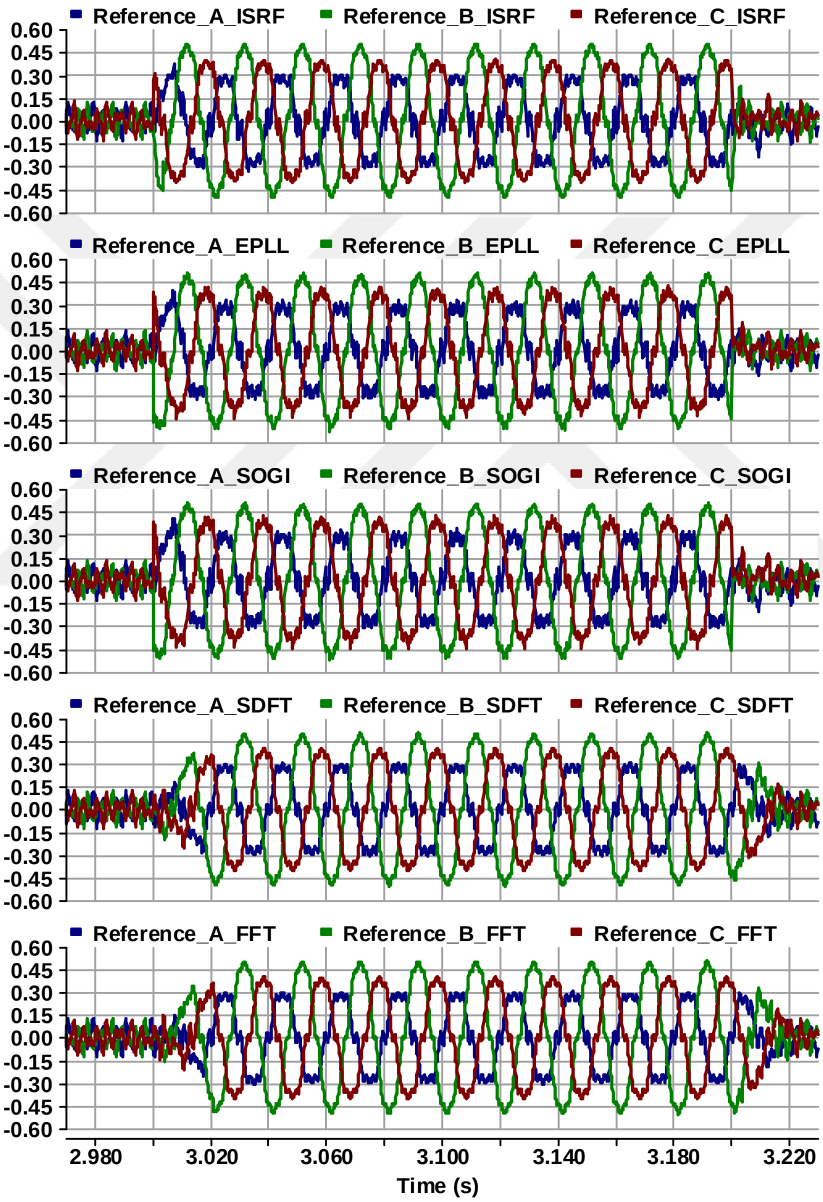

Figure 6.9 Generated reference signals by using different detection methods

After asymmetrical voltage dip situation starts, ISRF achieves the detection of voltage dips within 3.1 ms, 0.2 ms and 1.1 ms for phase-a, phase-b and phase-c, respectively. When voltage dips finish, ISRF detects the ends of voltage dips within 2.3 ms, 1 ms and 3.2 ms. The results show that ISRF based dip/swell detection give faster response compared to other methods.

The performance comparison results and detection speeds of start/end times of proposed method and SCSRF are given in Table 6.2 and 6.3, respectively.

Table 6.2 Performances of examined methods for detection of starting time of voltage dips

	Phase-a	Phase-b	Phase-c
ISRF	3.1 ms	0.2 ms	1.1 ms
EPLL	3.8 ms	0.2 ms	1.9 ms
SOGI	6.9 ms	0.8 ms	4.8 ms
SDFT	14. 5 ms	2.3 ms	7.6 ms
FFT	15.8 ms	3.1 ms	8.7 ms

Table 6.3 Performances of examined methods for detection of ending time of voltage dips

	Phase-a	Phase-b	Phase-c
ISRF	2.3 ms	1 ms	3.2 ms
EPLL	3.5 ms	1.7 ms	5.8 ms
SOGI	5.5 ms	10.2 ms	9.1 ms
SDFT	14.1 ms	13.0 ms	17.3 ms
FFT	14.9 ms	13.6 ms	18. 2 ms

6.3. Performance Results of Simultaneous Compensation of Voltage Dips and Voltage Harmonics

In this section, the performance results for compensation of voltage harmonics+dips, performance results of ISRF, EPLL, SOGI-PLL, SDFT and FFT based controllers are presented.

Figure 6.10 shows the performance results for ISRF controlled DVR in order to provide LVRT during voltage dips and continuous voltage harmonic compensation, simultaneously.

Figure 6.11 shows the performance results for EPLL controlled DVR in order to provide LVRT during voltage dips and continuous voltage harmonic compensation, simultaneously.

Figure 6.12 shows the performance results for SOGI-PLL controlled DVR in order to provide LVRT during voltage dips and continuous voltage harmonic compensation, simultaneously.

Figure 6.13 shows the performance results for SDFT controlled DVR in order to provide LVRT during voltage dips and continuous voltage harmonic compensation, simultaneously.

Figure 6.14 shows the performance results for FFT controlled DVR in order to provide LVRT during voltage dips and continuous voltage harmonic compensation, simultaneously.

6.3.1. ISRF

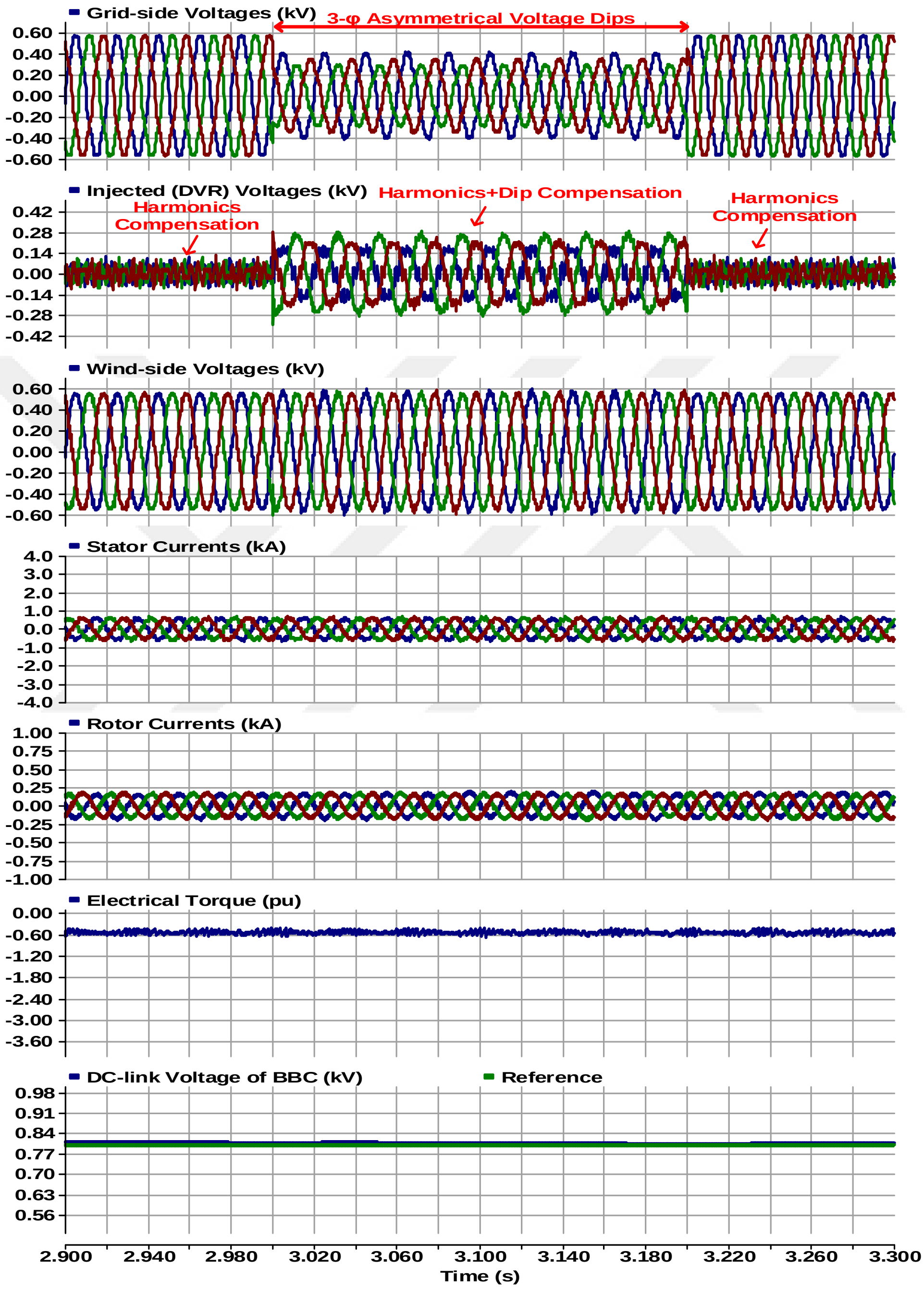

Figure 6.10 Compensation of voltage harmonics+dips by using ISRF method

6.3.2. EPLL

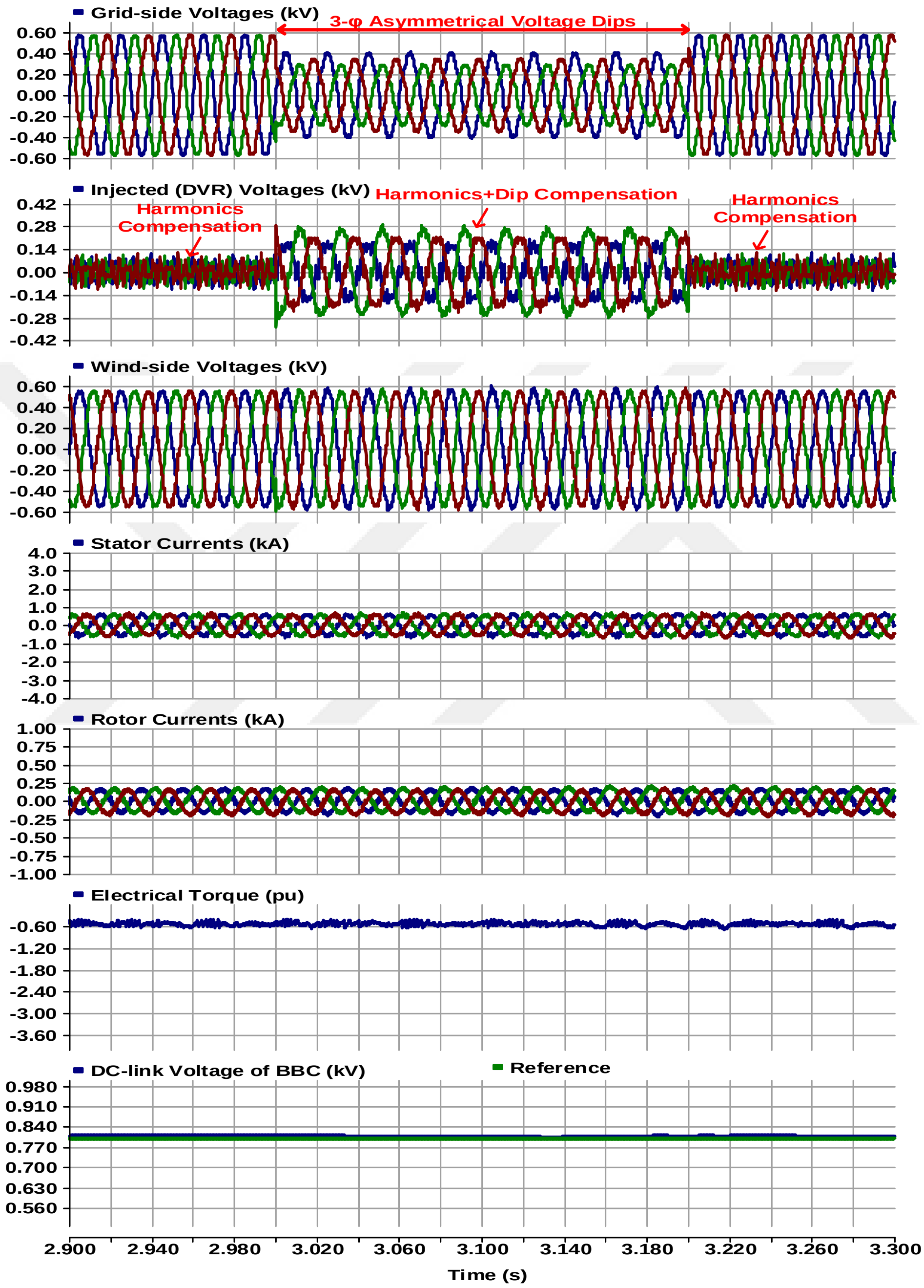

Figure 6.11 Compensation of voltage harmonics+dips by using EPLL method

6.3.3. SOGI-PLL

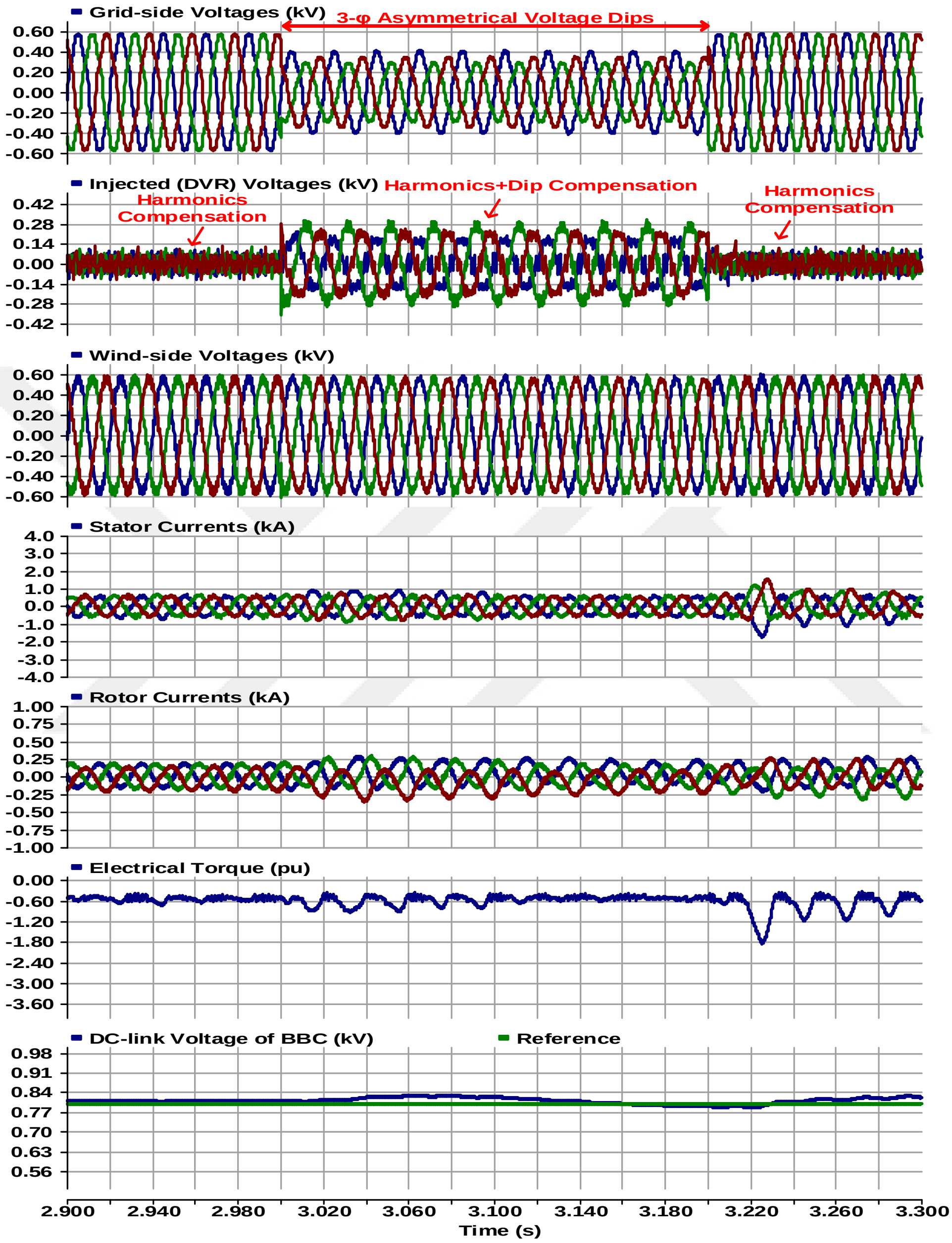

Figure 6.12 Compensation of voltage harmonics+dips by using SOGI-PLL

6.3.4. SDFT

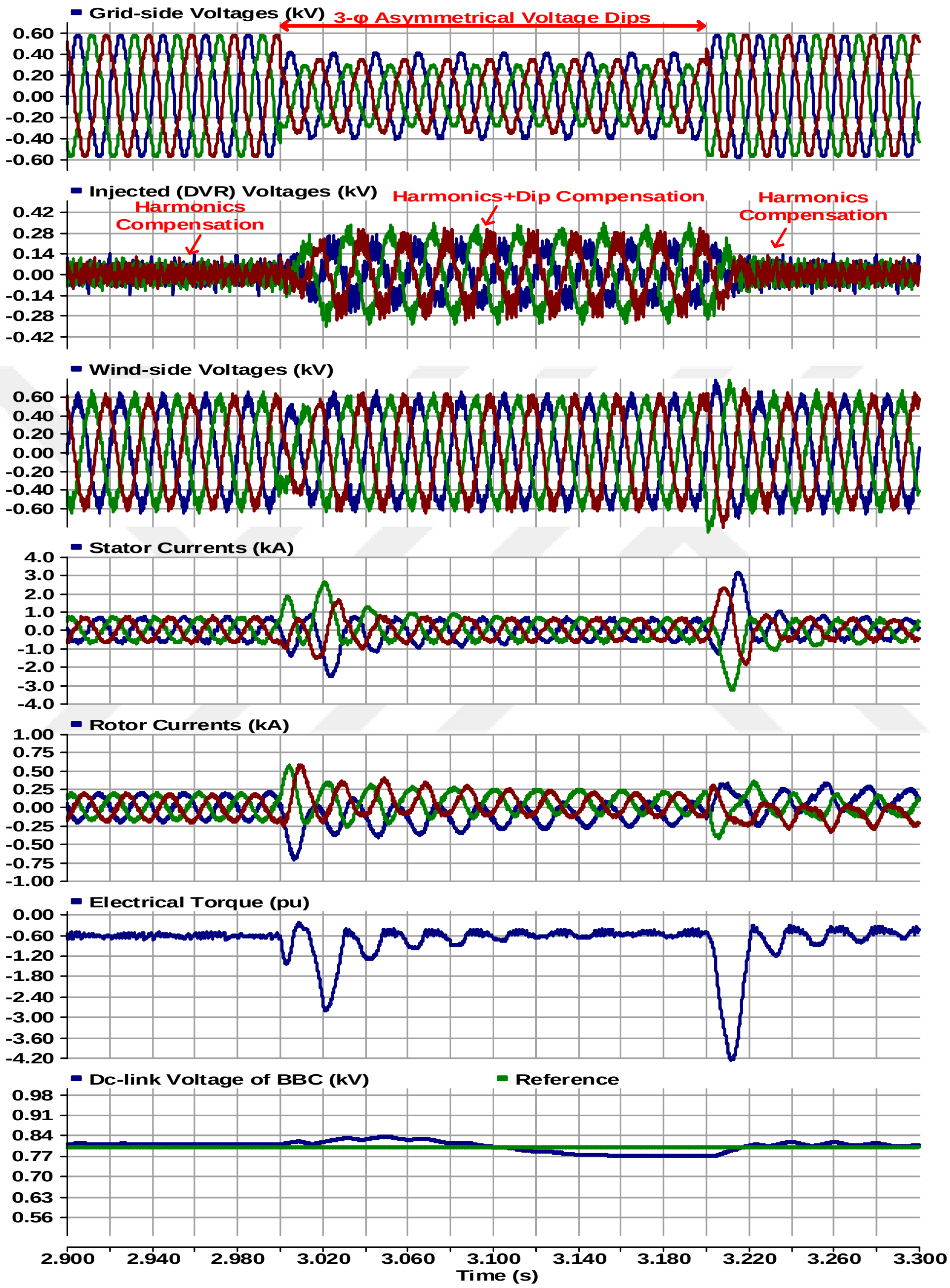

Figure 6.13 Compensation of voltage harmonics+dips by using SDFT method

6.3.5. FFT

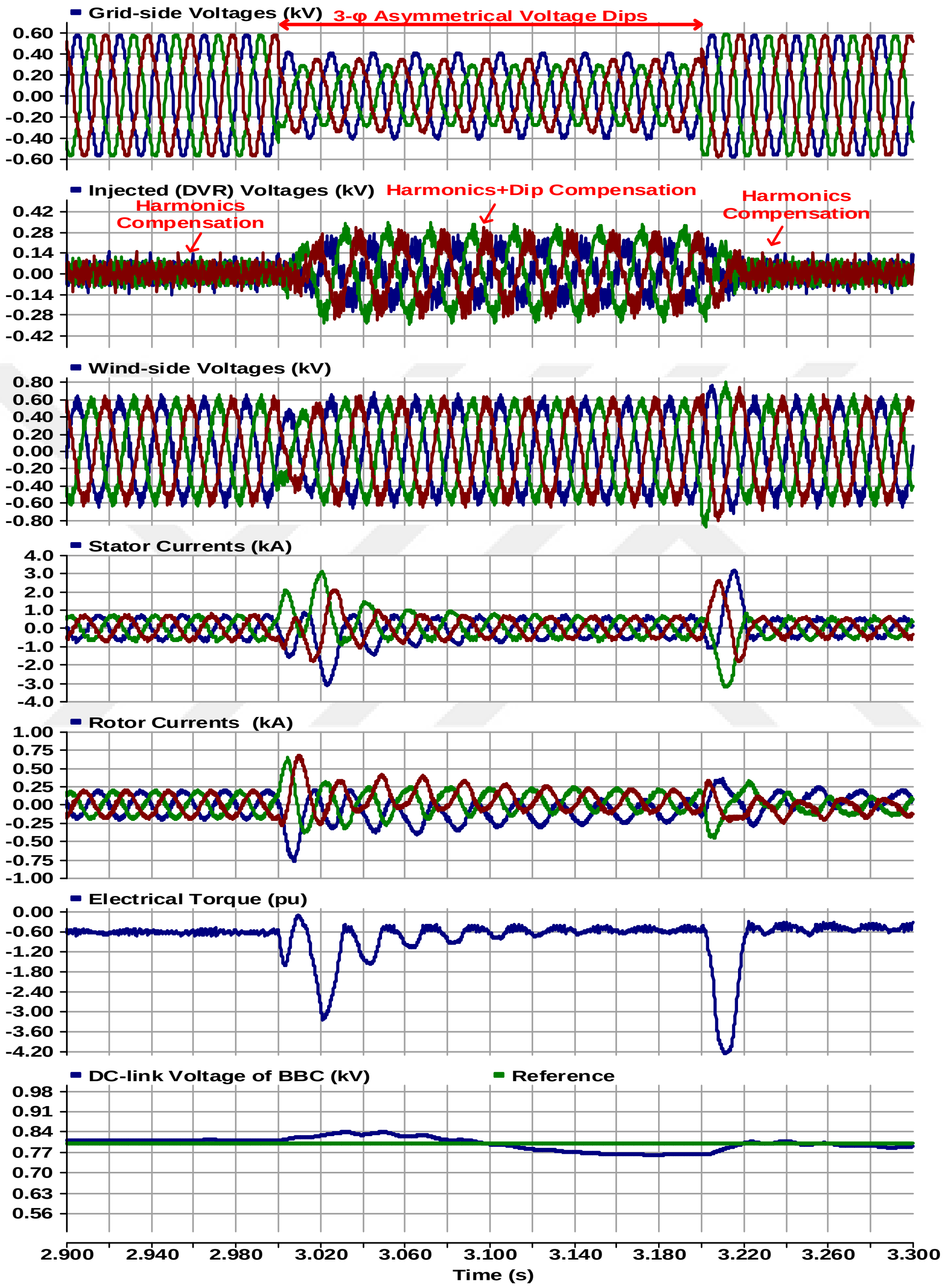

Figure 6.14 Compensation of voltage harmonics+dips by using FFT method

6.4. THD Values According to Controller Methods

In performance results, THD values are tested for steady-state and transient conditions.

6.4.1. THD Values for Steady-State Conditions

THD values at grid-side voltages are equal to 7.45% for phase- a, phase-b and phase-c. Figure 6.15 presents the performances of harmonic compensation by using ISRF method. It is shown that ISRF achieves the mitigation of harmonics from 7.45% to nearly 1.55 %. Figure 6.16 and Figure 6.17 introduces the performance results for EPLL and SOGI-PLL methods. It is shown that these methods can mitigate to nearly 1.8 % and 2.1% at wind-side voltages, respectively. Also, the performances of SDFT and FFT are presented in Figure 6.(18-19), respectively. SDFT and FFT reduce THD levels less than 2% at wind-side.

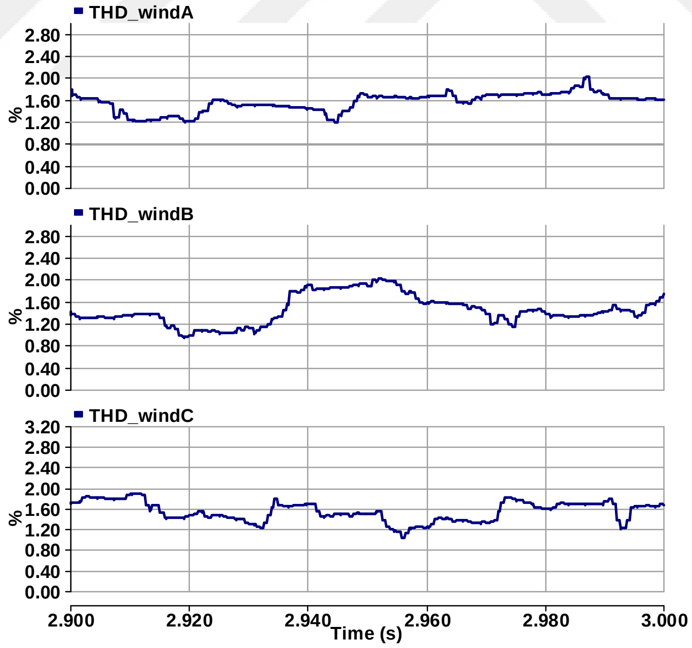

Figure 6.15 THD values for ISRF method

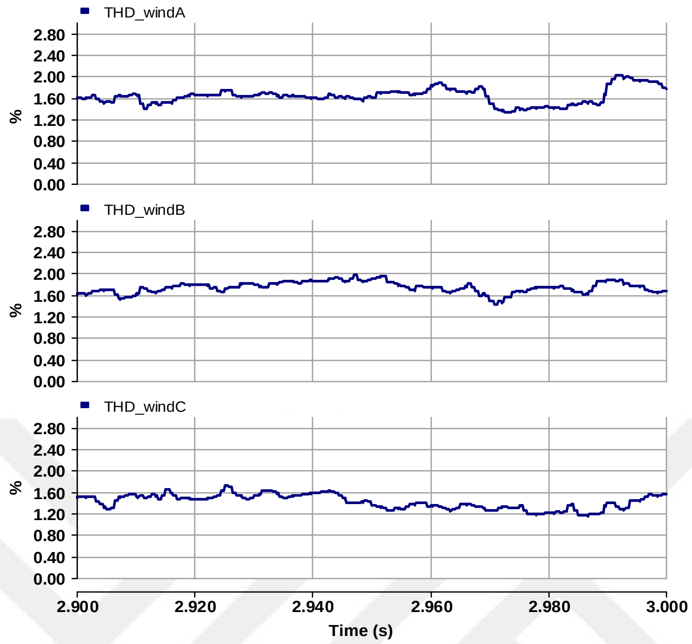

Figure 6.16 THD values for EPLL method

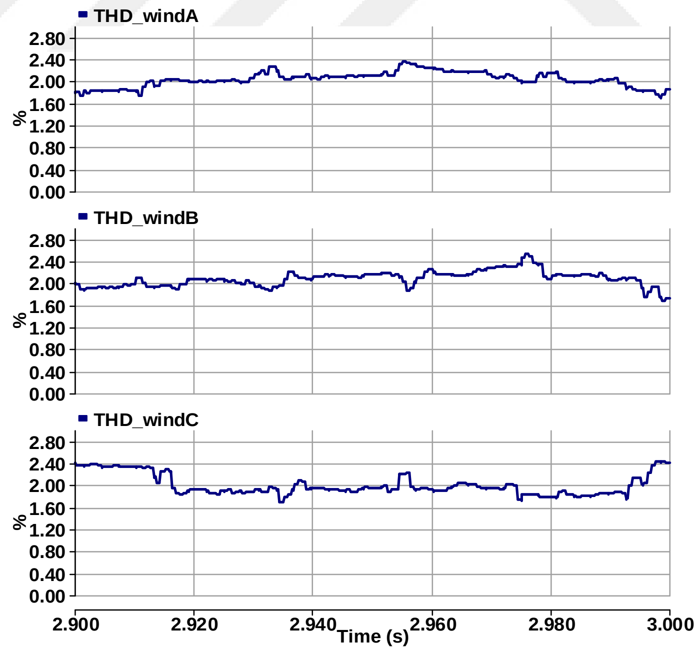

Figure 6.17 THD values for SOGI-PLL based method

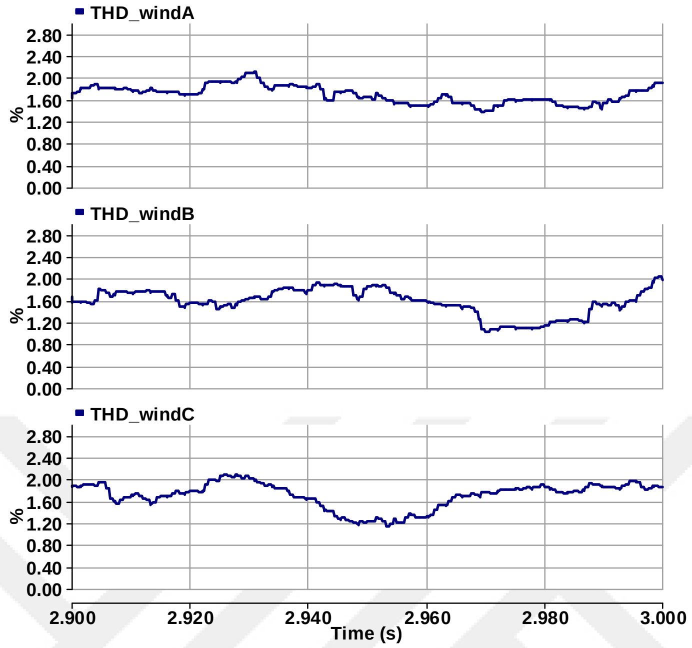

Figure 6.18 THD values for SDFT based method

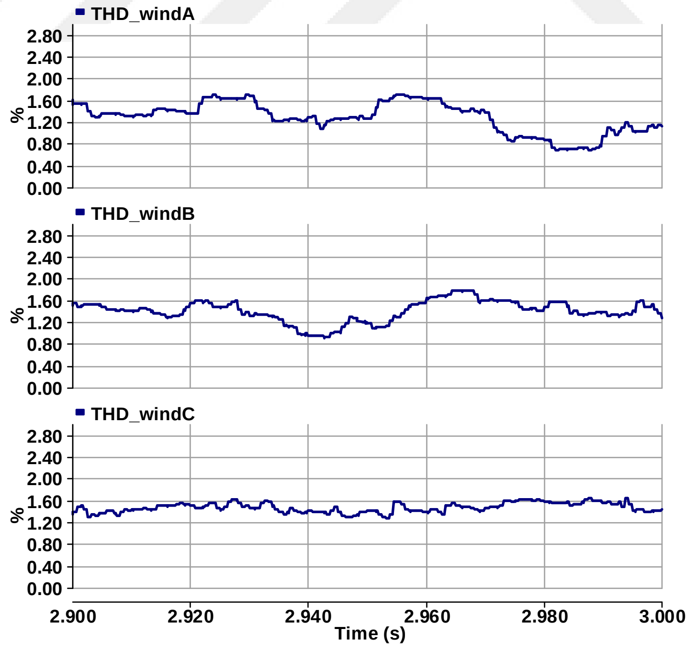

Figure 6.19 THD values for FFT based method

THD value at grid-side voltages is equal to nearly 7.45%. After compensation, THD values at wind side voltages by using different reference generation methods are introduced in Table 6.4.

Table 6.4 THD values at wind-side voltages according to different methods

THD:7.45%	ISRF	EPLL	SOGI	SDFT	FFT
Wind-side	1.55%	1.8%	2.1%	1.8%	1.45%

6.4.2. THD Values for Transient Conditions

In transient conditions, THD values in grid-side voltages are nearly 16 % for phase a, 36% for phase b and 25.5 % for phase c. Figure 6.20 presents ISRF based harmonic compensation under transient conditions. It can achieve superior performance for transient condition and keeps THD values less than 2%. Figure 6.21 and Figure 6.22 introduce the transient performance results of EPLL and SOGI-PLL, respectively. The results show that EPLL and SOGI-PLL have the worse performances compared to ISRF. The performances of SDFT and FFT are presented in Figure 6.23 and Figure 6.24, respectively. These methods show the worst performances among all examined methods.

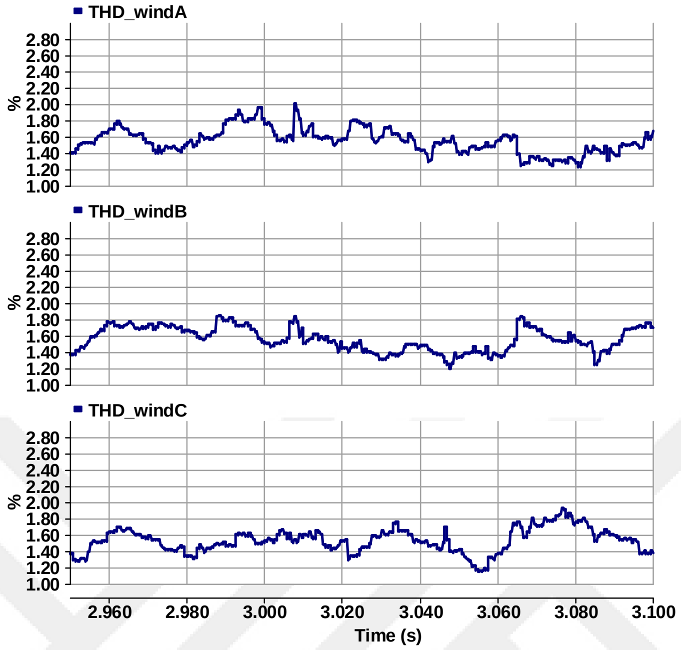

Figure 6.20 Transient condition: THD values for ISRF method

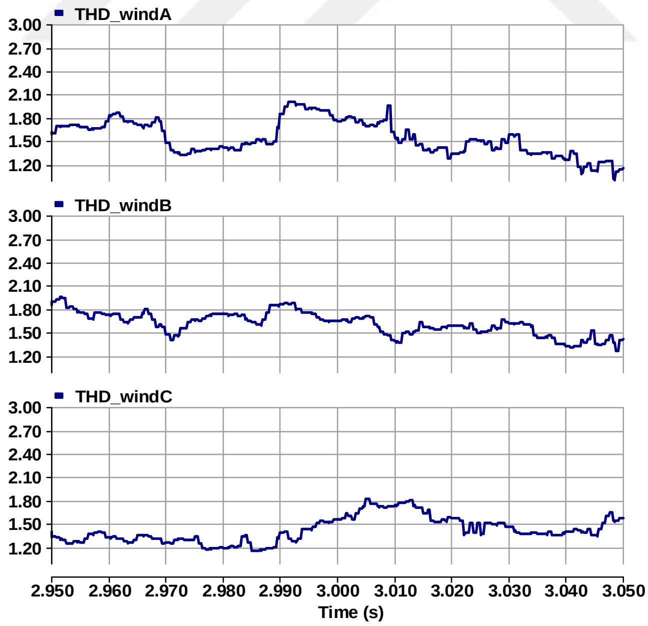

Figure 6.21 Transient condition: THD values for EPLL method

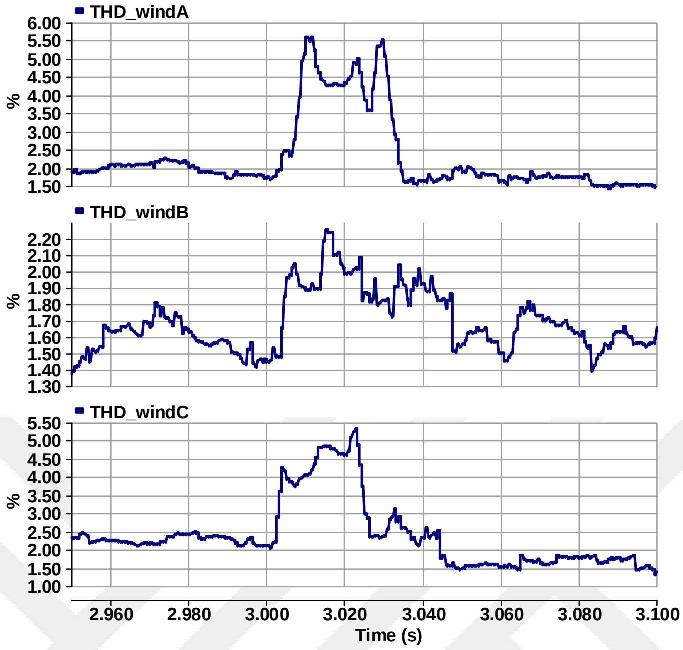

Figure 6.22 Transient condition: THD values for SOGI-PLL method

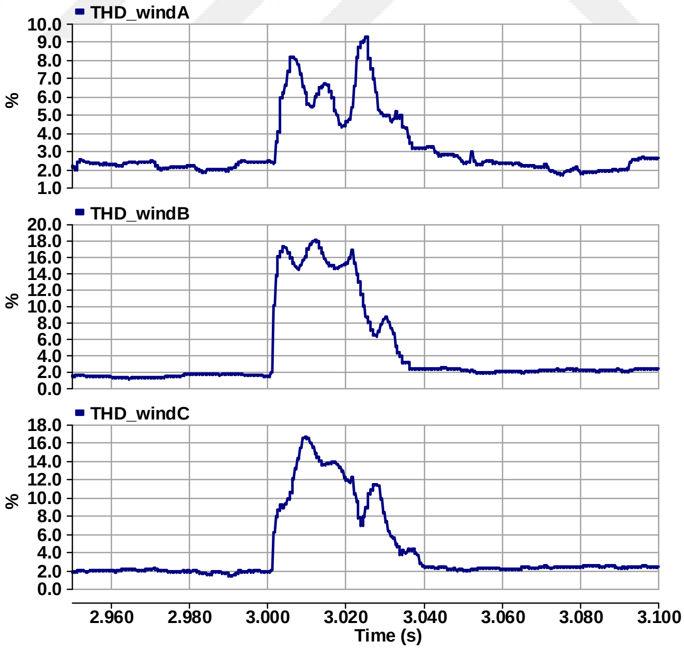

Figure 6.23 Transient condition: THD values for SDFT method

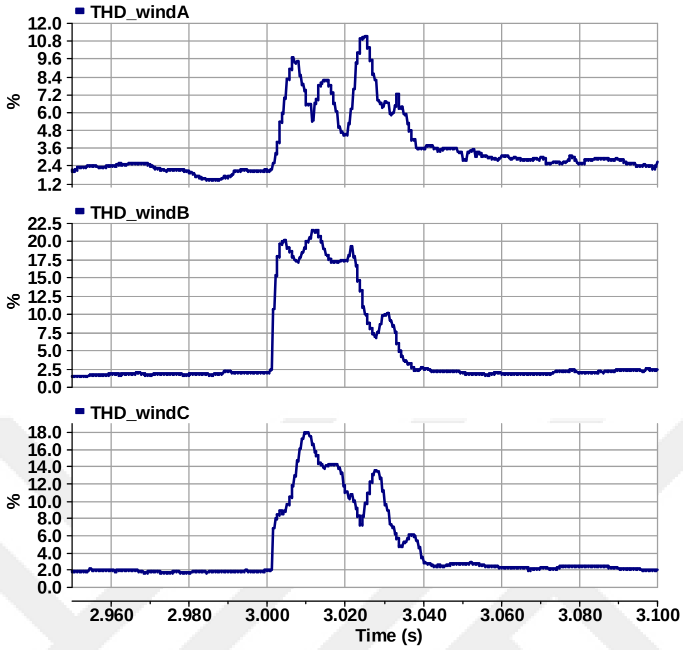

Figure 6.24 Transient condition: THD values for FFT method

After compensation, THD values at grid side and wind side voltages by using different reference generation methods for transient conditions are introduced in Table 6.5.

Table 6.5 THD values at grid-side and wind-side voltages by using different methods under transient conditions

		Phase A	Phase B	Phase C
Before	THD	16 %	35.5 %	25 %
After	ISRF	1.7 %	1.7 %	1.7 %
	EPLL	1.8 %	1.8 %	1.8 %
	SOGI	5.6 %	2.3 %	5.4 %
	SDFT	9.2 %	18.1 %	16.4 %
	FFT	11.9 %	21.9 %	17.9 %

6.5. Discussion

In this chapter, the compensation results of 3-ϕ asymmetrical voltage dips at grid-side voltages with harmonics and their affects have been presented in order to fulfill voltage stability at wind-side voltages. In order to prevent the negative influences like high stator/rotor currents and torque oscillations, ISRF, EPLL, SOGI-PLL, SDFT and FFT are used to generate reference signals for compensation of voltage dips/swells and harmonics. The main property of all methods is that they are applicable for each phase, separately. Also, they can compensate voltage dips/swell and voltage harmonics simultaneously. However, they shows different responses against voltage dips/swells and voltage harmonics. In Table 6.5, the general properties and capabilities of examined methods are presented.

Table 6.6 Comparison of examined methods

	ISRF	EPLL	SOGI	SDFT	FFT
Speed for detection of dips/swell	+++	+++	++	+	+
Harmonic mitigation	+++	+	++	+++	+++
Mitigation of Harmonics Types	All	All	All	Selective	Selective
Additional PLL	Yes	No	No	No	No
Magnitude information	Yes	Yes	Yes	Yes	Yes

+++=Very Good, ++=Good, += Not Good

According to comparison values of examined methods, ISRF and EPLL are the fastest methods to detect voltage dips after the occurrence of faults. The responses of ISRF, EPLL, SOGI are enough to compensate voltage dips and prevent the occurrence of high generator currents. However, performance results show that SDFT and FFT aren’t fast enough to detect voltage dips after the faults. In harmonic compensation capabilities, ISRF achieves the better harmonic mitigation compared to other methods. SDFT and FFT can compensate selective voltage harmonics in contrast to other methods.

7. PERFORMANCE RESULTS AND CASE STUDIES

In this section, different case studies are tested to show the performance results of Topology-I and Topology-II for LVRT/HVRT capability under dip/swell conditions and harmonic compensation. ISRF based controller method is used to generate reference signals for compensation processes in case studies.

7.1. Performance of Topology-I

The single line scheme of ISRF controlled Topology I is presented in Figure 7.1. As shown in scheme, the dc-link capacitor is supplied through a battery.

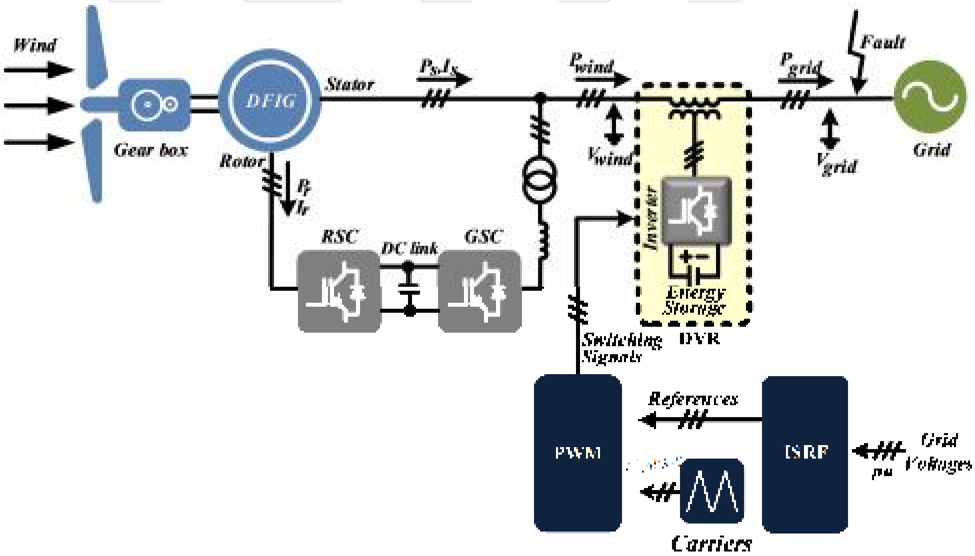

Figure 7.1 Single line scheme of ISRF controlled Topology I

Different case studies are presented for voltage stability of wind system by using Topology I. These case studies are:

Case I: Simultaneous compensation of symmetrical 3-ϕ voltage dips and symmetrical voltage harmonics (THD=6.91%).

Case II: Simultaneous compensation of asymmetrical 2-ϕ voltage dips and asymmetrical voltage harmonics.

Case III: Simultaneous compensation of symmetrical 3-ϕ voltage swells for HVRT and symmetrical voltage harmonics.

Case IV: Simultaneous compensation of asymmetrical single-ϕ voltage swells and asymmetrical voltage harmonics.

7.1.1. Case I

In Case I, a symmetrical fault situation and its effect on DFIG are analyzed. A voltage dip of 30%, symmetrical fault occurs at three phases for 5 cycles which starts at t=3.6 s. Also, voltage harmonics (THD for all phases is 6.91%) distorts voltage waveform continuously at grid-side voltages. The rms value of three-phase grid side voltage decreases to 278.6 Vrms (0.7 pu) from 398 Vrms (1 pu) at all phases. Figure 7.2 presents the influence of three-phase 30% voltage dips with harmonics voltage at grid-side voltages. In the absence of voltage dip compensation, the fault at grid-side induces higher rotor/stator currents during fault and immediately after the fault. Additionally, the oscillations of electrical torque are other important problems. With compensation by using DVR, generator side voltages are kept almost constant by an in-phase injection of voltage in series. As shown in Figure 7.3, the results show that DVR prevents current transients of rotor/stator by compensation of faults. In addition to mitigation of the high values in stator/rotor currents and it keeps electrical torque at prior values during faults. Figure 7.4 presents clear voltage waveforms for voltage harmonic compensation between t=3.52 s and t=3.58 s. The general information on Case I is given in Table 7.1. The THD values at grid-side and wind-side voltages are presented in Figure 7.5. As shown in THD values, DVR reduces THD values to approximately 1.55% for three phases at wind side voltages.

Table 7.1 Dip depth, THD, the fundamental and selective components of distorted grid-side voltages for Case I

		Phase A	Phase B	Phase C
Dip Depth		0.3 pu	0.3 pu	0.3 pu
THD at grid-side		6.91%	6.91%	6.91%
THD at wind-side		≈1.6%	≈1.55%	≈1.5%
The components of Grid-side Voltages	f1=50 Hz	560 V	560 V	560 V
	f5=250 Hz	28 V	28 V	28 V
	f7=350 Hz	23V	23V	23V
	f11=550 Hz	12 V	12 V	12 V
	f13=650 Hz	8 V	8 V	8 V

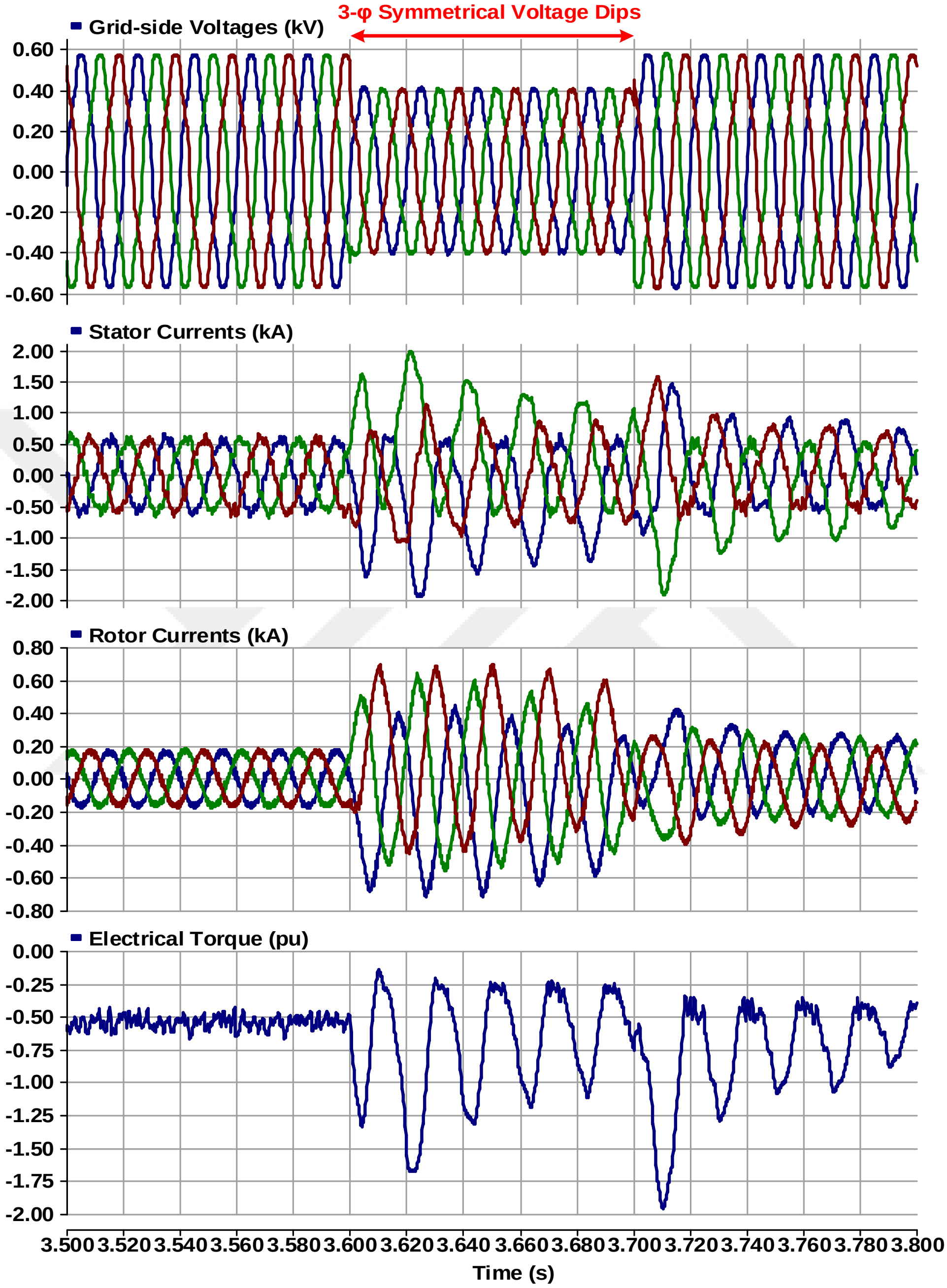

Figure 7.2 The effects of symmetrical 30% voltage dips under distorted grid

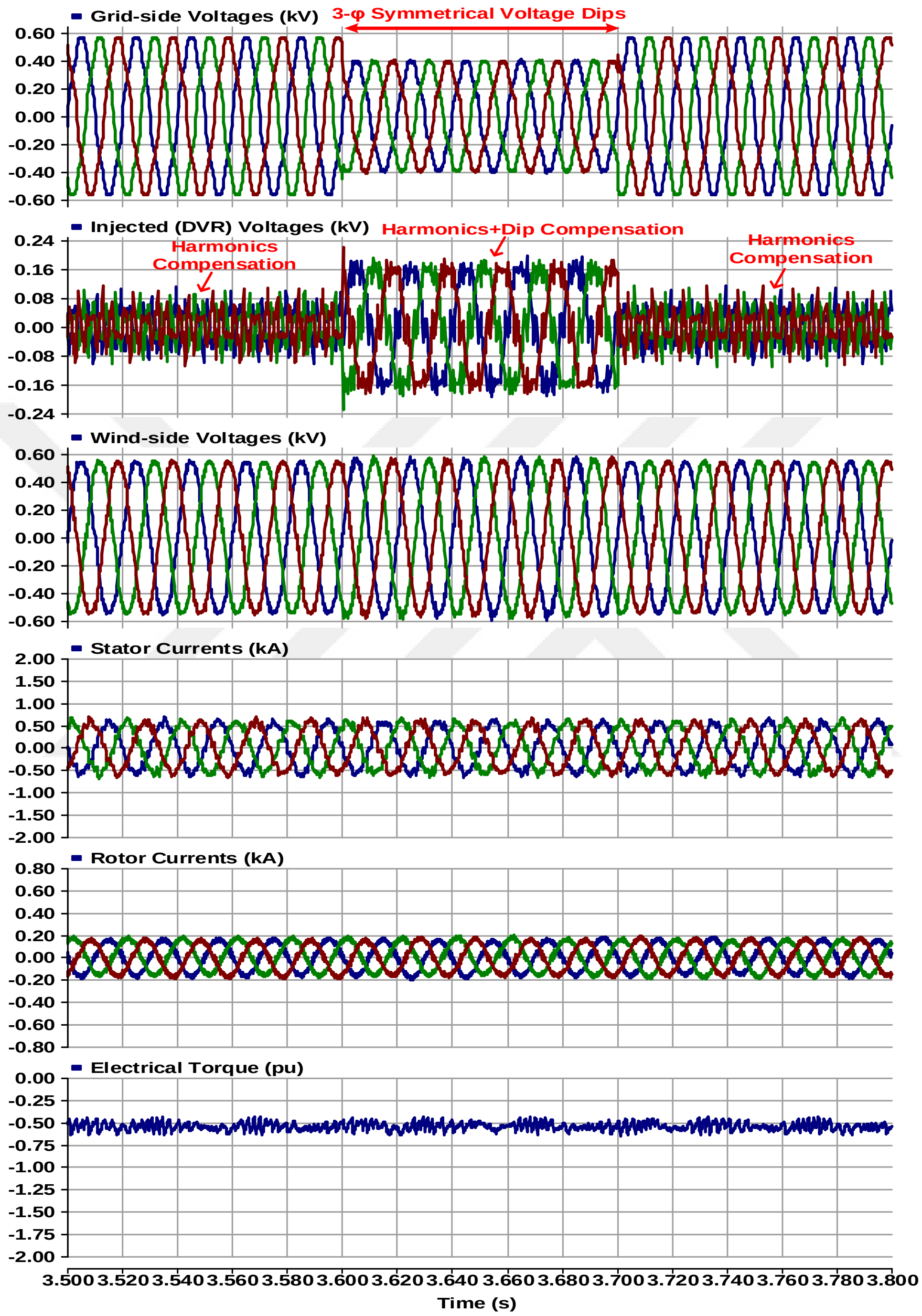

Figure 7.3 Compensation results of symmetrical 30% voltage dips and harmonics for Case I

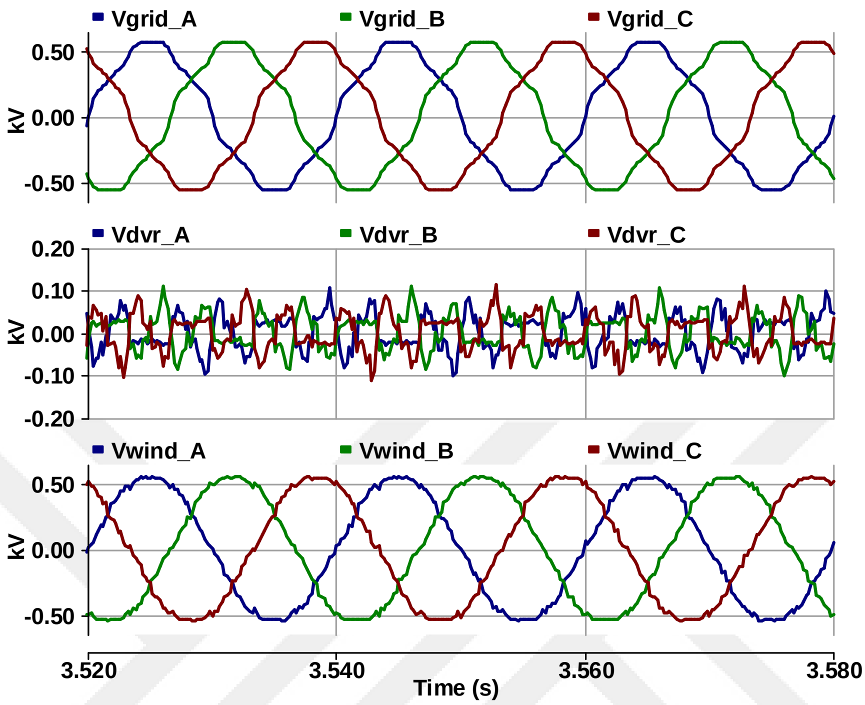

Figure 7.4 Compensation of voltage harmonics for Case I

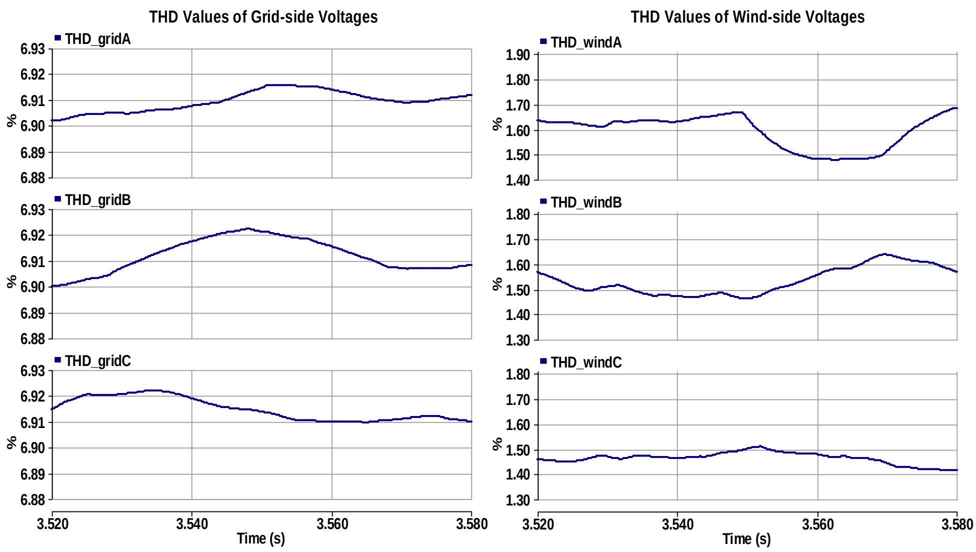

Figure 7.5 THD values of grid- and wind-side voltages for Case I

7.1.2. Case II

In second case called as Case II, asymmetrical fault situation and its effect on DFIG are analyzed. Voltage dips of 0.3 pu and 0.5 pu occur at phase a and phase b and start at t=4.4 s with 160 ms duration. Also, asymmetrical voltage harmonics (THD for phase a is 5.78%, THD for phase b is 9.52% and THD for phase c is 8.23%) distorts voltage waveform continuously at grid-side voltages. The rms value of grid side voltage at phase-a decreases to 278.6 Vrms (0.7 pu) from 398 Vrms (1 pu). The grid side voltage at phase-b decreases to 199 Vrms (0.5 pu) from 398 Vrms (1 pu). Figure 7.6 presents the influence of two-ϕ voltage dips with harmonics voltage at grid-side voltages. In the absence of two-ϕ voltage dip compensation, the fault at grid-side induces higher rotor/stator currents during fault and immediately after the fault, as shown in Figure 7.6. Additionally, the oscillations of electrical torque are other important problems. With compensation by using DVR, generator side voltages are kept almost constant by an in-phase injection of voltage in series. As shown in Figure 7.7, the results show that DVR prevents current transients of rotor/stator by compensation of faults. In addition to mitigation of the high values in stator/rotor currents and it keeps electrical torque at prior values during faults. Figure 7.8 presents clear voltage waveforms for voltage harmonic compensation between t=4.30 s and t=4.36 s. The general information on Case II is given in Table 7.2. The THD values at grid-side and wind-side voltages are presented in Figure 7.9. As shown in THD values, DVR reduces THD values below 1.5% for three phases at wind side voltages.

Table 7.2 Dip depth, THD, the fundamental and selective components of distorted grid-side voltages for Case II

		Phase A	Phase B	Phase C
Dip Depth		0.3 pu	0.5 pu	No dip
THD at Grid-side		5.78%	9.52%	8.23%
THD at Wind-side		≈1.25%	≈1.3%	≈1.45%
The components of Grid-side Voltages	f1=50 Hz	560 V	560 V	560 V
	f5=250 Hz	24 V	38 V	33 V
	f7=350 Hz	19 V	32 V	28 V
	f11=550 Hz	9 V	16 V	14 V
	f13=650 Hz	7 V	13 V	10 V

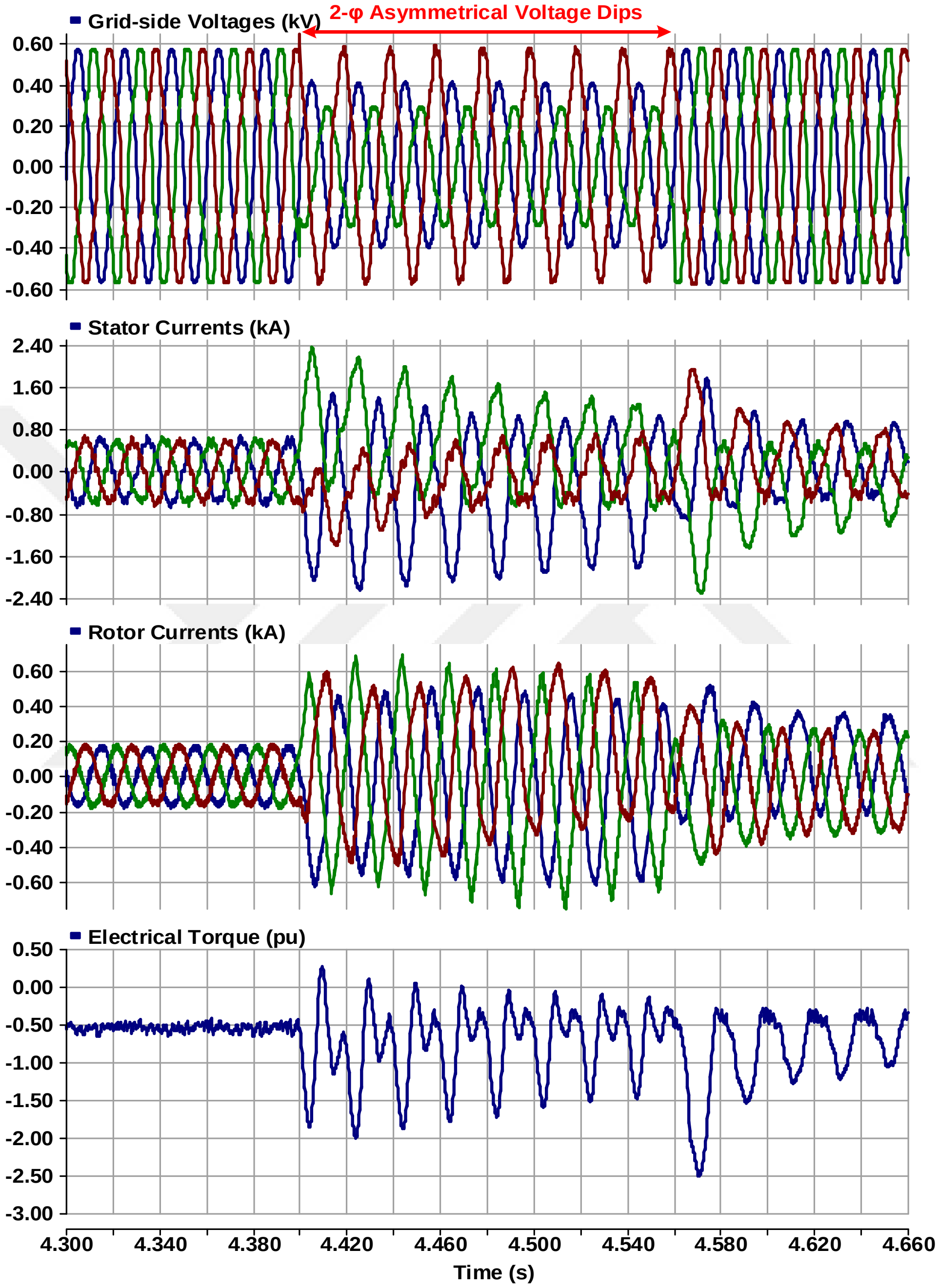

Figure 7.6 The effects of asymmetrical 2-ϕ voltage dips under distorted grid

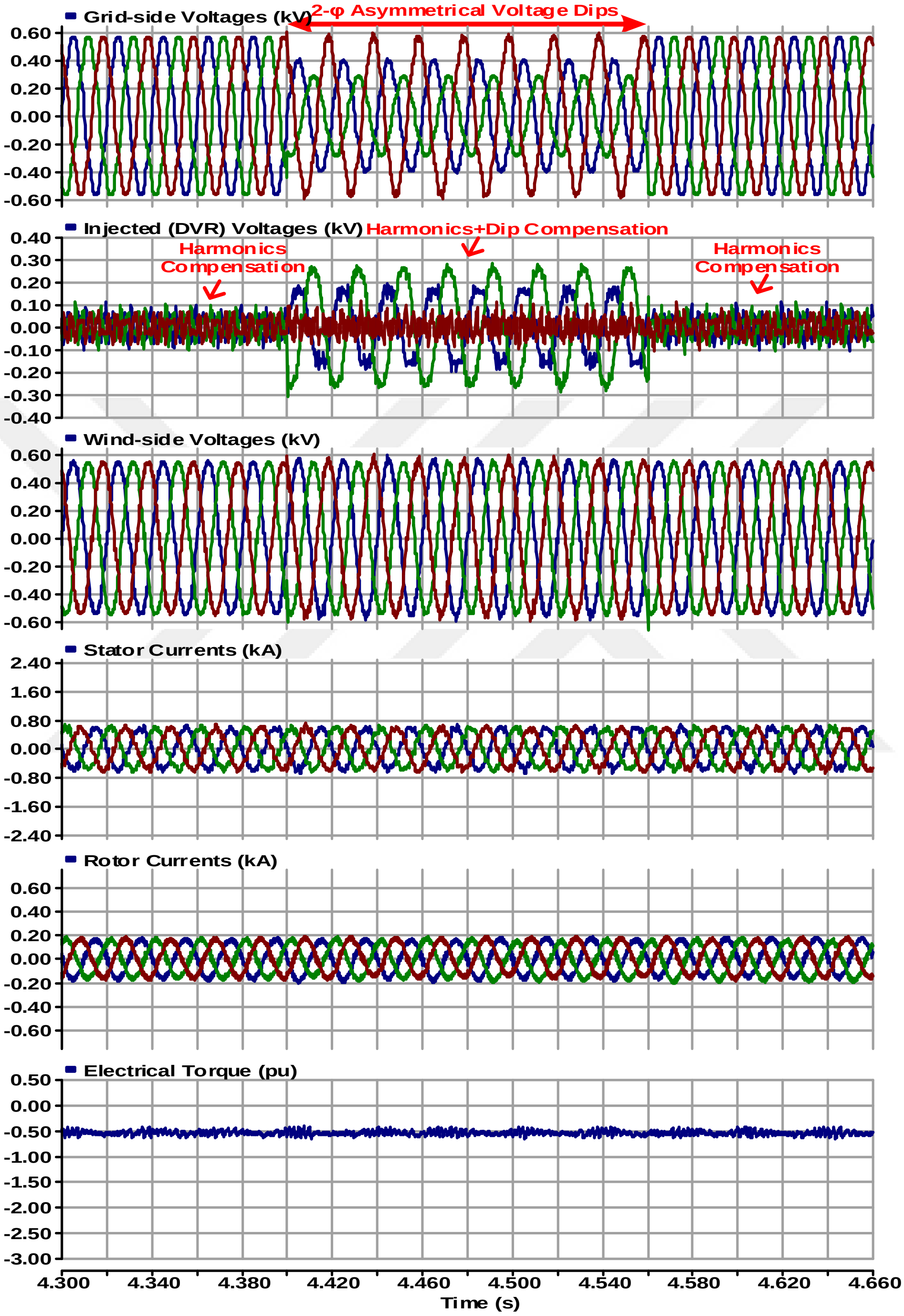

Figure 7.7 Compensation results of asymmetrical 2-ϕ voltage dips and harmonics for Case II

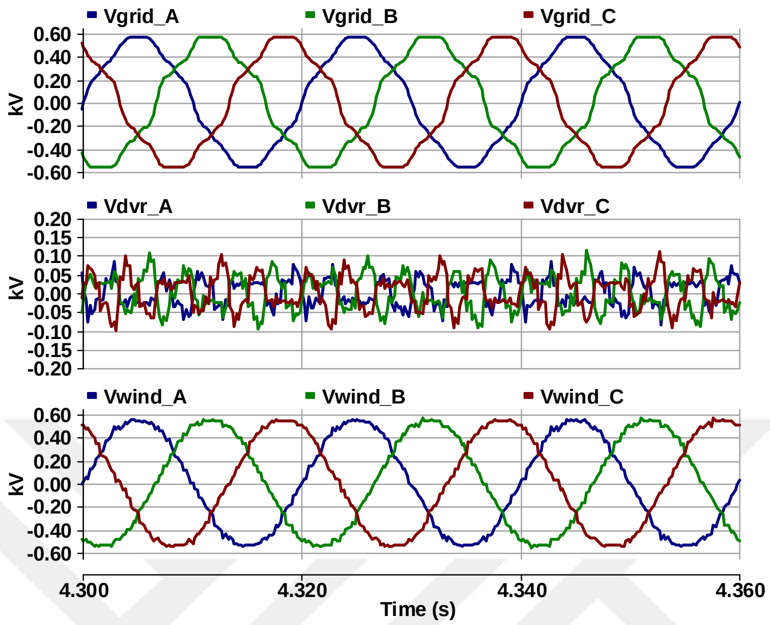

Figure 7.8 Compensation of voltage harmonics for Case II

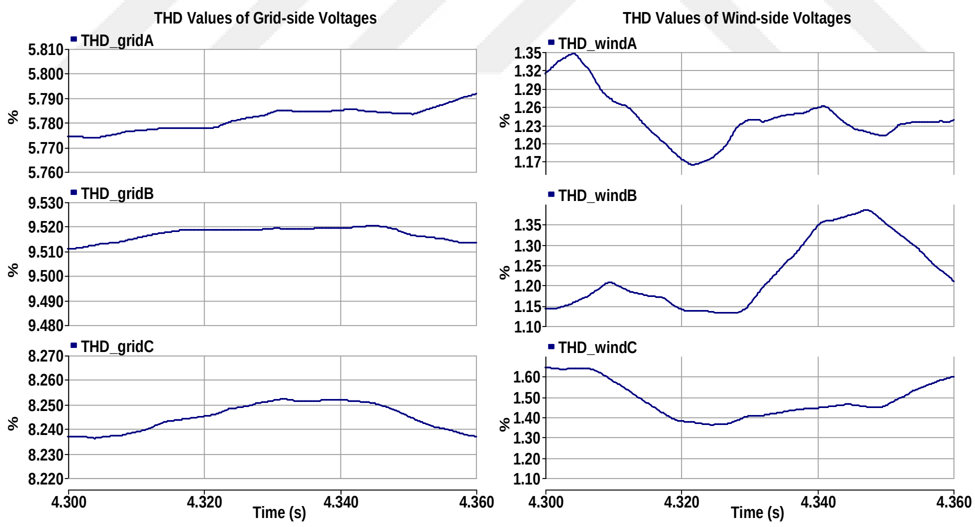

Figure 7.9 THD values of grid- and wind-side voltages for Case II

7.1.3. Case III

In Case III, a symmetrical fault situation and its effect on DFIG are analyzed for HVRT requirement. Symmetrical 30% voltage swell occurs at three phases for 5 cycles which starts at t=5.4 s. Also, voltage harmonics (THD for all phases is 9.08%) distorts voltage waveform continuously at grid-side voltages. The rms value of three-phase grid side voltage increases to 517.4 Vrms (0.7 pu) from 398 Vrms (1 pu) at all phases. Figure 7.10 presents the influence of three-phase 30% voltage swells with harmonics voltage at grid-side voltages. In the absence of voltage swell compensation, the fault at grid-side induces higher rotor/stator currents during fault and immediately after the fault, as shown in Figure 7.10. Additionally, the oscillations of electrical torque are other important problems. With compensation by using DVR, generator side voltages are kept almost constant by an in-phase injection of voltage in series. As shown in Figure 7.11, the results show that DVR prevents current transients of rotor/stator by compensation of faults. In addition to mitigation of the high values in stator/rotor currents and it keeps electrical torque at prior values during faults. Figure 7.12 presents clear voltage waveforms for voltage harmonic compensation between t=5.32 s and t=5.38 s. The general information on Case III is given in Table 7.3. The THD values at grid-side and wind-side voltages are presented in Figure 7.13. As shown in THD values, DVR reduces THD to less values than 2% for three phases at wind side voltages.

Table 7.3 Swell depth, THD, the fundamental and selective components of distorted grid-side voltages for Case III

		Phase A	Phase B	Phase C
Swell Depth		0.3 pu	0.3 pu	0.3 pu
THD at Grid-side		9.08%	9.08%	9.08%
THD at Wind-side		≈1.6%	≈1.2%	≈1.3%
The components of Grid-side Voltages	f1=50 Hz	560 V	560 V	560 V
	f5=250 Hz	36 V	36 V	36 V
	f7=350 Hz	31 V	31 V	31 V
	f11=550 Hz	15 V	15 V	15 V
	f13=650 Hz	12 V	12 V	12 V

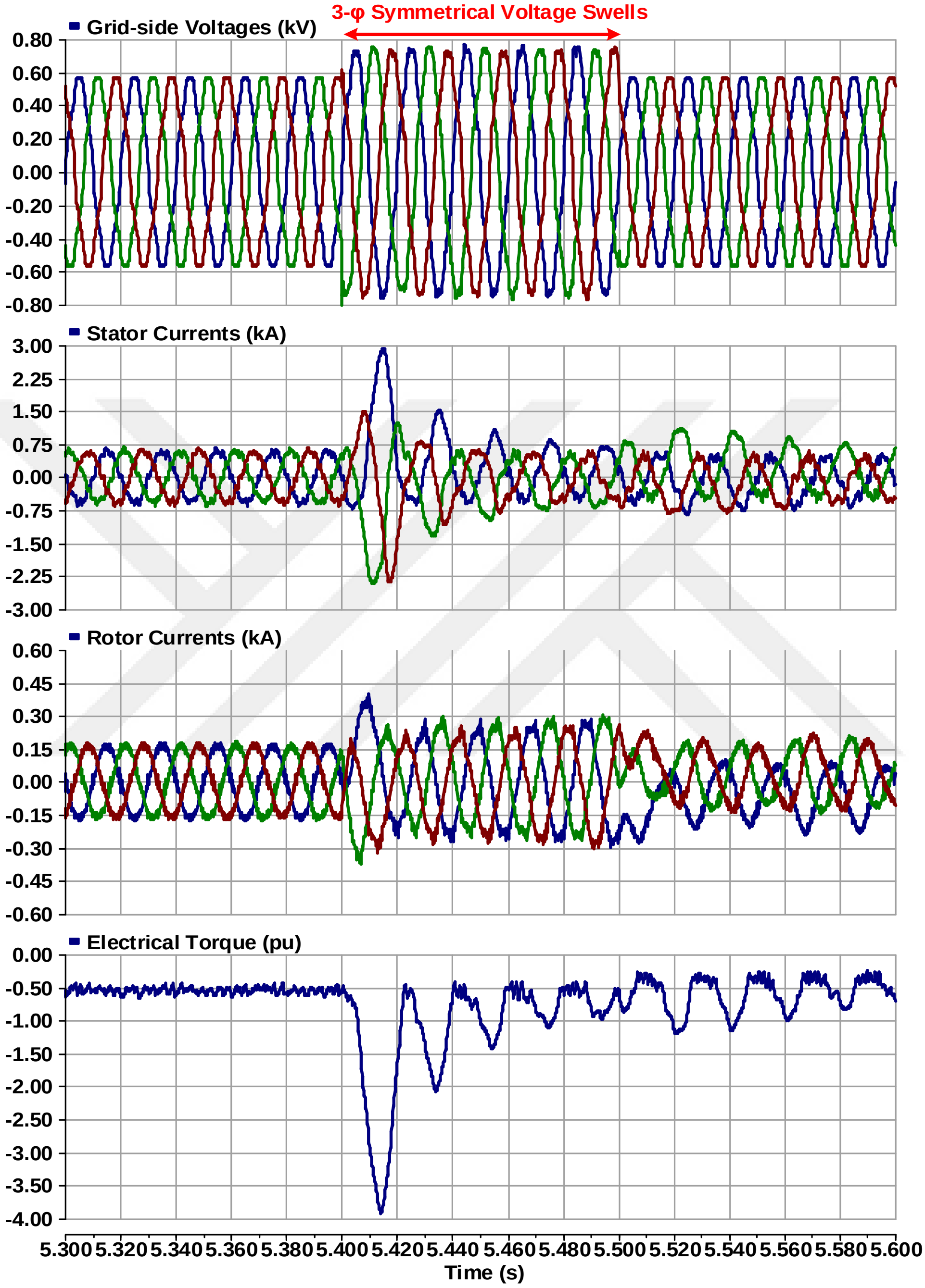

Figure 7.10 The effects of symmetrical 30% voltage swells with distorted grid

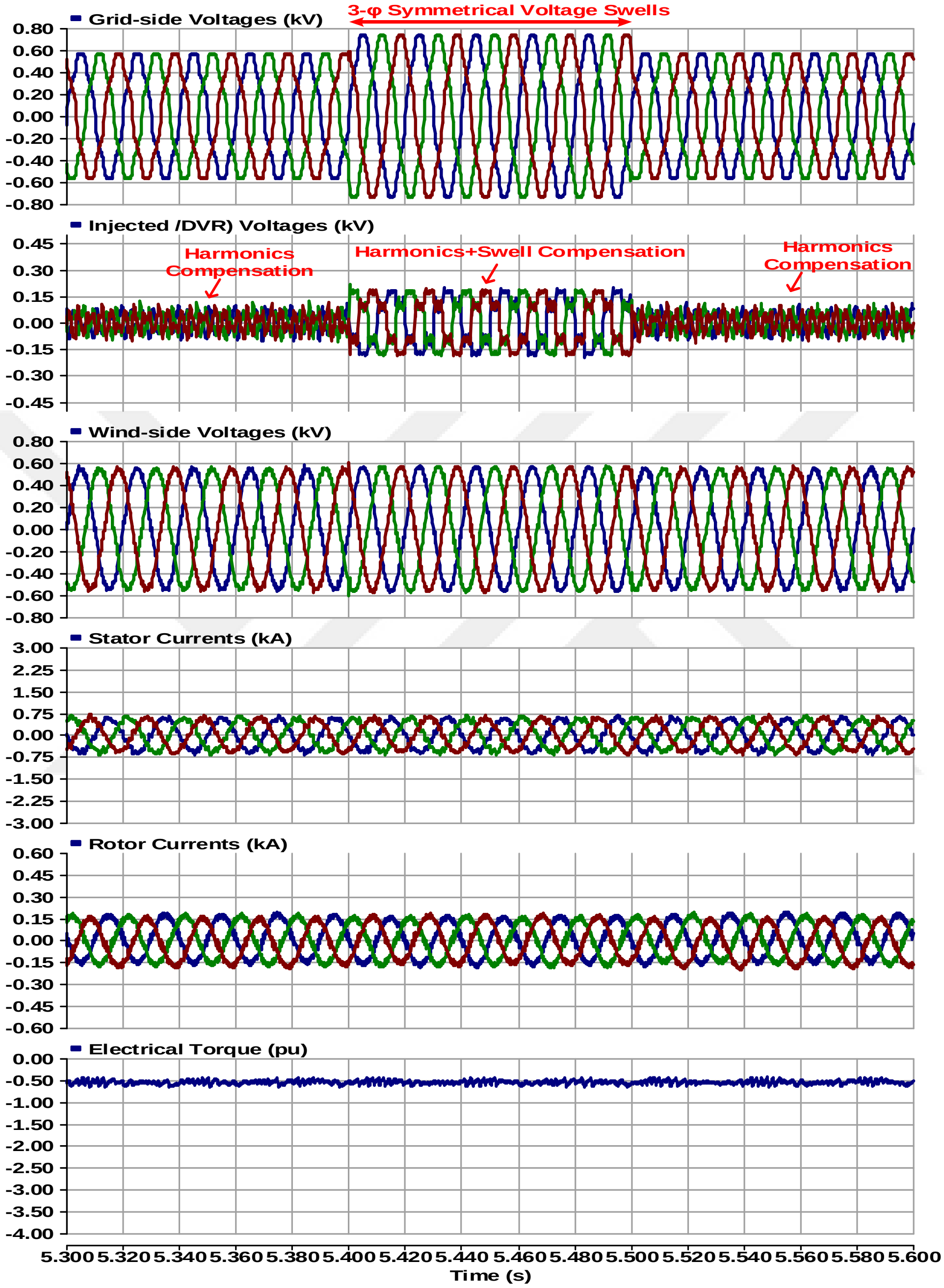

Figure 7.11 Compensation results of symmetrical 30% voltage swells and harmonics for Case III

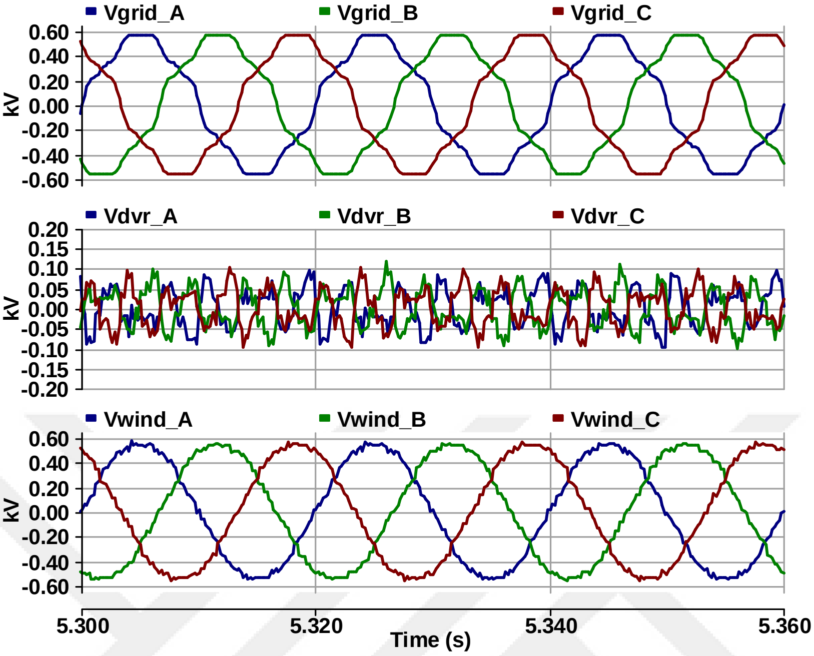

Figure 7.12 Compensation of voltage harmonics for Case III

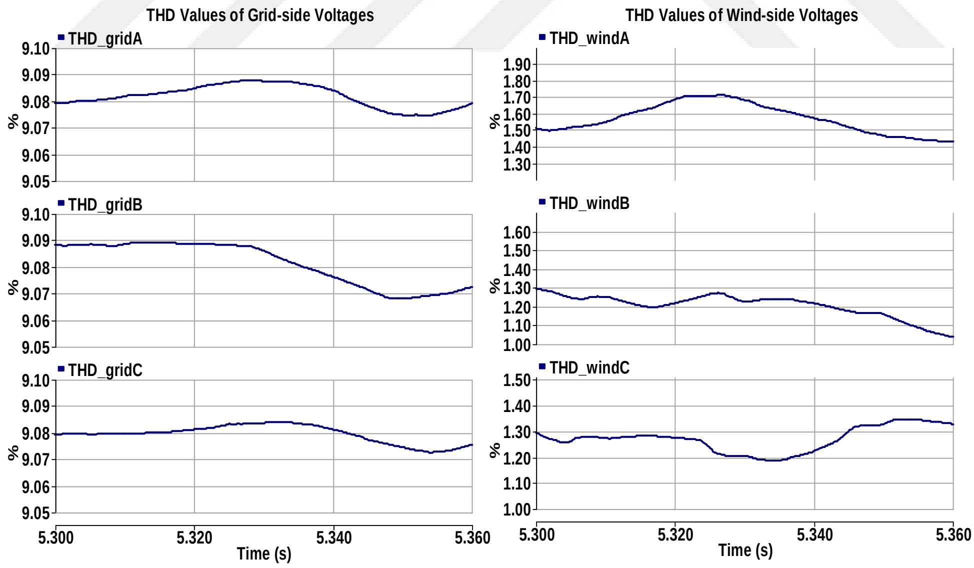

Figure 7.13 THD values of grid- and wind-side voltages for Case III

7.1.4. Case IV

In fourth case called as Case IV, single phase voltage swells and its effect on DFIG are analyzed. Asymmetrical single phase of 0.3 pu voltage swell occurs at phase – b. Voltage swell starts at t=6.1 s and its duration is 120 ms. Also, asymmetrical voltage harmonics (THD for phase a is 6.75%, THD for phase b is 7.54% and THD for phase c is 5.85%) distorts voltage waveform continuously at grid-side voltages. The rms value of grid side voltage at phase-b increases to 517.4 Vrms (1.3 pu) from 398 Vrms (1 pu). Figure 7.14 presents the influence of two-ϕ voltage dips with harmonics voltage at grid-side voltages. In the absence of single-ϕ voltage swell compensation, the fault at grid-side induces higher rotor/stator currents during fault and immediately after the fault, as shown in Figure 7.14. Additionally, the oscillations of electrical torque occur in DFIG. Thanks to compensation by using DVR, generator side voltages are kept almost constant by an in-phase injection of voltage in series. As shown in Figure 7.15, the results show that DVR prevents current transients of rotor/stator by compensation of faults. In addition to mitigation of the high values in stator/rotor currents and it keeps electrical torque at prior values during faults. Figure 7.16 presents clear voltage waveforms for voltage harmonic compensation between t=6.0 s and t=6.06 s. The general information on Case IV is given in Table 7.4. The THD values at grid-side and wind-side voltages are presented in Figure 7.17. As shown in THD values, DVR reduces THD values nearly 1.55%, 1.6% and 1.35% for phase-a, phase-b and phase-c, respectively.

Table 7.4 Swell depth, THD, the fundamental and selective components of distorted grid-side voltages for Case IV

		Phase A	Phase B	Phase C
Swell Depth		No swell	0.3 pu	No swell
THD at Grid-side		6.75%	7.54%	5.85%
THD at Wind-side		≈1.6%	≈1.6%	≈1.4%
The components of Grid-side Voltages	f1=50 Hz	560 V	560 V	560 V
	f5=250 Hz	27 V	30 V	23 V
	f7=350 Hz	22 V	25 V	20 V
	f11=550 Hz	12 V	13 V	10 V
	f13=650 Hz	10 V	11 V	8 V

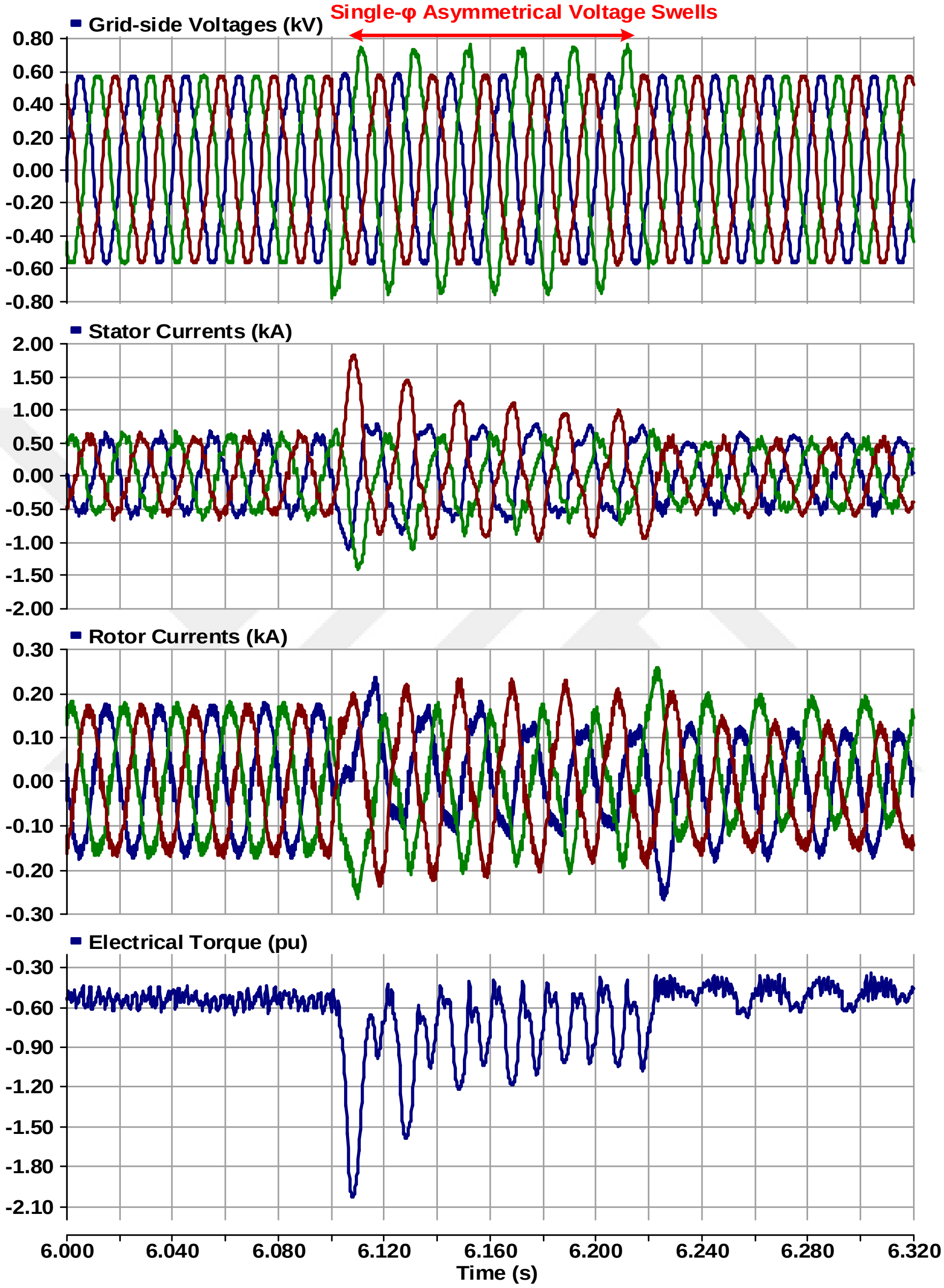

Figure 7.14 The effects of single-ϕ voltage swells under distorted grid

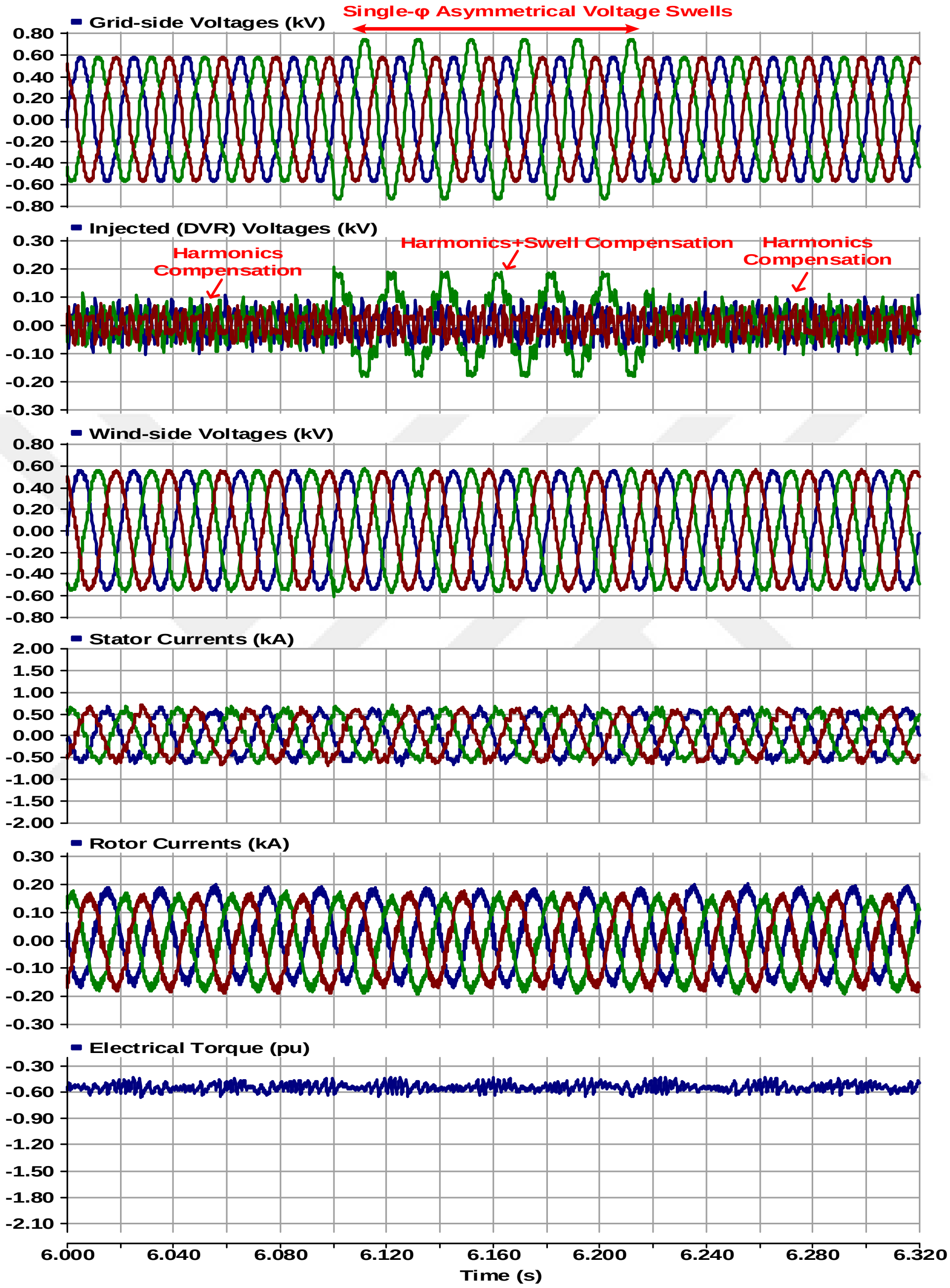

Figure 7.15 Compensation results of asymmetrical single-ϕ voltage swell and voltage harmonics for Case IV

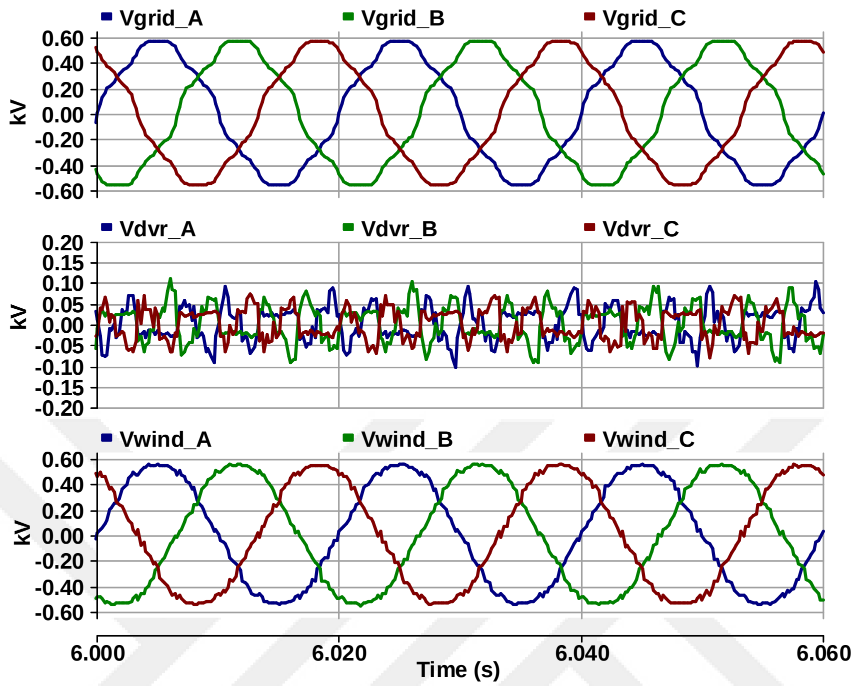

Figure 7.16 Compensation results of asymmetrical voltage harmonics for Case IV

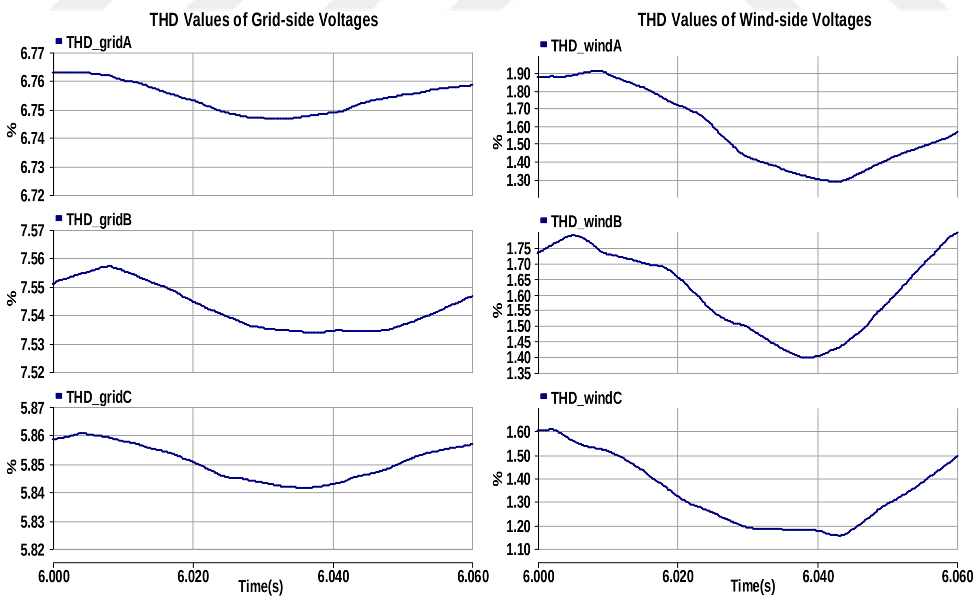

Figure 7.17 THD values of grid- and wind-side voltages for Case IV

7.2. Performance of Topology-II

The single line scheme of ISRF controlled Topology II is presented in Figure 7.18. It is shown that DVR uses the common dc-link capacitors of back-back converters in DFIG.

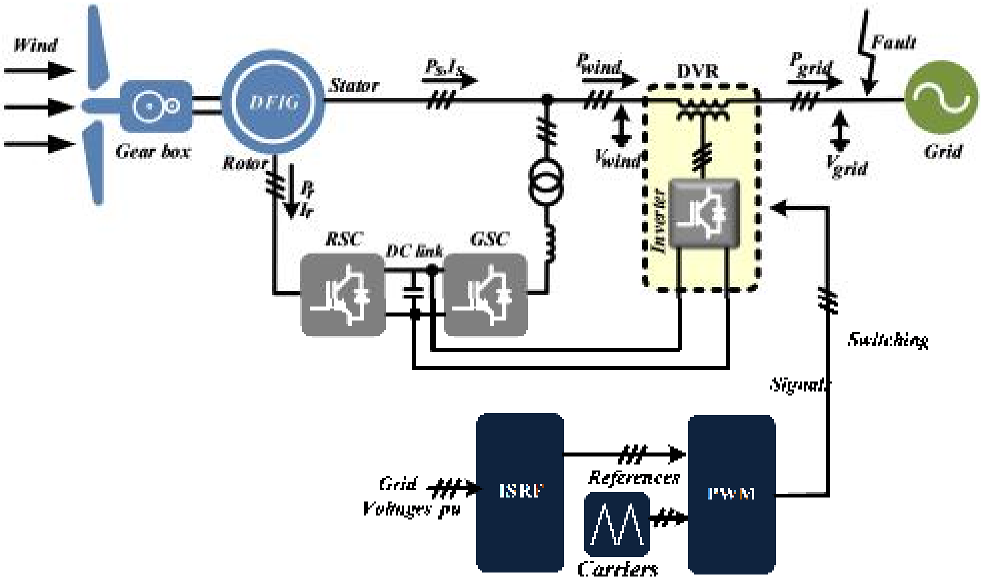

Figure 7.18 Single line scheme of ISRF controlled Topology II

Two different case studies are presented for voltage stability of wind system by using Topology II. These case studies are:

Case V: Simultaneous compensation of asymmetrical two-ϕ voltage dips and asymmetrical voltage harmonics.

Case VI: Simultaneous compensation of asymmetrical two-ϕ voltage swells and asymmetrical voltage harmonics.

7.2.1. Case V

In Case V, asymmetrical 2-ϕ voltage dips and their effects on DFIG are analyzed. Two phase voltage dips at two phases (a and b) occur for 220 ms which starts at t=4.1 s. Also, voltage harmonics (THD for all phases are 6.27%, 8.06% and 7.38%, respectively) distorts voltage waveform continuously at grid-side voltages. The rms value of grid side voltage decreases to 199 Vrms (0.5 pu) from 398 Vrms (1 pu) at phase-a. Figure 7.19 presents the influences of two-phase voltage dips at grid-side voltages with harmonics voltage. In the absence of voltage dip compensation, the fault at grid-side induces higher rotor/stator currents during fault and immediately after the fault, as shown in Figure 7.19. Additionally, the oscillations of electrical torque occur at generator-side. With compensation by using DVR, generator side voltages are kept almost constant by an in-phase injection of voltage in series. As shown in Figure 7.20, the results show that DVR prevents current transients of rotor/stator by compensation of faults. In addition to mitigation of the high values in stator/rotor currents and it keeps electrical torque at prior values during faults. Figure 7.21 presents clear voltage waveforms for voltage harmonic compensation between t=4.04 s and t=4.1 s. The general information on Case V is given in Table 7.5. The THD values at grid-side and wind-side voltages are presented in Figure 7.22. As shown in THD values, DVR reduces THD values nearly 1.7%, 1.65% and 1.8% for three phases at wind side voltages.

Table 7.5 Dip depth, THD, the fundamental and selective components of distorted grid-side voltages for Case V

		Phase A	Phase B	Phase C
Dip Depth		0.4 pu	No dip	0.2 pu
THD at grid-side		6.27%	8.06%	7.38%
THD at wind-side		≈1.7%	≈1.65%	≈1.8%
The components of Grid-side Voltages	f1=50 Hz	560 V	560 V	560 V
	f5=250 Hz	25 V	32 V	29 V
	f7=350 Hz	20 V	26 V	24 V
	f11=550 Hz	12 V	15 V	14 V
	f13=650 Hz	9 V	12 V	11 V

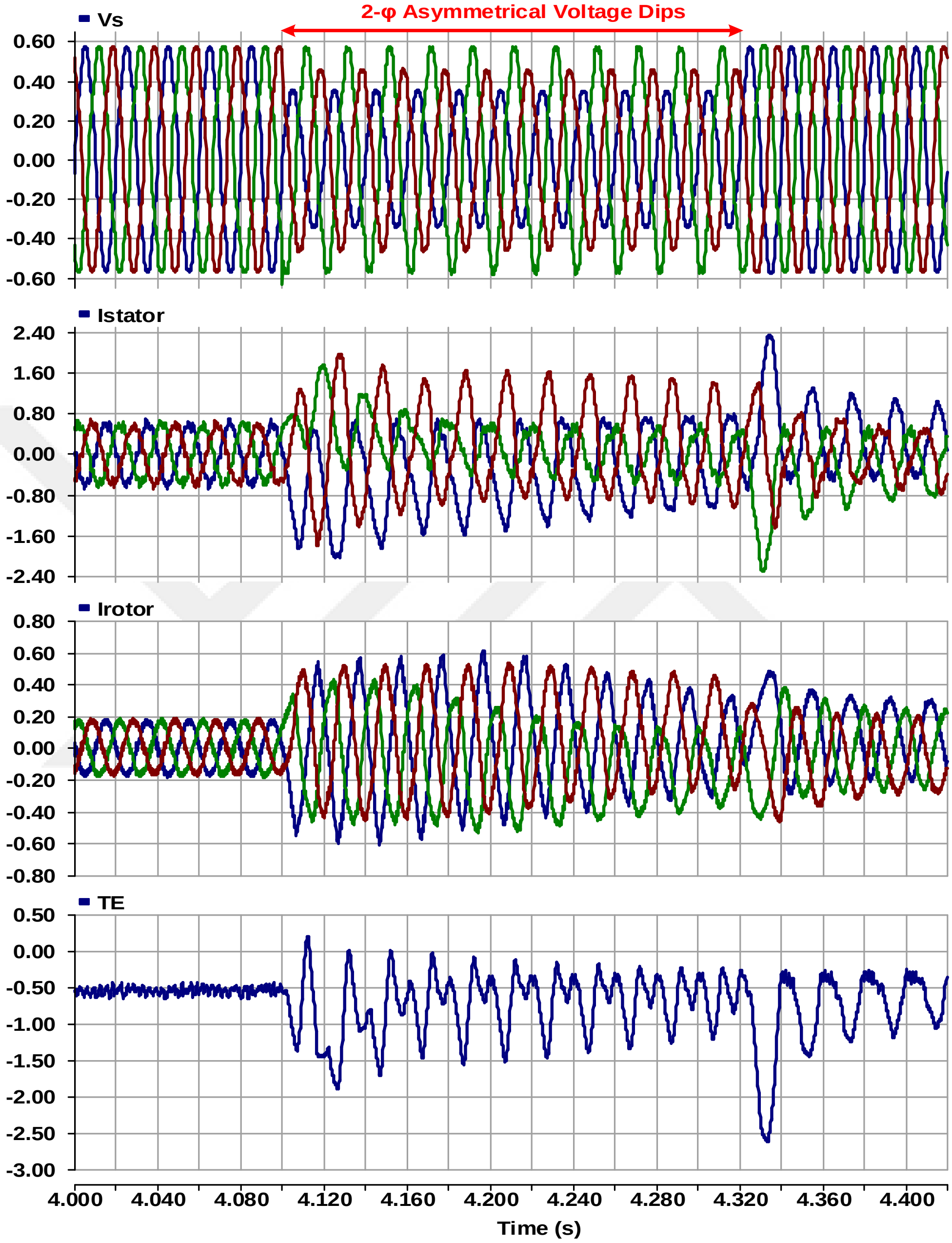

Figure 7.19 The effects of 2-ϕ asymmetrical voltage dips under distorted grid

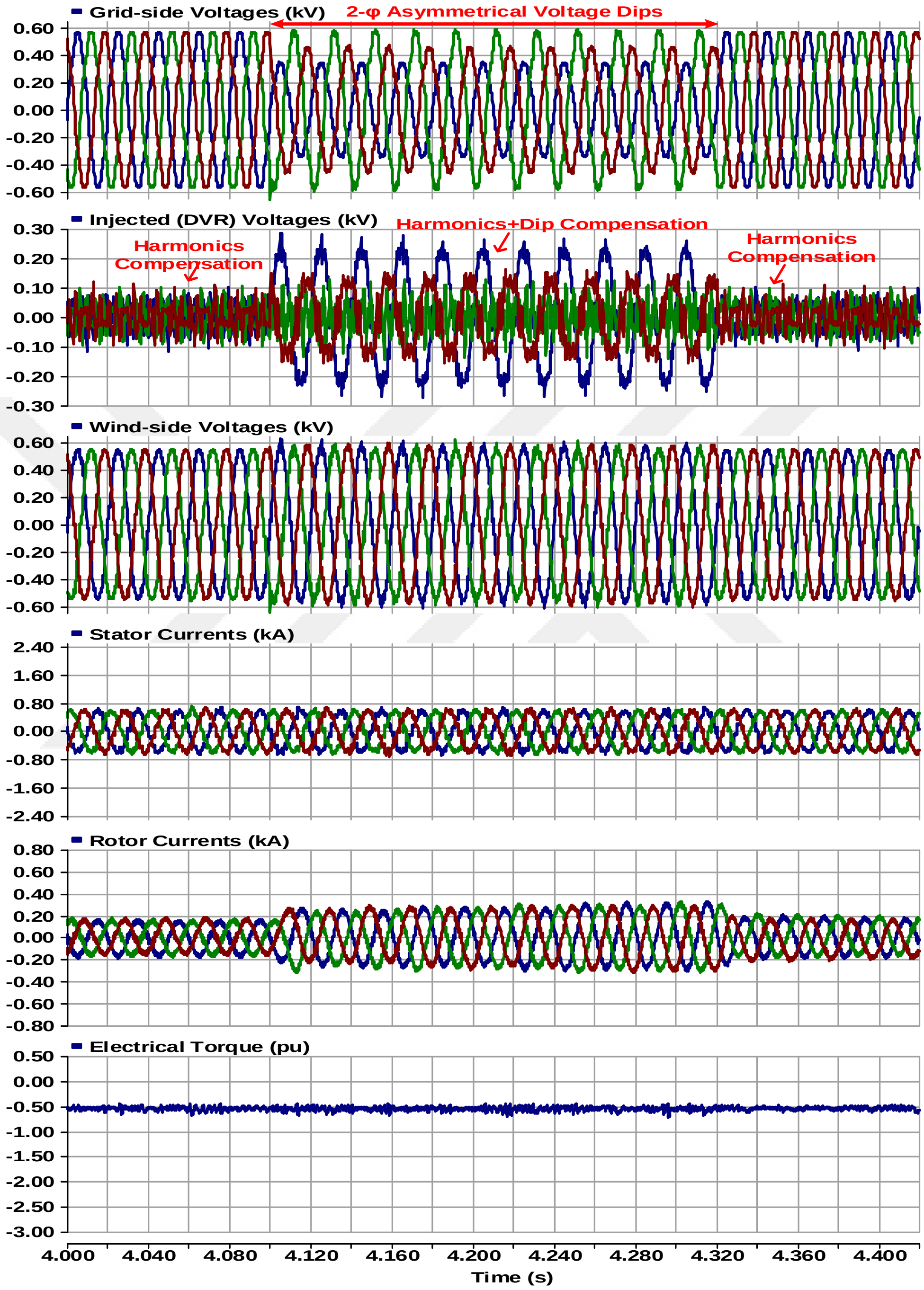

Figure 7.20 Compensation results of asymmetrical 2-ϕ voltage dips and voltage harmonics for Case V

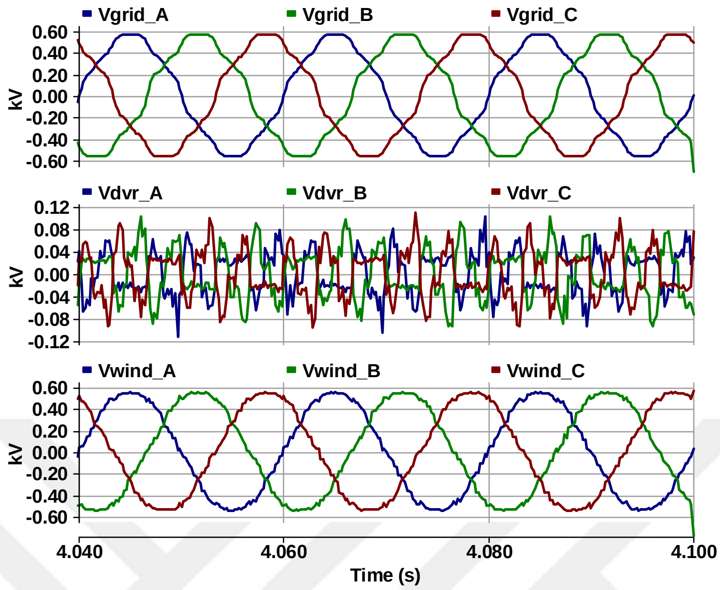

Figure 7.21 Compensation results of voltage harmonics for Case V

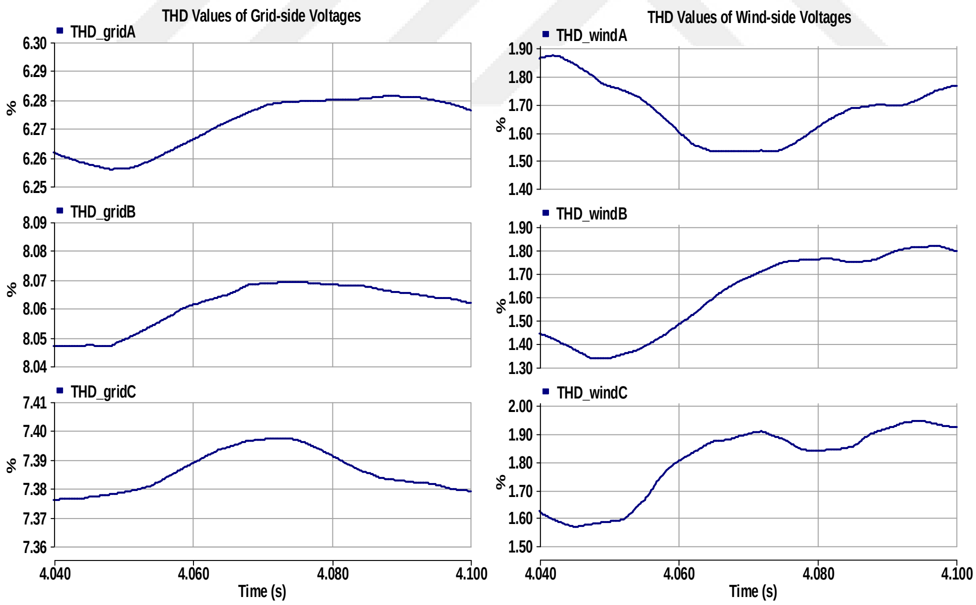

Figure 7.22 THD values of grid-side and wind-side voltages for Case V

7.2.2. Case VI

In Case VI, 2-ϕ voltage swells and its effects on DFIG are analyzed for Topology II. Asymmetrical two-ϕ swells for 0.2 and 0.3 pu occur at phase a and phase b. Voltage swell starts at t=6.1 s and its duration is 160 ms. Also, asymmetrical voltage harmonics (THD for phase a is 6.14%, THD for phase b is 7.93% and THD for phase c is 7.26%) distorts voltage waveform continuously at grid-side voltages. The rms value of grid side voltage at phase-b increases to 517.4 Vrms (1.3 pu) from 398 Vrms (1 pu). Figure 7.23 presents the influence of two-ϕ voltage dips with harmonics voltage at grid-side voltages. In the absence of 2-ϕ voltage swell compensation, the fault at grid-side induces higher rotor/stator currents during fault and immediately after the fault, as shown in Figure 7.23. Additionally, the oscillations of electrical torque occur in DFIG. Thanks to compensation by using DVR, generator side voltages are kept almost constant by an in-phase injection of voltage in series. As shown in Figure 7.24, the results show that DVR prevents current transients of rotor/stator by compensation of faults. In addition to mitigation of the high values in stator/rotor currents and it keeps electrical torque at prior values during faults. Figure 7.25 presents clear voltage waveforms for voltage harmonic compensation between t=6.02 s and t=6.08 s. The general information on Case VI is given in Table 7.6. The THD values at grid-side and wind-side voltages are presented in Figure 7.26. As shown in THD values, DVR reduces THD values nearly 1.8%, 1.75% and 1.7% for phase-a, phase-b and phase-c, respectively.

Table 7.6 Dip depth, THD, the fundamental and selective components of distorted grid-side voltages for Case VI

		Phase A	Phase B	Phase C
Swell Depth		0.2 pu	0.3 pu	No swell
THD at grid-side		6.14%	7.93%	7.26%
THD at wind-side		≈1.8%	≈1.75%	≈1.7%
The components of Grid-side Voltages	f1=50 Hz	560 V	560 V	560 V
	f5=250 Hz	24 V	31 V	28 V
	f7=350 Hz	20 V	26 V	24 V
	f11=550 Hz	12 V	15 V	14 V
	f13=650 Hz	9 V	12 V	11 V

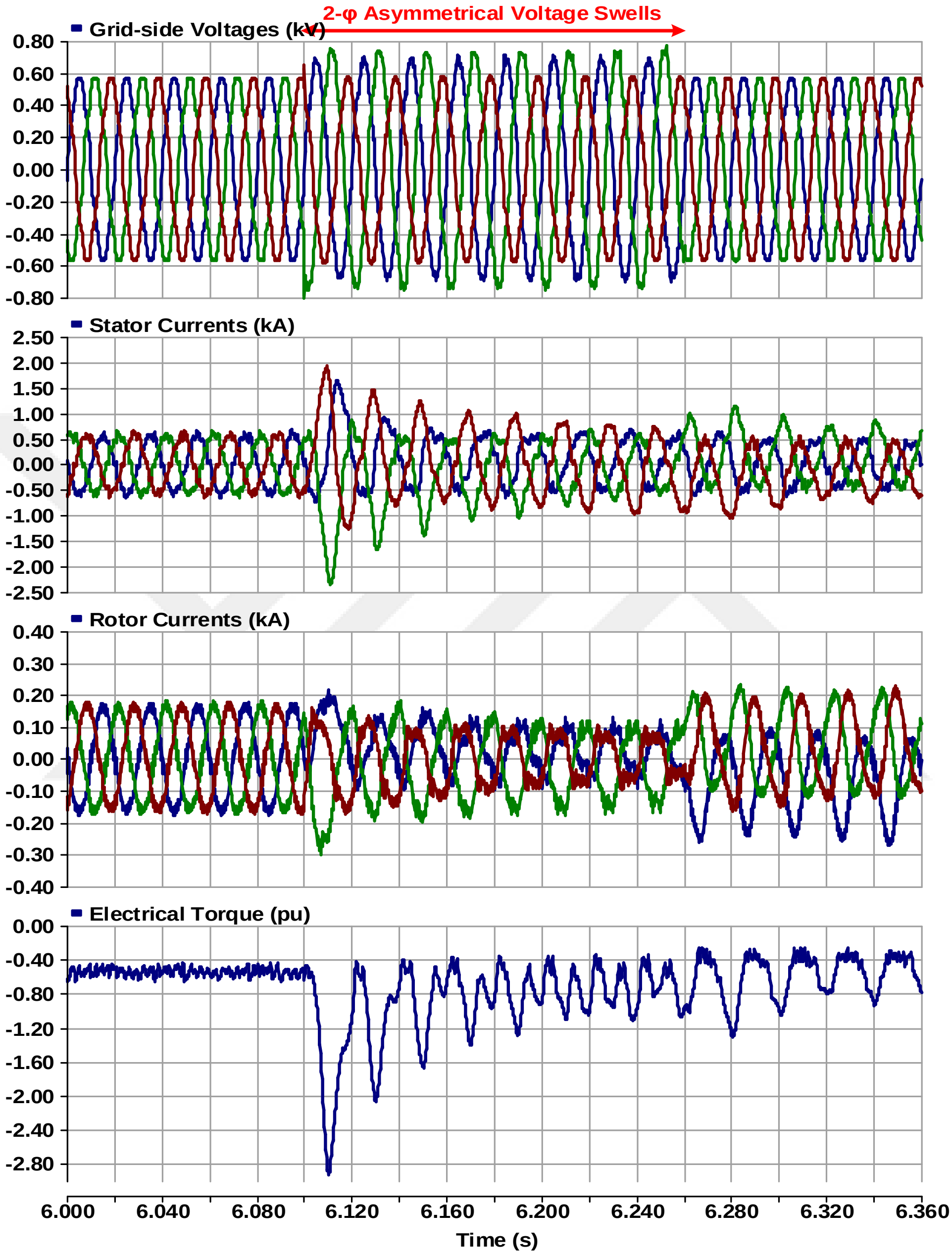

Figure 7.23 The effects of asymmetrical 2-ϕ voltage swell under distorted grid

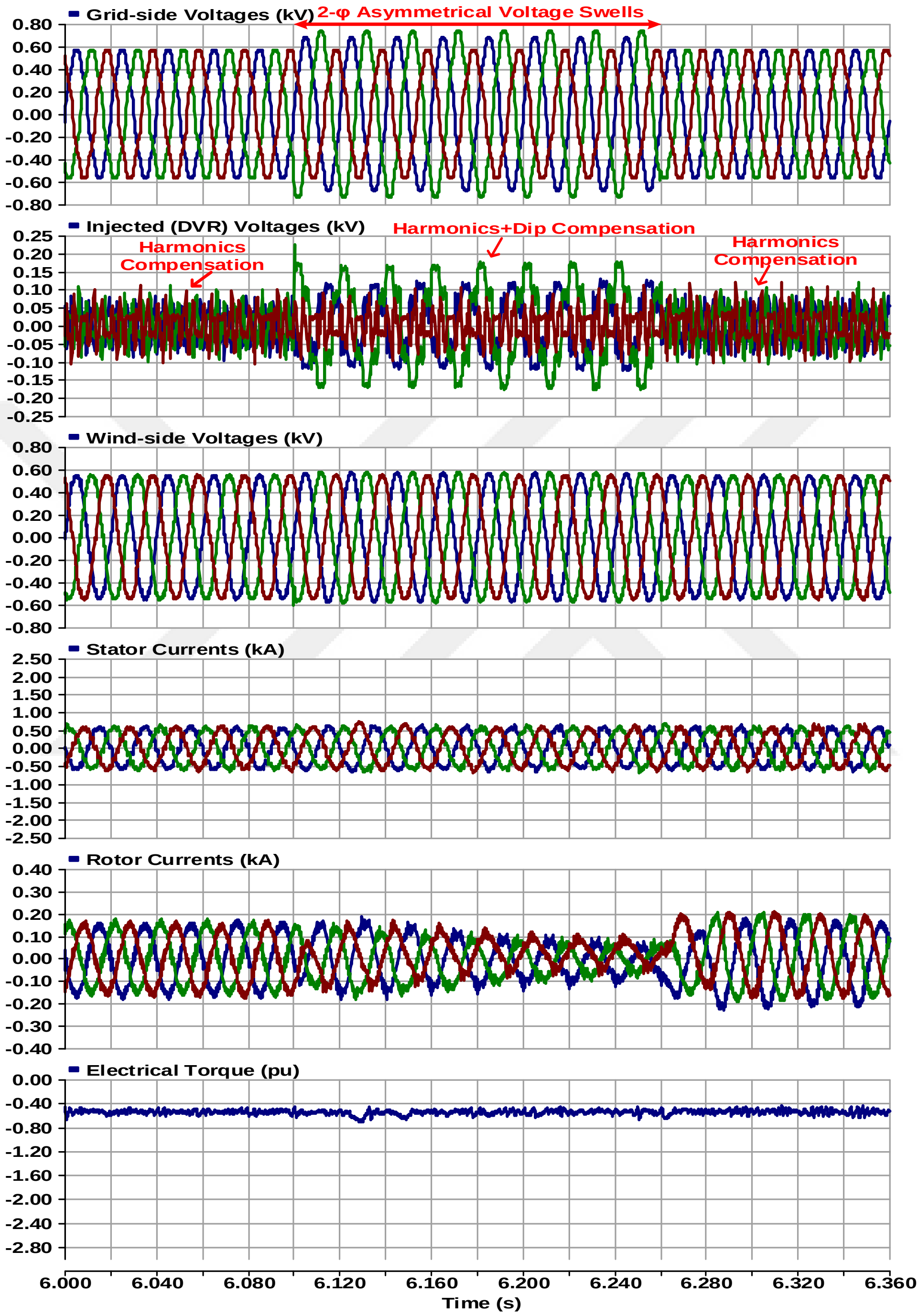

Figure 7.24 Compensation results of asymmetrical 2-ϕ voltage swells and voltage harmonics for Case VI

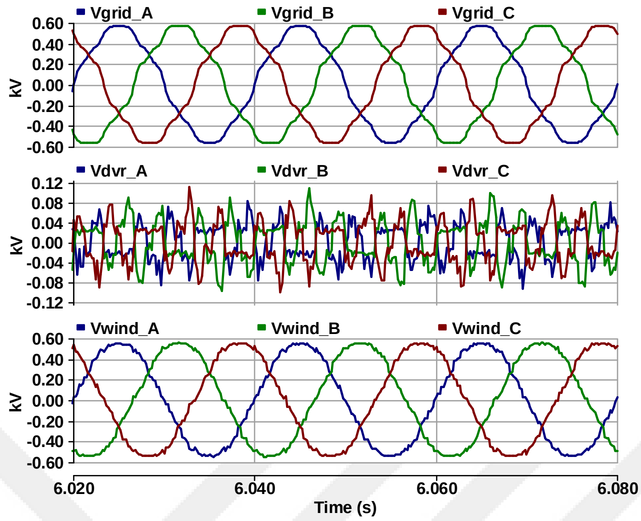

Figure 7.25 Compensation of voltage harmonics for Case VI

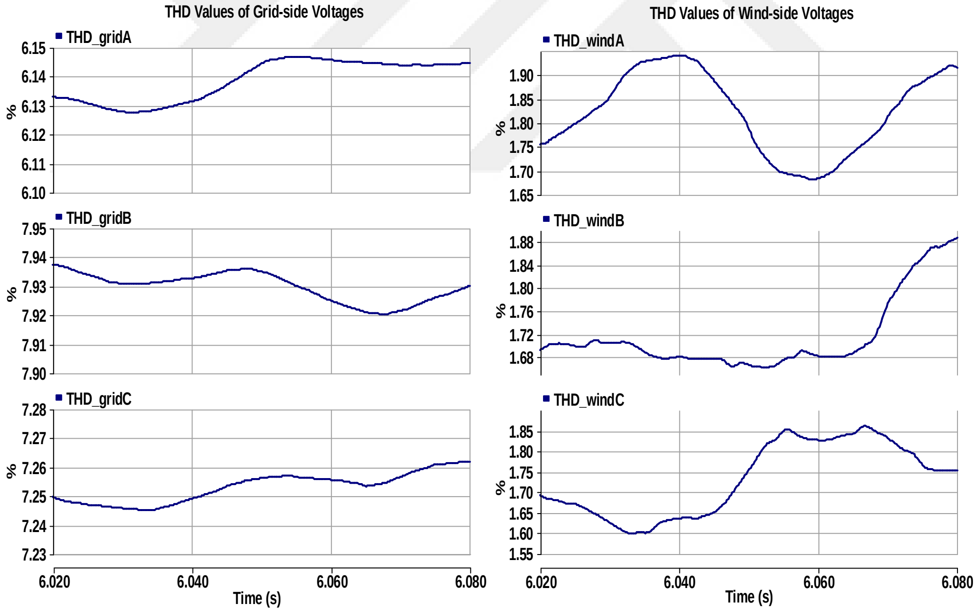

Figure 7.26 THD values of grid-side and wind-side voltages for Case VI

7.3. Discussion

In this chapter, different case studies are tested for Topology I and Topology II. The performance results are obtained up to 50% voltage dips, 30 % voltage swells and 9.52 % THD at grid-side voltages. Topology I uses a battery in dc-input of inverter in order to enhance LVRT, HVRT and voltage harmonic compensation. In topology II, back-back converter in DFIG and DVR shares common dc-link capacitors for fault ride through capabilities and harmonic compensation. In this way, it eliminates an extra dc energy storage unit compared to Topology I. But, it can achieve limited compensation due to power rating of back-back converter in DFIG system. Due to battery usage in Topology I, it can achieve more severe and long-term voltage dips/swells compared to Topology II. In harmonic compensation capability, two topologies achieves effective harmonic mitigation which reduces to approximately 1.6 % for different THD levels.

8. CONCLUSION AND FUTURE

8.1. Concluding Remarks and Discussion

This thesis investigates the power quality (PQ) problems, their affects and their compensation results in grid connected wind energy systems (GCWES) by using multilevel dynamic voltage restorer. Among PQ problems, the most hazardous voltage problems which affect the stability of wind turbine are known as voltage dips and swells. Voltage dips and swells cause high generator currents and electrical torque by losing voltage stability in GCWESs. After occurrence of grid faults, wind turbines are required to remain grid connected during voltage variations and to prevent high stator/rotor currents and power losses without losing the voltage stability of turbine. This condition is defined as low voltage ride through (LVRT) capability for voltage dips and high Voltage ride through (HVRT) for voltage swells. Besides, voltage harmonics is a serious voltage problem which cause over heating of transformer/generators and fault operation of protective equipments. The PQ standards and grid requirements of grid connected systems are specified by IEC Standard 61400-21 of IEC-Technical Committee 88.

In GCWES, Doubly fed induction generator (DFIG) is the most widely used generator type. In DFIG structure, it includes two back-back converters named as rotor-side converter (RSC) and grid-side converter (GSC). The main functions of RSC is to control active/reactive power and speed of machine. GSC is used to provide fixed dc-link voltage and unity power factor.

DFIG wind energy generation systems have to fulfill international standards and remain connected to the energy network. The most hazardous voltage problems (voltage dips and swells) provoke high stator/rotor currents and electrical torque oscillations during fault. Crowbar, Statcom and Dynamic voltage restorer (DVR) are the most common solution techniques in DFIG in order to prevent the negative effects of severe voltage disturbances. Compared to Crowbar and Statcom, DVR is more effective tool to provide voltage stability at wind-side voltages with voltage controlled inverter based structure. The advantages/disadvantages of solution techniques are compared in thesis, and capabilities of conventional DVR tied GCWES are expressed in study. DVR is tied between grid and wind-turbine, and injects controlled voltage to grid voltage for compensation of only voltage dips.

In this thesis, multilevel DVR is tied between grid and wind system in order to compensate multi-voltage problems such as voltage dips, voltage swell and voltage harmonics at wind-side voltages. In order to test DVR tied wind system, DFIG based GCWES is first implemented in PSCAD program. It is designed according to 0.69 kV/50 Hz wind turbine model. It generates approximately 700 kW active power at output of generator. In modeling system, vector control scheme is applied to control RSC and GSC. In second part, DVR is designed according to wind turbine model. In beginning, it is connected between grid and sensitive load. It is tested to keep constant voltage at load-side against voltage dips, swells and voltage harmonics. In final part of modeling, the optimization of DVR and DFIG system is achieved. The optimization of DVR tied system is realized in two topologies. In first topology called as Topology I, DVR provides active energy from a separate battery. In Topology II, the dc-link capacitor of back-back converter in DFIG is shared to compensate voltage problems. The system is designed and performed to compensate up to %50 voltage dips and voltage harmonics with approximately %9 total harmonics distortion (THD). The performance results of the system is tested and verified for different case studies in PSCAD/EMDTC 4.2.

In proposed system, five level H-bridge diode clamped multilevel inverter (H-DCMI) is used to obtain low THD values at injected voltages. Multilevel DVR is first tested to compensate different voltage problems called as voltage dips/swells and voltage harmonics, simultaneously. For this purpose, multifunctional controller algorithm is improved in order to compensate different voltage problems. Different controller schemes are first analyzed to compare performance results during severe voltage dips in multifunctional algorithm. The common property of examined detection methods is that they can be applied in compensation of both symmetrical and asymmetrical problems. In order to realize this comparison, ISRF, EPLL, SOGI-PLL, SDFT and FFT based detection methods are performed to obtain the depth of voltage dip and extract the voltage harmonics. After the generation of reference signals for voltage dip/swell and voltage harmonics, reference signals are compared with carrier signals to generate controlled injection voltages for compensation of voltage dips and harmonics. The modeled controller methods gives different responses to compensate voltage dips in order provide fault ride through capability. Among these methods, ISRF based controller algorithm shows superior performance results compared to other methods. ISRF achieves faster response for detection of voltage dips/swells and reduces to THD levels less than 1.8%. for different THD levels at grid-side voltages.

DVR topologies with battery (Topology I) and dc-link capacitor of back-back converter in DFIG (Topology II) are also performed for LVRT, HVRT and voltage harmonics. In compensation of voltage problems, ISRF method is applied in Topology I and Topology II. Topology I provides energy requirement from an additional energy storage unit to compensate voltage problems. Topology II shares the common dc-link capacitor with back-back converter. Topology I and Topology II are performed for symmetrical and asymmetrical case studies at grid-side voltages. Both topologies are tested to compensate voltage dips, voltage swells and voltage harmonics. As shown in case studies, they can prevent the high stator/rotor currents during voltage dips and swell after the occurrence of faults. Due to battery usage in Topology I, it can achieve more severe and long-term voltage dips/swells compared to Topology II. However, Topology II eliminates an additional energy storage unit. In harmonic compensation capability, two topologies achieves effective harmonic mitigation which reduces to 1.5-1.8 % from 9.52 % for up level THD results.

8.2. Future Work

Numerous original contributions have been tested and accomplished in this thesis, In addition, several future research topics are interesting. In order to improve the performance of grid connected wind energy systems, various subjects for future studies are listed in the following.

- The effects of voltage dips/swells with phase jump can be analyzed in GCWES.
- High-speed voltage detection methods can be improved to reduce detection time of voltage dips/swells.
- Unified power quality conditioner (UPQC) can be performed to compensate current harmonics in addition to voltage dips/swells and voltage harmonics.
- Switch reduces inverters can be used in DVR structures in order to reduce cost.
- The power quality issue can be considered in popular trends such as smart grid and micro-grid.

REFERENCES

Abbey, C., Li, W., Owatta, L. and Joos, G. (2006). Power Electronic Converter Control Techniques for Improved Low Voltage Ride Through Performance in WTGs. 2006 37th IEEE Power Electronics Specialists Conference.

Abdel-Baqi, O. and Nasiri, A., (2011). "Series Voltage Compensation for DFIG Wind Turbine Low-Voltage Ride-Through Solution." IEEE Transactions on Energy Conversion 26(1): 272-280.

Ackermann, T. (2005). Wind power in power systems. West Sussex PO19 8SQ, England, John Wiley & Sons Inc.

Aga, J.M. and Jadhav, H.T. (2013). Improving fault ride-through capability of DFIG connected wind turbine system: A review. Power, Energy and Control (ICPEC), 2013 International Conference on.

Aggarwal Archna, Saini Lalit Mohan and Bhim, S., (2014). "Control Strategies for DFIG Based Grid Connected Wind Energy Conversion System." International Journal of Grid Distribution Computing 7(3): 49-60.

Ahmad, A. and Loganathan, R. (2010). Development of LVRT and HVRT control strategy for DFIG based wind turbine system. Energy Conference and Exhibition (EnergyCon), 2010 IEEE International.

Al-Hadidi, H.K., Gole, A.M. and Jacobson, D.A., (2008). "Minimum power operation of cascade inverter-based dynamic voltage restorer." IEEE Transactions on Power Delivery 23(2): 889-898.

Al-Hadidi, H.K., Gole, A.M. and Jacobson, D.A., (2008). "A novel configuration for a cascade inverter-based dynamic voltage restorer with reduced energy storage requirements." IEEE Transactions on Power Delivery 23(2): 881-888.

Alaraifi, S., Moawwad, A., El Moursi, M.S. and Khadkikar, V., (2013). "Voltage Booster Schemes for Fault Ride-Through Enhancement of Variable Speed Wind Turbines." IEEE Transactions on Sustainable Energy 4(4): 1071-1081.

Almoataz Y. Abdelaziz, A.M.I., Ahmed M. Asim, Ahmed H. Abdel Razek, (2013). "Dynamic Behaviour Of Dfig-Based Wind Turbines During Symmetrical Voltage Dips." Electrical and Electronics Engineering: An International Journal (ELELIJ) 2(2): 47-59.

Amutha, N. and Kumar, B.K., (2013). "Improving fault ride-through capability of wind generation system using DVR." International Journal of Electrical Power & Energy Systems 46: 326-333.

Asiminoaei, L., Blaabjerg, F. and Hansen, S. (2005). Evaluation of harmonic detection methods for active power filter applications. Twentieth Annual IEEE Applied Power Electronics Conference and Exposition, 2005. APEC 2005.

Babaei, E. and Kangarlu, M.F., (2011). "Voltage quality improvement by a dynamic voltage restorer based on a direct three-phase converter with fictitious DC link." IET Generation Transmission & Distribution 5(8): 814-823.

Babaei, E. and Kangarlu, M.F., (2012). "Sensitive load voltage compensation against voltage sags/swells and harmonics in the grid voltage and limit downstream fault currents using DVR." Electric Power Systems Research 83(1): 80-90.

Babaei, E., Kangarlu, M.F. and Sabahi, M., (2010). "Compensation of voltage disturbances in distribution systems using single-phase dynamic voltage restorer." Electric Power Systems Research 80(12): 1413-1420.

Babaei, E., Kangarlu, M.F. and Sabahi, M., (2010). "Mitigation of Voltage Disturbances Using Dynamic Voltage Restorer Based on Direct Converters." IEEE Transactions on Power Delivery 25(4): 2676-2683.

Babaei, E., Kangarlu, M.F. and Sabahi, M., (2014). "Dynamic voltage restorer based on multilevel inverter with adjustable dc-link voltage." IET Power Electronics 7(3): 576-590.

Barros, J.D. and Silva, J.F., (2010). "Multilevel Optimal Predictive Dynamic Voltage Restorer." IEEE Transactions on Industrial Electronics 57(8): 2747-2760.

Bhumkittipich, K., Chankhamrian, W. and Mithulananthan, N., (2013). "Application of Three-level Diode-clamped Converter on 10 kW Distribution Voltage Restorer." 10th Eco-Energy and Materials Science and Engineering Symposium 34: 116-129.

Blaabjerg, F. and Chen, Z. (2006). Power Electronics for Modern Wind Turbines. United States of America, Morgan & Claypool Publishers.

Blaabjerg, F. and Ma, K., (2013). "Future on Power Electronics for Wind Turbine Systems." IEEE Journal of Emerging and Selected Topics in Power Electronics 1(3): 139-152.

Boukhris, Y., Makrini, A.E., Moussaoui, H.E. and Markhi, H.E. (2015). High voltage ride-through capability using series grid side converter for doubly fed induction generator based wind turbines. 2015 3rd International Renewable and Sustainable Energy Conference (IRSEC).

Chandrasekaran, S., (2014). Grid Connected Doubly Fed Induction Generator Based Wind Turbine under LVRT. PhD Thesis PhD Thesis, University Of Bologna.

Chaudhary, M., Brahma, S.M. and Ranade, S.J. (2013). Circuit breaker selection in a wind farm with Type-2 wind turbine generators. 2013 IEEE Power & Energy Society General Meeting.

Chen, W., Xu, D., Zhu, N., Chen, M. and Blaabjerg, F., (2016). "Control of Doubly-Fed Induction Generator to Ride-Through Recurring Grid Faults." IEEE Transactions on Power Electronics 31(7): 4831-4846.

Chen, W.L. and Wang, M.J., (2014). "Control Design of a Dynamic Voltage Restorer for Wind-Driven Induction Generators during a Low Voltage Fault at Grid Bus." Electric Power Components and Systems 42(14): 1553-1564.

Chen, Z. (2005). Issues of Connecting Wind Farms into Power Systems. 2005 IEEE/PES Transmission & Distribution Conference & Exposition: Asia and Pacific.

Chen, Z., Guerrero, J.M. and Blaabjerg, F., (2009). "A Review of the State of the Art of Power Electronics for Wind Turbines." IEEE Transactions on Power Electronics 24(8): 1859-1875.

Choi, S.S., Li, B.H. and Vilathgamuwa, D.M., (2000). "A comparative study of inverter- and line-side filtering schemes in the dynamic voltage restorer." 2000 IEEE Power Engineering Society Winter Meeting - Vols 1-4, Conference Proceedings: 2967-2972.

Choi, S.S., Li, B.H. and Vilathgamuwa, D.M., (2002). "Design and analysis of the inverter-side filter used in the dynamic voltage restorer." IEEE Transactions on Power Delivery 17(3): 857-864.

Chouhan, N.S., (2010). Doubly fed induction generator with integrated energy storage system for smoothening of output power. Master Science, Missouri University of Science and Technology.

Ditkovich, Y., Kuperman, A., Yahalom, A. and Byalsky, M., (2012). "A Generalized Approach to Estimating Capacity Factor of Fixed Speed Wind Turbines." IEEE Transactions on Sustainable Energy 3(3): 607-608.

Ebrahimzadeh, E., Farhangi, S., Iman-Eini, H., Ajaei, F.B. and Iravani, R., (2015). "Improved Phasor Estimation Method for Dynamic Voltage Restorer Applications." IEEE Transactions on Power Delivery 30(3): 1467-1477.

Edrah, M., Lo, K.L. and Anaya-Lara, O., (2015). "Impacts of High Penetration of DFIG Wind Turbines on Rotor Angle Stability of Power Systems." IEEE Transactions on Sustainable Energy 6(3): 759-766.

Emanuel, H., Schellschmidt, M., Wachtel, S. and Adloff, S. (2009). Power quality measurements of wind energy converters with full-scale converter according to IEC 61400-21. 2009 10th International Conference on Electrical Power Quality and Utilisation.

Ezoji, H., Sheikholeslami, A., Rezanezhad, M. and Livani, H., (2010). "A new control method for Dynamic Voltage Restorer with asymmetrical inverter legs based on fuzzy logic controller." Simulation Modelling Practice and Theory 18(6): 806-819.

Feltes, C., Engelhardt, S., Kretschmann, J., Fortmann, J., Koch, F. and Erlich, I. (2008). High voltage ride-through of DFIG-based wind turbines. Power and Energy Society General Meeting - Conversion and Delivery of Electrical Energy in the 21st Century, 2008 IEEE.

Flannery, P.S. and Venkataramanan, G., (2009). "Unbalanced Voltage Sag Ride-Through of a Doubly Fed Induction Generator Wind Turbine With Series Grid-Side Converter." IEEE Transactions on Industry Applications 45(5): 1879-1887.

Fortman, J. (2015). Modeling of Wind Turbines with Doubly Fed Generator System, Springer Vieweg.

Ghosh, A., Jindal, A.K. and Joshi, A., (2004). "Design of a capacitor-supported dynamic voltage restorer (DVR) for unbalanced and distorted loads." IEEE Transactions on Power Delivery 19(1): 405-413.

Gkavanoudis, S.I. and Demoulias, C.S., (2015). "Fault ride-through capability of a DFIG in isolated grids employing DVR and supercapacitor energy storage." International Journal of Electrical Power & Energy Systems 68: 356-363.

Gonzalez, M., Cardenas, V. and Espinosa, G., (2014). "Advantages of the passivity based control in dynamic voltage restorers for power quality improvement." Simulation Modelling Practice and Theory 47: 221-235.

Göksu, Ö., (2013). Control of Wind Turbines during Symmetrical and Asymmetrical Grid Faults. PhD, Aalborg University.

Guo, S. and Liu, D. (2011). Analysis and design of output LC filter system for dynamic voltage restorer. Applied Power Electronics Conference and Exposition (APEC), 2011 Twenty-Sixth Annual IEEE.

Hansen, A.D., Iov, F., Blaabjerg, F. and Hansen, L.H., (2004). "Review of Contemporary Wind Turbine Concepts and Their Market Penetration." Wind Engineering 28(3): 247-263.

Hansen, A.D. and Michalke, G., (2007). "Fault ride-through capability of DFIG wind turbines." Renewable Energy 32(9): 1594-1610.

He, Y., Hu, J. and Zhao, R. (2005). Modeling and control of wind-turbine used DFIG under network fault conditions. 2005 International Conference on Electrical Machines and Systems.

Ho, C.N.M. and Chung, H.S.H., (2010). "Implementation and Performance Evaluation of a Fast Dynamic Control Scheme for Capacitor-Supported Interline DVR." IEEE Transactions on Power Electronics 25(8): 1975-1988.

Holdsworth, L., Wu, X.G., Ekanayake, J.B. and Jenkins, N., (2003). "Comparison of fixed speed and doubly-fed induction wind turbines during power system disturbances." IEE Proceedings - Generation, Transmission and Distribution 150(3): 343-352.

Hosseini, S.H., Sharifian, M.B.B. and Shahnia, F., (2005). "Dynamic performance of double fed induction generator for wind turbines." ICEMS 2005: Proceedings of the Eighth International Conference on Electrical Machines and Systems, Vols 1-3: 1261-1266.

Hussein, A.A. and Ali, M.H., (2016). "Comparison among series compensators for transient stability enhancement of doubly fed induction generator based variable speed wind turbines." IET Renewable Power Generation 10(1): 116-126.

Ibrahim, A.O., Nguyen, T.H., Lee, D.C. and Kim, S.C., (2011). "A Fault Ride-Through Technique of DFIG Wind Turbine Systems Using Dynamic Voltage Restorers." IEEE Transactions on Energy Conversion 26(3): 871-882.

Iec (2005). Wind turbines – Part 1: Design requirements. International Standard IEC 61400-1. Geneva, Switzerland, International Electrotechnical Commission: 1-92.

Ieee (1993). IEEE Recommended Practices and Requirements for Harmonic Control in Electrical Power Systems. IEEE Std 519-1992: 1-112.

Ieee (1995). IEEE Recommended Practice for Monitoring Electric Power Quality. IEEE Std 1159-1995: i.

Ieee (2009). IEEE Recommended Practice for Monitoring Electric Power Quality. IEEE Std 1159-2009 (Revision of IEEE Std 1159-1995): c1-81.

Ieee (2014). IEEE Trial-Use Recommended Practice for Voltage Sag and Short Interruption Ride-Through Testing for End-Use Electrical Equipment Rated Less than 1000 V. IEEE Std 1668-2014: 1-92.

İnci, M., Bayındır, K.Ç. and Tümay, M., (2016). "Improved Synchronous Reference Frame based controller method for multifunctional compensation." Electric Power Systems Research 141: 500-509.

İnci, M., Bayındır, K.Ç. and Tümay, M., (2016). "A novel method improvement for detection of voltage problems in dynamic voltage restorers." Journal of the Faculty of Engineering and Architecture of GaziUniversity 31(4): 997-1006.

Islam, F.R. and Pota, H.R., (2013). "Plug-in-hybrid electric vehicles park as virtual DVR." Electronics Letters 49(3): 211-212.

Jacobsen, E. and Lyons, R., (2003). "The sliding DFT." IEEE Signal Processing Magazine 20(2): 74-80.

Jayaprakash, P., Singh, B., Kothari, D.P., Chandra, A. and Al-Haddad, K., (2014). "Control of Reduced-Rating Dynamic Voltage Restorer With a Battery Energy Storage System." IEEE Transactions on Industry Applications 50(2): 1295-1303.

Jiang, F., Tu, C.M., Shuai, Z.K., Xiao, F. and Lan, Z., (2016). "Combinational voltage booster technique for fault ride-through capability enhancement of squirrel-cage induction generator." Electric Power Systems Research 136: 163-172.

Jimichi, T., Fujita, H. and Akagi, H., (2008). "Design and experimentation of a dynamic voltage restorer capable of significantly reducing an energy-storage element." IEEE Transactions on Industry Applications 44(3): 817-825.

Jing, X., (2009). Modeling and Control of a Doubly-Fed Induction Generator for Wind Turbine-Generator Systems. Master of Science MSc Thesis, Marquette University.

Karaipoom, T. and Ngamroo, I., (2015). "Optimal Superconducting Coil Integrated Into DFIG Wind Turbine for Fault Ride Through Capability Enhancement and Output Power Fluctuation Suppression." IEEE Transactions on Sustainable Energy 6(1): 28-42.

Karimi-Ghartemani, M., (2014). "Linear and Pseudolinear Enhanced Phased-Locked Loop (EPLL) Structures." IEEE Transactions on Industrial Electronics 61(3): 1464-1474.

Karimi-Ghartemani, M. and Iravani, M.R., (2002). "A nonlinear adaptive filter for online signal analysis in power systems: Applications." IEEE Transactions on Power Delivery 17(2): 617-622.

Karimi-Ghartemani, M., Iravani, M.R. and Katiraei, F., (2005). "Extraction of signals for harmonics, reactive current and network-unbalance compensation." IEE Proceedings-Generation Transmission and Distribution 152(1): 137-143.

Karimi-Ghartemani, M., Mokhtari, H., Iravani, M.R. and Sedighy, M., (2004). "A signal processing system for extraction of harmonics and reactive current of single-phase systems." IEEE Transactions on Power Delivery 19(3): 979-986.

Kim, H.S. and Lu, D.D.C. (2010). Review on wind turbine generators and power electronic converters with the grid-connection issues. 2010 20th Australasian Universities Power Engineering Conference.

Koç, E., (2010). Modeling and Investigation of Fault Ride Through Capability of Variable Speed Wind Turbines Master of Science MSc Thesis, Middle East Technical University.

Konuray, M. (2016). Turkish Wind Energy Statistics Report. Turkey: 1-90.

Kyaw, M.M. and Ramachandaramurthy, V.K., (2011). "Fault ride through and voltage regulation for grid connected wind turbine." Renewable Energy 36(1): 206-215.

Larsson, A., (2000). The power quality of wind turbines. PhD PhD Thesis, Chalmers University of Technology.

Leon, A.E., Farias, M.F., Battaiotto, P.E., Solsona, J.A. and Valla, M.I., (2011). "Control Strategy of a DVR to Improve Stability in Wind Farms Using Squirrel-Cage Induction Generators." IEEE Transactions on Power Systems 26(3): 1609-1617.

Li, B.H., Choi, S.S. and Vilathgamuwa, D.M., (2000). "On the injection transformer used in the dynamic voltage restorer." 2000 International Conference on Power System Technology, Vols I-Iii, Proceedings: 941-946.

Li, B.H., Choi, S.S. and Vilathgamuwa, D.M., (2002). "Transformerless dynamic voltage restorer." IEE Proceedings-Generation Transmission and Distribution 149(3): 263-273.

Li, G.J., Zhang, X.P., Choi, S.S., Lie, T.T. and Sun, Y.Z., (2007). "Control strategy for dynamic voltage restorers to achieve minimum power injection without introducing sudden phase shift." IET Generation Transmission & Distribution 1(5): 847-853.

Li, Y.W., (2009). "Control and Resonance Damping of Voltage-Source and Current-Source Converters With LC Filters." IEEE Transactions on Industrial Electronics 56(5): 1511-1521.

Li, Y.W., Vilathgamuwa, D.M., Loh, P.C. and Blaabjerg, F., (2006). "A dual-functional medium voltage level DVR to limit downstream fault currents." 2006 IEEE Power Electronics Specialists Conference, Vols 1-7: 1326-1332.

Limin, X., Weisheng, X. and Youling, Y. (2007). A Fast Harmonic Detection Method Based on Recursive DFT. 2007 8th International Conference on Electronic Measurement and Instruments.

Lütfü Sarıbulut, Ahmet Teke and Tümay, M., (2013). "Fundamentals and literature review of Fourier transform in power quality issues." Journal of Electrical and Electronics Engineering Research 5(1): 9-22.

Manoj Kumar Swain, R.R.S., Balaram Das, Rakesh Sahu, (2013). "Enhancement of Power Quality for Grid Connected Wind Energy System using Smart-STATCOM." International Journal of Emerging Technology and Advanced Engineering 3(10): 232-235.

Marei, M.I., Eltantawy, A.B. and Abd El-Sattar, A., (2012). "An energy optimized control scheme for a transformerless DVR." Electric Power Systems Research 83(1): 110-118.

Massoud, A.M., Ahmed, S., Enjeti, P.N. and Williams, B.W., (2010). "Evaluation of a Multilevel Cascaded-Type Dynamic Voltage Restorer Employing Discontinuous Space Vector Modulation." IEEE Transactions on Industrial Electronics 57(7): 2398-2410.

Md. Arifujjaman , M.T. Iqbal and Quaicoe, J.E., (2009). "Vector Control of a DFIG Based Wind Turbine." Istanbul University – Journal of Electrical & Electronics En Gineering 9(2): 1057-1066.

Mohamed, M.B., Jemli, M., Gossa, M. and Jemli, K. (2004). Doubly fed induction generator (DFIG) in wind turbine modeling and power flow control. Industrial Technology, 2004. IEEE ICIT '04. 2004 IEEE International Conference on.

Mohammadpour, H., Zadeh, S.G. and Tohidi, S., (2015). "Symmetrical and asymmetrical low-voltage ride through of doubly-fed induction generator wind turbines using gate controlled series capacitor." IET Renewable Power Generation 9(7): 840-846.

Mohod, S.W. and Aware, M.V., (2010). "A STATCOM-Control Scheme for Grid Connected Wind Energy System for Power Quality Improvement." IEEE Systems Journal 4(3): 346-352.

Moursi, M.S.E., Goweily, K., Kirtley, J.L. and Abdel-Rahman, M., (2014). "Application of Series Voltage Boosting Schemes for Enhanced Fault Ridethrough Performance of Fixed Speed Wind Turbines." IEEE Transactions on Power Delivery 29(1): 61-71.

Naidoo, R. and Pillay, P., (2007). "A New Method of Voltage Sag and Swell Detection." IEEE Transactions on Power Delivery 22(2): 1056-1063.

Naidu, S.R. and Fernandes, D.A., (2009). "Dynamic voltage restorer based on a four-leg voltage source converter." IET Generation Transmission & Distribution 3(5): 437-447.

Nami, A., Zare, F., Ghosh, A. and Blaabjerg, F., (2011). "A Hybrid Cascade Converter Topology With Series-Connected Symmetrical and Asymmetrical Diode-Clamped H-Bridge Cells." IEEE Transactions on Power Electronics 26(1): 51-65.

Newman, M.J., Holmes, D.G., Nielsen, J.G. and Blaabjerg, F., (2003). "A dynamic voltage restorer (DVR) with selective harmonic compensation at medium voltage level." 2003 Ieee Industry Applications Conference, Vols 1-3: 1228-1235.

Omar, R. and Rahim, N.A., (2012). "Voltage unbalanced compensation using dynamic voltage restorer based on supercapacitor." International Journal of Electrical Power & Energy Systems 43(1): 573-581.

Pan, X.P., Ju, P., Wu, F. and Jin, Y.Q., (2013). "Parameter estimation of drive system in a fixed-speed wind turbine by utilising turbulence excitations." IET Generation, Transmission & Distribution 7(7): 665-673.

Pannell, G., Atkinson, D.J. and Zahawi, B., (2010). "Minimum-Threshold Crowbar for a Fault-Ride-Through Grid-Code-Compliant DFIG Wind Turbine." IEEE Transactions on Energy Conversion 25(3): 750-759.

Pena, R., Clare, J.C. and Asher, G.M., (1996). "Doubly fed induction generator using back-to-back PWM converters and its application to variable-speed wind-energy generation." IEE Proceedings-Electric Power Applications 143(3): 231-241.

Perera, K., Salomonsson, D., Atputharajah, A. and Alahakoon, S. (2006). Automated Control Technique for a Single Phase Dynamic Voltage Restorer. 2006 International Conference on Information and Automation.

Petersson, A., (2005). Analysis, Modeling and Control of Doubly-Fed nduction Generators for Wind Turbines. The Degree Of Doctor Of Philosophy PhD Thesis, Chalmers University Of Technology.

Pillay, P. and Manyage, M., (2001). "California Electricity Situation." IEEE Power Engineering Review 21(5): 10-12.

Polinder, H., Ferreira, J.A., Jensen, B.B., Abrahamsen, A.B., Atallah, K. and Mcmahon, R.A., (2013). "Trends in Wind Turbine Generator Systems." IEEE Journal of Emerging and Selected Topics in Power Electronics 1(3): 174-185.

Qiao, W. and Harley, R.G. (2008). Grid Connection Requirements and Solutions for DFIG Wind Turbines. 2008 IEEE Energy 2030 Conference.

Qiao, W., Venayagamoorthy, G. and Harley, R., (2009). "Real-Time Implementation of a STATCOM on a Wind Farm Equipped With Doubly Fed Induction Generators." IEEE Transactions on Industry Applications 45(1): 98-107.

Raju, R.V.R., Karthikeyan, A. and Nagamani, C. (2012). Enhanced decoupled power control of wind turbine driven DFIG using DVR under unbalanced grid voltage. Advances in Power Conversion and Energy Technologies (APCET), 2012 International Conference on.

Ramasamy, M. and Thangavel, S., (2012). "Photovoltaic based dynamic voltage restorer with power saver capability using PI controller." International Journal of Electrical Power & Energy Systems 36(1): 51-59.

Ramirez, D., Martinez, S., Platero, C.A., Blazquez, F. and De Castro, R.M., (2011). "Low-Voltage Ride-Through Capability for Wind Generators Based on Dynamic Voltage Restorers." IEEE Transactions on Energy Conversion 26(1): 195-203.

Rauf, A.M. and Khadkikar, V., (2015). "An Enhanced Voltage Sag Compensation Scheme for Dynamic Voltage Restorer." IEEE Transactions on Industrial Electronics 62(5): 2683-2692.

Reid, W.E. (1994). Power quality issues-standards and guidelines. Pulp and Paper Industry Technical Conference, 1994., Conference Record of 1994 Annual.

Rojas, C.A., Kouro, S., Edwards, D., Wu, B. and Rivera, S. (2014). Five-level H-bridge NPC central photovoltaic inverter with open-end winding grid connection. IECON 2014 - 40th Annual Conference of the IEEE Industrial Electronics Society.

Romlie, M.F.B., (2014). Impact of Energy Storage on the Stability and Transmission Efficiency of a Remote Grid. PhD PhD Thesis, The University of Nottingham.

Roncero-Sanchez, P. and Acha, E., (2009). "Dynamic Voltage Restorer Based on Flying Capacitor Multilevel Converters Operated by Repetitive Control." Ieee Transactions on Power Delivery 24(2): 951-960.

S.Tripathi, C.S.S., (2014). "Power Quality Improvement in Wind Grid Energy System using STATCOM With BESS -Control Scheme." International Journal of Innovation and Scientific Research 9(2): 237-245.

Sadigh, A.K. and Smedley, K.M., (2016). "Fast and precise voltage sag detection method for dynamic voltage restorer (DVR) application." Electric Power Systems Research 130: 192-207.

Saraf, P., (2012). Fault Analysis of an Unbalanced Distribution System with Distributed Generation. Master of Science MSc, Clemson University.

Shafiei, F., (2012). Modelling and Verification of Doubly Fed Induction Generator (DFIG) using Real Time Digital Simulator (RTDS). Master Science MSc Thesis, Chalmers University of Technology.

Shi, J., Tang, Y.J., Yang, K., Chen, L., Ren, L., Li, J.D. and Cheng, S.J., (2010). "SMES Based Dynamic Voltage Restorer for Voltage Fluctuations Compensation." IEEE Transactions on Applied Superconductivity 20(3): 1360-1364.

Shin, H., Jung, H.S. and Sul, S.K. (2011). Low Voltage Ride Through(LVRT) control strategy of grid-connected variable speed Wind Turbine Generator System. 8th International Conference on Power Electronics - ECCE Asia.

Silva, S.M., Da Silveira, S.B., Reis, A.D. and Cardoso, B.J., (2005). "Analysis of a dynamic voltage compensator with reduced switch-count and absence of energy storage system." IEEE Transactions on Industry Applications 41(5): 1255-1262.

Sivasankar, G. and Kumar, V.S., (2014). "Improving Low Voltage Ride through Capability of Wind Generators Using Dynamic Voltage Restorer." Journal of Electrical Engineering-Elektrotechnicky Casopis 65(4): 235-241.

Springer, T., (1988). "Sliding Fft Computes Frequency-Spectra in Real-Time." Edn 33(20): 161-170.

Sree, H. and Mohan, N., (2000). "High-frequency-link cycloconverter-based DVR for voltage sag mitigation." Conference Record of the 2000 Twenty-Fourth International Power Modulator Symposium, 50th Anniversary: 97-100.

Sree, H. and Mohan, N., (2000). "Voltage sag mitigation using a high-frequency-link cycloconverter-based DVR." IECON 2000: 26th Annual Conference of the Ieee Industrial Electronics Society, Vols 1-4: 344-349.

Steve Sawyer and Rave, K. (2016). GWEC - Global Wind Report 2015. www.gwec.net: 1-76.

Sugirtha, M.G. and Latha, P. (2011). Analysis of power quality problems in grid connected wind power plant. Recent Advancements in Electrical, Electronics and Control Engineering (ICONRAEeCE), 2011 International Conference on.

Sun, Y.Z., Lin, J., Li, G.J. and Li, X. (2009). A review on the integration of wind farms with variable speed wind turbine systems into power systems. 2009 International Conference on Sustainable Power Generation and Supply.

Sunil, T.P. and Loganathan, N. (2012). Power quality improvement of a grid-connected wind energy conversion system with harmonics reduction using FACTS device. Advances in Engineering, Science and Management (ICAESM), 2012 International Conference on.

Tao, S., (2004). Power Quality of Grid-Connected Wind Turbines with DFIG and Their Interaction with the Grid. Doctor of Philosophy in Electrical Engineering PhD Thesis, Aalborg University.

Tourou, P. and Sourkounis, C. (2014). Investigation of fault ride-through behavior of DFIG-based wind energy conversion systems. Energy Conference (ENERGYCON), 2014 IEEE International.

Tunaboylu, N.S., Collins, E.R. and Chaney, P.R. (1998). Voltage disturbance evaluation using the missing voltage technique. Harmonics and Quality of Power Proceedings, 1998. Proceedings. 8th International Conference On.

Tuscaloosa, A., (2009). Control Design and Analysis of Doubly- Fed Induction Generator in Wind Power Application Master of Science MSc Thesis, The University of Alabama

Vilathgamuwa, D.M., Wijekoon, M. and Choi, S.S., (2006). "A novel technique to compensate voltage sags in multiline distribution system - The interline dynamic voltage restorer." IEEE Transactions on Industrial Electronics 53(5): 1603-1611.

Vilathgamuwa, M., Perera, A.a.D.R. and Choi, S.S., (2002). "Performance improvement of the dynamic voltage restorer with closed-loop load voltage and current-mode control." IEEE Transactions on Power Electronics 17(5): 824-834.

Wang, B.S. and Venkataramanan, G., (2009). "Dynamic Voltage Restorer Utilizing a Matrix Converter and Flywheel Energy Storage." IEEE Transactions on Industry Applications 45(1): 222-231.

Wang, B.S., Venkataramanan, G. and Illindala, M., (2006). "Operation and control of a dynamic voltage restorer using transformer coupled H-bridge converters." IEEE Transactions on Power Electronics 21(4): 1053-1061.

Wang, J., Hu, X. and Chen, S. (2012). Research on detection algorithm of voltage sag characteristics. 2012 7th IEEE Conference on Industrial Electronics and Applications (ICIEA).

Wang, L. and Truong, D.N., (2013). "Stability Enhancement of DFIG-Based Offshore Wind Farm Fed to a Multi-Machine System Using a STATCOM." IEEE Transactions on Power Systems 28(3): 2882-2889.

Wenjie, C., Blaabjerg, F., Nan, Z., Min, C. and Dehong, X., (2016). "Doubly Fed Induction Generator Wind Turbine Systems Subject to Recurring Symmetrical Grid Faults." IEEE Transactions on Power Electronics 31(2): 1143-1160.

Wessels, C., Gebhardt, F. and Fuchs, F.W., (2011). "Fault Ride-Through of a DFIG Wind Turbine Using a Dynamic Voltage Restorer During Symmetrical and Asymmetrical Grid Faults." IEEE Transactions on Power Electronics 26(3): 807-815.

Wessels, C., Lohde, R. and Fuchs, F.W. (2010). Transformer based voltage sag generator to perform LVRT and HVRT tests in the laboratory. Proceedings of 14th International Power Electronics and Motion Control Conference EPE-PEMC 2010.

Xie, Z., Zhang, X.G., Zhang, X., Yang, S.Y. and Wang, L.X., (2015). "Improved Ride-Through Control of DFIG During Grid Voltage Swell." IEEE Transactions on Industrial Electronics 62(6): 3584-3594.

Xiong, P.H. and Sun, D., (2016). "Backstepping-Based DPC Strategy of a Wind Turbine-Driven DFIG Under Normal and Harmonic Grid Voltage." IEEE Transactions on Power Electronics 31(6): 4216-4225.

Yao, J., Li, H., Chen, Z., Xia, X.F., Chen, X.Y., Li, Q. and Liao, Y., (2013). "Enhanced Control of a DFIG-Based Wind-Power Generation System With Series Grid-Side Converter Under Unbalanced Grid Voltage Conditions." IEEE Transactions on Power Electronics 28(7): 3167-3181.

Yuvaraj, V., Raj, E.P., Mowlidharan, A. and Thirugnanamoorthy, L. (2011). Power quality improvement for grid connected wind energy system using FACTS device. Proceedings of the Joint INDS'11 & ISTET'11.

Zhan, C.J., Ramachandaramurthy, V.K., Arulampalam, A., Fitzer, C., Kromlidis, S., Barnes, M. and Jenkins, N., (2001). "Dynamic voltage restorer based on voltage-space-vector PWM control." IEEE Transactions on Industry Applications 37(6): 1855-1863.

Zhan, C.J., Wu, X.G., Kromlidis, S., Ramachandaramurthy, V.K., Barnes, M., Jenkins, N. and Ruddell, A.J., (2003). "Two electrical models of the lead-acid battery used in a dynamic voltage restorer." IEE Proceedings-Generation Transmission and Distribution 150(2): 175-182.

Zhang, S., Tseng, K.J., Choi, S.S., Nguyen, T.D. and Yao, D.L., (2012). "Advanced Control of Series Voltage Compensation to Enhance Wind Turbine Ride Through." IEEE Transactions on Power Electronics 27(2): 763-772.

Zheng, Z., Yang, G. and Geng, H., (2013). "High Voltage Ride-through Control Strategy of Grid-side Converter for DFIG-based WECS." 39th Annual Conference of the Ieee Industrial Electronics Society (Iecon 2013): 5282-5287.

Zhu, R., Deng, F., Chen, Z. and Liserre, M., (2016). "Enhanced Control of DFIG Wind Turbine Based on Stator Flux Decay Compensation." IEEE Transactions on Energy Conversion 31(4): 1366-1376.

Zhu, R.W., Chen, Z., Tang, Y., Deng, F.J. and Wu, X.J., (2016). "Dual-Loop Control Strategy for DFIG-Based Wind Turbines Under Grid Voltage Disturbances." IEEE Transactions on Power Electronics 31(3): 2239-2253.

BIOGRAPHY

Mustafa İNCİ was born in Şanlıurfa, Turkey in 1987. He received his BSc. And MSc from Electrical and Electronics Engineering Department of Çukurova University in 2011 and 2013, respectively. Now, he has been working as research assistant in Electrical and Electronics Engineering Department of Çukurova University since 2011. His research interests include power quality, wind energy systems and multilevel inverters.

SCI/SCI-Expanded Publications

Büyük, M., **İnci, M.,** Tümay, M., "Performance Comparison of Voltage Sag/Swell Detection Methods Implemented in Custom Power Devices", Rev. Roum. Sci. Tech.- Electrotechnique at Energetique, vol.62, 2, pp. 129-133, June 2017.

İnci, M., Bayındır, K.Ç., Tümay, M., "The performance improvement of dynamic voltage restorer based on bidirectional dc–dc converter", Electrical Engineering, vol. 9, 1, pp.285-300, March 2017

İnci, M., Bayındır, K.Ç., Tümay, M., "Improved Synchronous Reference Frame Based Controller Method for Multifunctional Compensation", Electric Power Systems Research, vol. 141, pp. 500-509, December 2016

İnci, M., Bayındır, K.Ç., Tümay, M., "A Novel Method Improvement For Detectıon Of Voltage Dısturbances In Dynamıc Voltage Restorers", Journal of The Faculty of Engineering and Architecture of Gazi University, vol. 31, 4, pp. 997-1006, December 2016